Biomarkers for Obesity: *In Vivo* Monitoring of Bioamine Metabolism in Adipose Tissue and Skeletal Muscle Using Online Microdialysis-Capillary Electrophoresis

A THESIS
SUBMITTED TO THE FACULTY OF
UNIVERSITY OF MINNESOTA
BY

Megan Marie Weisenberger

IN PARTIAL FULFILLMENT OF THE REQUIREMENTS
FOR THE DEGREE OF
DOCTOR OF PHILOSOPHY

Michael T. Bowser, Advisor

May, 2017

Acknowledgements

There have been countless individuals who have contributed to my growth as not only a scientist, but towards becoming a better human being. I am forever grateful for all their support, wisdom, and kindness extended to me throughout the years.

On a professional note, I would first and foremost like to thank Dr. David Clemmer. There have been so many moments over the last few years where I've realized just how much you and your analytical course are the reason I am currently on this career path. As a professor, you managed to make analytical chemistry fun and exciting, with personal touches of home-made cookies for the class during exam weeks. I greatly appreciate how much time and effort you dedicated to all of your students. The time spent working in your lab not only taught me the endless practical applications of instrument-development analytical work, but also opened my eyes to a world of career opportunities I had never dared to envision for myself. Thank you for believing in me and pushing me further than I ever expected.

I would also like to thank Dr. Michael Bowser and the members of the Bowser research group, both past and present. I would especially like to thank Dr. Nic Frost, Thane Taylor, Dr. Amy Stading, Dr. Matt Geiger, Alex Johnson, Kailey Soller, and Sean Dembowski. I sincerely enjoyed the creative and productive work space you all helped create. It's a special treat when one genuinely enjoys working with their colleagues; thank you all for maintaining that atmosphere.

The veterinary staff at Research Animal Resources have been incredibly helpful and supportive throughout the years. Thank you for all of your hard work, researchers are

truly indebted to your services. Dr. David Bernlohr, Dr. Renee Frontiera, and Dr. Phil Buhlmann have offered advice and support which has been much appreciated during my graduate studies. Dr. Vivian Feng allowed me the opportunity to teach an analytical laboratory course at Augsburg College during graduate school. It was an amazing experience that allowed me to grow and develop as an educator, thank you.

On a personal level, I would like to acknowledge my family, especially my parents, my sisters, and my grandma. Dad, thank you for all of your help throughout the years. All of your trips out to visit, only to be met with a laundry-list of tasks often absurd in length, helped me tremendously. Thank you. Grandma, your kindness and open heart are truly appreciated by everyone around you. Thank you for your love and kindness over the last 15 years. Tori, whisperer of technology, you demonstrate each and every day what it means to be a female in science. I am in awe of your determination, drive, and wit. There is no doubt your future holds amazing things, and I hope to be a little more like you each day. Mom, where do I even begin? Your support, your love, your helpfulness, and your willingness to listen are just some of the reasons why I owe so much of this work to you. Without question, I am the person I am today because of you. Thank you isn't enough. I love all of you.

To my friends, Kailey, Victoria, Lindsay, and Alex. Five years ago we all were strangers, exchanging nervous smiles as we entered into our first entrance exam, first luncheon, or first graduate class. It's difficult to picture this journey without the input and support from all of you through the years. Thank you for the joy, wisdom, and humor you each have uniquely provided in my life. I'm excited to see where the future takes all of you.

And lastly, my fiancé, Steve. It's hard to imagine this all started over a dinner seating at a conference in Canada. You've been by my side during some of the most difficult times in my life, and I'm forever grateful for all of your support. Thank you for the laughs, the goofy smiles, the unwavering support, and the endless love. The future is always bright when you have your best friend at your side, and I can't wait to see what it holds for us. I love you.

Dedicated to my amazing family.
Their love and support made all of this possible.

Abstract

Significant work has been done studying the metabolism of adipose tissue in recent years, in an effort to more effectively combat the obesity epidemic. Adipose tissue has been found to participate in the metabolism signaling network, with BCAAs playing a vital role as messengers relating the amino acid content of high protein meals. BCAA plasma levels have also been found to be elevated in individuals with obesity or type 2 diabetes, with their increased levels often occurring prior to elevated resting glucose levels and insulin resistance. Their dynamics under various metabolic conditions must still be examined however, on a metabolically relevant time scale. Current methods are limited in their time response for *in vivo* studies, with time-points ranging from minutes to hours. Metabolic dynamics must be studied in near real time, in order to establish these bioamines as metabolic biomarkers.

In this work, an *in vivo* platform is developed for monitoring bioamine metabolism dynamics in adipose tissue and skeletal muscle with 22 second temporal resolution. A high-speed online microdialysis-CE assay, capable of detecting BCAAs and their related metabolites, is utilized to monitor dynamics in near real time. Inguinal adipose tissue and quadriceps skeletal muscle serve as the sampling locations in C57BL6 mice. A systemic stimulation of insulin demonstrated our assay's ability to detect induced metabolic dynamics. Stimulations of glucose, saccharin, and ace K provide further information regarding the metabolism of bioamines in adipose tissue.

Table of Contents

List of Figures

List of Abbreviations

β-ABA	β-Amino-n-Butyric-Acid
Ace K	Acesulfame K
aCSF	Artificial Cerebral Spinal Fluid
ADI	Acceptable Daily Intake
BAT	Brown Adipose Tissue
BCAA	Branched Chain Amino Acid
BCAT2	Branched Chain Aminotransferase
BCKDHC	Branched Chain Ketoacid Dehydrogenase Complex
CE	Capillary Electrophoresis
CZE	Capillary Zone Electrophoresis
DI	Deionized
DMEM	Dulbecco's Modified Eagle Medium
EC	Electrochemical
FBS	Fetal Bovine Serum
FDA	Fluorescein Diacetate
FITC	Fluorescein 5-Isothiocyanate
GABA	γ-Amino-n-Butyric-Acid
IACUC	Institutional Animal Care and Use Committee
KCl	Potassium Chloride
LC	Liquid Chromatography
LIF	Laser Induced Fluorescence

LOD	Limit of Detection
MD	Microdialysis
mEq	milli-Equivalent
MS	Mass Spectrometry
MWCO	Molecular Weight Cutoff
NBDF	4-Fluoro-7-Nitro-2,1,3-Benzoxadiazole
NDA	Naphthalene-2,3-Dicarboxyaldehyde
OPA	Opthalaldehyde
P/S	Penicillin/Streptomycin
PTFE	Polytetrafluorethylene
RAR	Research Animal Resources
RFU	Relative Fluorescence Units
SEC	Size Exclusion Chromatography
SOP	Standard Operating Procedure
SPF	Specific Pathogen Free
UCP1	Uncoupling Protein-1
UV	Ultra-Violet
WAT	White Adipose Tissue

Chapter 1

Introduction

1.1 The Obesity Epidemic

1.1.1 Obesity and Adipose Tissue

Obesity is a widely prevalent health epidemic in the United States, with nearly 70% of adults labeled as obese or overweight.[1,2] Obesity is generally defined as the unproportioned accumulation of adipose tissue resulting from an energy imbalance, where the energy intake of an individual is greater than the energy spent. Total energy expenditure is comprised of active energy and resting energy, the latter of which describes the thermic effect of metabolism.[3] Traditional methods of reducing energy intake through restricted diet and increasing total energy expenditure through physical activity have proven insufficient in effectively curbing this epidemic. Therefore current research has focused on more fully understanding this disease's development and mechanisms.

Brown adipose tissue (BAT), white adipose tissue (WAT), and beige adipose tissue are all found throughout the body.[4-6] BAT usually contains one large lipid vesicle and contains high amounts of mitochondria with uncoupling protein-1 (UCP1).[6] Its primary role is thermogenesis.[7] WAT contains multiple smaller lipid vesicles utilized as storage for excess triglycerides until needed for gluconeogenesis.[8,9] This was assumed to be WAT's sole responsibility, until recently it was discovered that it plays an active role in the signaling network with the brain, liver, muscle, and pancreas.[10-12] Participation in this signaling network to relay information regarding energy balance and appetite, suggests WAT should be classified as an endocrine organ.[13,14] Beige adipose tissue describes clusters of adipocytes which form in WAT, but have similar lipid droplet

conformation to BAT and contain UCP1. These clusters also have thermogenic capabilities.[6,15]

The accumulation of WAT during obesity is due to both an increase in the number of adipocytes present and their expansion. Size expansion of adipocytes is believed to aide in the progression of disease development.[16,17] Adverse health effects related to obesity include, but are not limited to, type 2 diabetes, hypertension, and heart disease.[18]

Adipocytes have been found to regulate several small molecules acting as messengers to relate energy functions throughout the body.[19] These small molecules, the branched chain amino acids (BCAAs) – leucine, isoleucine, and valine – are utilized by adipocytes for the citric acid cycle and lipogenesis.[19,20] Complete understanding of adipose tissue's role in the regulation of various small molecule messenger mechanisms could yield insight into potential dysregulation leading to the development of obesity.

1.1.2 Branched Chain Amino Acids

The BCAAs (Figure 1.1), promote metabolism due to a spike in their plasma levels following a high protein meal. The increase in plasma BCAA levels is due to the liver's poor ability to metabolize them as they pass through. Plasma BCAAs are then able to regulate insulin secretion from the pancreas,[21] protein synthesis and degradation in muscle,[12] and food uptake control in the brain.[11,20]

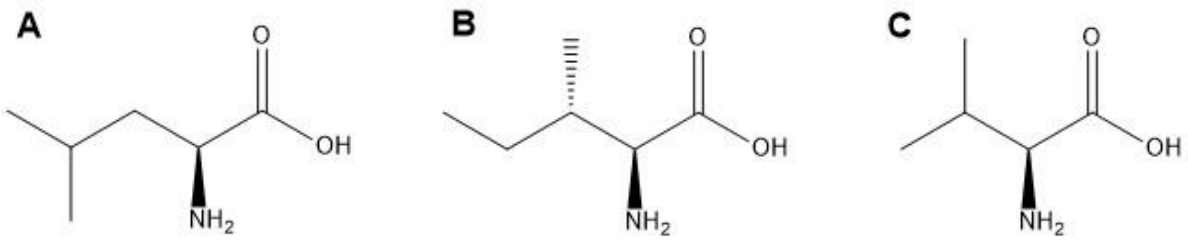

Figure 1.1. The branched chain amino acids: (A) leucine, (B) isoleucine, and (C) valine.

The first step in BCAA catabolism requires the enzyme mitochondrial branched chain aminotransferase (BCAT2), which is present only at very low levels in the liver.[22,23] This reversible transamination conversion yields α-ketoacids for each respective BCAA with a

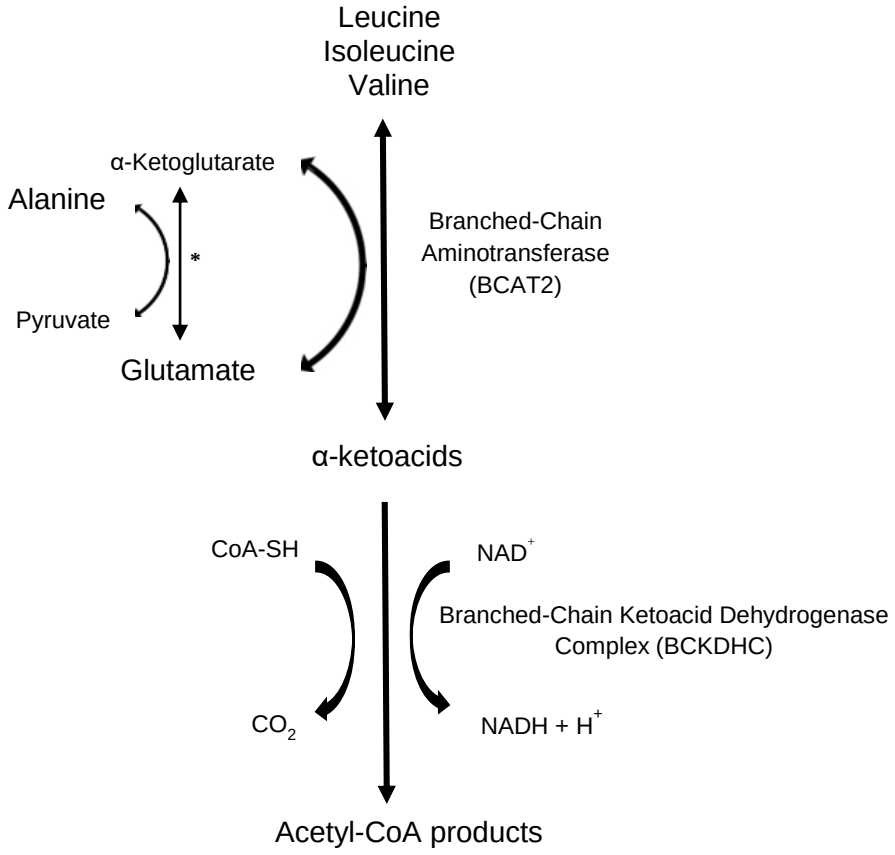

Figure 1.2. The BCAA catabolism cycle. Acetyl CoA products are utilized in the citric acid cycle, and downstream products of glutamate and alanine are also present. *Glutamate-pyruvate transaminase.

by-product of glutamate. These α-ketoacids then react with branched chain ketoacid dehydrogenase complex (BCKDHC) in an irreversible and rate limiting oxidative decarboxylation yielding acetyl-CoA products. Alanine is a by-product of the glutamate to α-ketoglutarate conversion.[24] The catabolism cycle has been shown to operate as a feedback loop, in which BCAAs themselves can act as inhibitors when an imbalance arises.[25]

Circulating levels of BCAAs have been found elevated in individuals affected by obesity or type 2 diabetes.[21,26-29] Upon weight loss, either naturally or by gastric bypass surgery, circulating levels returned to normal.[30] This confirmed the ability of adipose tissue to regulate these small molecule messengers.[30,31] Since elevated circulating BCAA levels often appear prior to elevated fasting glucose levels and insulin resistance, it has been determined these are one of the best predictors for metabolic disorders, including diabetes.[21,28]

1.1.3 Adipose Tissue Research Models

The prevalence of obesity has prompted both *in vitro* and *in vivo* analysis of adipose tissue. *In vitro* models most commonly use 3T3-L1 or 3T3-F422A cell lines.[32,33] Both cells lines originate from a 3T3 mouse, and then are differentiated to adipocytes under specified conditions.[34-37] While *in vitro* analysis avoids the complexities of an *in vivo* model, it does not allow for interworking bodily systems to be assessed. Within the human body, especially in regards to metabolism and metabolic dysregulation, adipose tissue does not function in isolation. It is part of a vast signaling network,[13,14] and to best replicate this scenario for analysis, *in vivo* models must be employed. Several rodent

models, along with human studies, have been utilized for obesity research.[38,39] Tissues are frequently excised and examined *ex vivo*,[40] however this does not allow for dynamic changes to be monitored. C57BL6 mice are commonly studied in obesity research due to the progression of their metabolic dysregulation mimicking that of humans.[41] Therefore, this model is an ideal choice for investigating dynamic changes occurring within metabolism.

1.2 Microdialysis Sampling

1.2.1 Probe Design and Function

Microdialysis probes are one of the preferred sampling techniques for *in vivo* studies due to minimal tissue disturbances at the tissue or organ of interest.[42,43] As shown in Figure 1.3, microdialysis probes of side-by-side geometry are constructed by inserting two narrow bore fused-silica capillaries into a hollow fiber semipermeable dialysis membrane.[42-44] The two capillaries, acting as inlet and outlet channels, are offset to create a sampling region. Sampling regions typically range from 3-10 mm in length, for use in *in vivo* versus *in vitro* studies respectively.[45-48] Perfusate, the solution pumped through the inlet channel, is chosen to mimic the composition of the external matrix surrounding

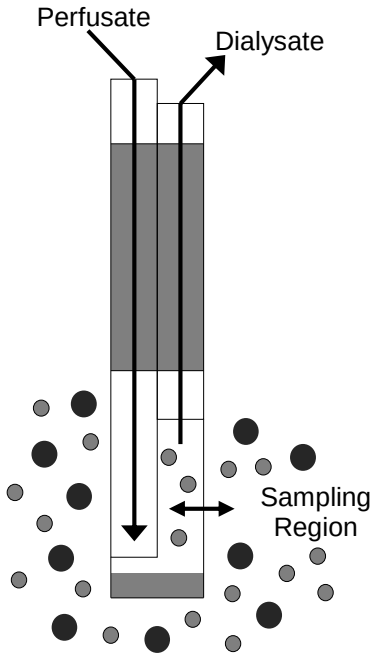

Figure 1.3. Schematic of a microdialysis probe with side-by-side geometry.

the probe in both pH and ionic composition. Matching the composition of the perfusate with the surrounding matrix allows analytes of interest to diffuse across the dialysis membrane due to a concentration gradient. Solution containing the sampled analytes, termed the dialysate, is then carried out through the outlet channel.[43,49]

Initial microdialysis probes were designed primarily for use in neuroscience research, consisting of a dialysis membrane located at the end of a rigid spherical cannula.[50] The rigid cannula was fashioned to be implanted through a guide cannula, which was screwed to the skull to hold the dialysis membrane securely in place (Figure 1.4A). This style functioned well for neuroscience experiments, however the rigidity was disadvantageous when working with other soft tissues. Furthermore, awake experiments ran the risk of puncturing the surrounding tissue with the rigid cannula. To address these concerns, a flexible cannula design was fashioned for intravenous sampling (Figure 1.4B).[51-53] The flexible design allowed the probe to be inserted away from any interfering movements of an awake animal and decreased the chances of puncturing blood vessel walls.

While the flexible probe design was successfully implemented for intravenous studies, it still damaged other soft tissues.[43] Linear probes were developed and successfully utilized in tumor tissue,[1,54,55] muscle,[54,56] liver,[57-59] and dermis[60-62] experiments (Figure 1.4C). The primary advantage of the developed design was the direct contact between the dialysis membrane and soft tissue, allowing for close proximity diffusion of analytes.

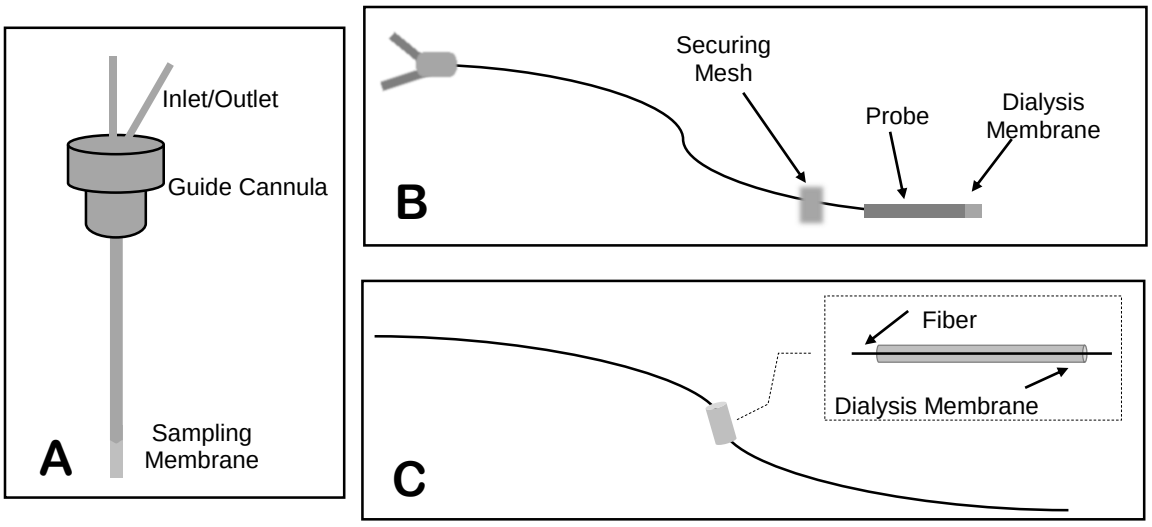

Figure 1.4. Schematic of various microdialysis probe designs. (A) A rigid cannula design inside a guide cannula, (B) an intravenous sampling dialysis probe, and (C) a linear probe intended for sampling of soft peripheral tissues.

All microdialysis probe designs serve as a continuous sampling technique with no net loss of surrounding extracellular fluid. The semipermeable dialysis tubing allows for diffusion of small molecules, with a specific molecular weight cutoff (MWCO) that can be selected based on the expected biological matrix.[63] In this way, microdialysis sampling enables continuous monitoring of biological phenomena in various tissues, while acting as a purification step to prevent large molecules from being collected.

1.2.2 Recovery and Resolution

One of the fundamental limitations of microdialysis sampling is that equilibrium is never established across the membrane, and thus the recovered concentration in the dialysate is a fraction of the concentration in the extracellular matrix.[49] Even at typical flow rates between 0.1-1.0 µL/min, equilibrium is still not reached, leading to an inability to acquire absolute quantification.[64] The description of collected analyte in the dialysate

can be defined as either absolute or relative recovery. Absolute recovery is the total amount of analyte that is collected in the perfusion medium, per rate of time. Relative recovery is the amount of analyte that is collected in perfusion medium relative to the amount of analyte present in the extracellular matrix.[49] Perfusion rates dramatically effect both recoveries, with decreased flow rates into the probe yielding increased relative recovery and decreased absolute recovery, as shown in Figure 1.5.[63,65,66]

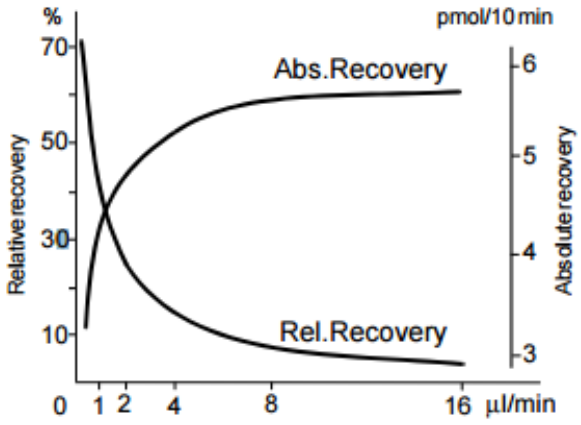

Figure 1.5. The absolute and relative recoveries as a function of flow rate from a microdialysis probe. Adapted from Ref. 63.

A mathematical representation of relative recovery as a function of various experimental parameters is defined as:

$$RR = \frac{C_d}{C_e} = 1 - e^{\frac{1}{Q_d(R_d + R_m + R_e)}} \quad (1.1)$$

Bungay *et al.* defined relative recovery, the fraction of analyte concentration in the dialysate (C_d) compared to the analyte concentration in the extracellular matrix (C_e), in terms of perfusion flow rate (Q_d) and resistance to solute movement in the dialysate, through the probe membrane, and in the tissue/solution (R_d, R_m, and R_e, respectively).[67]

Solute movement in the dialysate and through the probe membrane depends on factors such as flow properties of the dialysate through the probe membrane, diffusion coefficient of analyte through membrane, chemical interactions occurring between the probe membrane and analyte, analyte diffusion in the membrane, and the probe membrane's length, radius, and material.[68,69] Analyte movement in the tissue is dependent on the diffusion through the extracellular matrix to the probe.[68,70]

The relative recovery of the microdialysis probe must be calculated to relate the collected concentration of analyte back to the actual extracellular concentration. When undergoing *in vitro* studies, probe calibration can proceed by creating calibration curves from known concentrations of solution with a microdialysis probe and comparing these signals to those obtained through direct injection of identical concentrations.[71-73] Due to the fact that *in vivo* recoveries are typically less than *in vitro* results, *in vitro* probe calibration does not accurately predict *in vivo* results.[74,75] *In vivo* recoveries are subject to the influences of uptake/release mechanisms during an analyte's diffusion to the probe, as well as a more tortuous path of diffusion through tissue and extracellular space.[76]

Many *in vivo* calibration techniques have been employed such as retrodialysis, no-net-flux, and perfusion flow rate (also known as "zero flow rate"). Retrodialysis involves adding an internal standard to the perfusion solution, and the amount of internal standard delivered through the microdialysis probe to the tissue is assumed to be equivalent to the analyte of interest's diffusion efficiency into the dialysate.[77,78] No-net-flux determines the diffusion of analyte into the dialysate as a function of perfusate solution concentrations.[79,80] Zero flow rate monitors the concentration of analyte in the dialysate as a function of perfusion flow rate. Using a nonlinear regression, the concentrations of

the extracellular matrix can then be approximated.[66,75,81] Probe calibration is a laborious process and for most *in vivo* experiments, the relative recovery may not be accurately predicted. Relative changes are most often assessed for *in vivo* microdialysis sampling, thus negating the need for absolute concentrations.[43]

Complications often encountered with microdialysis sampling include limitations on the spatial and temporal resolutions achieved. The potential for surrounding tissue damage due to probe implantation causes spatial resolution to be an important consideration *in vivo*. Spatial resolution is also negatively impacted *in vivo* when probes are operated at higher flow rates, usually to improve absolute recovery, causing an increased concentration gradient extending outwards from the probe's location. The probe's sampling region is also limited to ~1-5 mm *in vivo*, further affecting spatial resolution.[74,82]

Temporal resolution is defined as the smallest amount of time it takes an analytical system to detect changes in analyte concentrations. This is determined by the microdialysis probe flow rates as well as the parameters of the analytical system.[64] To increase the efficiency of probe sampling, a slower perfusion rate is utilized, which results in longer sampling times. These longer sampling times decrease temporal resolution. When the dynamics being investigated occur on a slower timescale than probe sampling and instrument analysis time, the temporal resolution is simply the time required for signal intensity to increase from 10-90%, also known as the rise time.[63] Optimization between sample volume requirements, perfusion rate, and detection limits determines the temporal resolution attained.[64]

1.2.3 Coupling Microdialysis to an Analytical System

Despite their limitations, microdialysis probes remain heavily utilized as a sampling technique. Through offline and online analysis, analytical systems such as liquid chromatography (LC),[83-86] capillary electrophoresis (CE),[71,74,87,88] microchip electrophoresis,[89,90] mass spectrometry (MS),[91,92] and biosensors[93,94] have been coupled to microdialysis sampling, just to name a few. Microdialysis sampling is a continuous sampling technique while analytical systems typically require discrete samples for analysis, which pairs well for offline fraction collection. Offline fraction collection utilizes microdialysis to collect aliquots of sample, which are then subsequently run on an analytical system. This method is limited in its time response, as enough sample aliquot must be collected for the selected analytical system's volume requirements, as well as the potential for errors when handling such small volumes. Online analysis is highly desirable however, due to microdialysis sampling requiring no purification step prior to introduction onto an analytical system. An injection interface had to be designed to convert continuous dialysate flow from the probe into discrete sample plugs suitable for analysis on an analytical system.

Jorgenson and Lemmo utilized a flow-gate interface in the early 1990's to couple size exclusion chromatography (SEC) with capillary zone electrophoresis (CZE).[74,95] Lada and Kennedy adapted this design for use in microdialysis and CZE.[74] Two steel plates were separated by 75 µm of polytetrafluorethylene (PTFE), or Teflon. An inlet and outlet channel were incorporated into the PTFE for CE buffer, which ran perpendicular to channels positioned for the microdialysis probe outlet and CE separation capillary inlet. While CE buffer was flowing, dialysate samples were carried away and not injected onto

the separation capillary. To make an injection, voltage and buffer flow was stopped to allow sample volume to accumulate by the separation capillary inlet. Application of voltage then injected the dialysate sample. This interface yielded good temporal resolution, however it suffered from lack of reproducibility.[64]

Jorgenson and Hooker developed a new flow-gate interface using polycarbonate polymer for micro-HPLC and CZE.[96] As shown in Figure 1.6, the clear polymer allowed for easy visualization of capillary alignment, making construction much more reproducible. It's utilization in coupling microdialysis to high-speed analysis, especially CE,[97-99] led to slight modifications in construction materials. A Plexiglas block with solenoid valve[98] and a pneumatically actuated valve with polycarbonate[48] or acrylic[44] flow-gate interfaces have all been reported. In each of these designs, the reaction capillary, carrying the dialysate sample, and CE separation capillary are set 30-50 µm apart. Separation buffer is then pumped across the flow gate perpendicular to the fixed capillary positions to prevent dialysate from entering the inlet of the separation capillary. To inject a sample volume, flow of buffer is stopped using the valve and dialysate is allowed to accumulate in the gap between capillaries. After a delay, voltage is applied to the outlet of the separation capillary to pull the sample plug down into the capillary to begin separation. Buffer flow is then resumed to prevent any additional sample from entering the separation capillary.

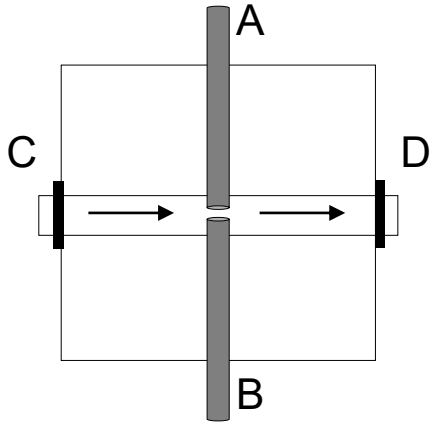

Figure 1.6. Schematic of the flow gate designed by Jorgenson and Hooker. The reaction capillary (A) and separation capillary (B) are spaced ~50 µm apart, with buffer flowing perpendicularly across the channel (C-D).

Online coupling of microdialysis probes to analytical system, due to the development of flow-gated interfaces, allows for more near real time analysis of events, which is highly advantageous when studying biological phenomena.[100] Temporal resolution of the overall system is now limited by the mass sensitivity, volume requirements, and analysis time of the instrument. When coupled with microdialysis sampling, HPLC's femtomolar limits of detection (LODs) result in 5-30 minute sampling times. CE's mass sensitivity and small volume requirements, attomolar LODs[88] and 1-10 nL of injected sample,[64] allow for temporal resolutions on the order of 10-30 seconds.[45,47,101] As low as a 5 second temporal resolution has been reported by Lada and Kennedy.[97]

The implementation of flow-gated interfaces have allowed for the online coupling of microdialysis sampling to an analytical system by converting continuous dialysate flow into discrete samples. The mass sensitivity and small volume requirements make CE an advantageous coupling for this sampling technique, while high-speed CE's fast analysis times yield temporal resolutions on the timescales of seconds. This is a clear advantage for the near real time analysis of biological phenomena. The primary limitation of coupling microdialysis online to CE is the sensitivity required for the detection scheme as a result of the small volumes being analyzed.[102]

1.2.4 Analyte Derivatization and Detection

Several detection methods have been used in conjugation with microdialysis (MD)-CE including ultraviolet (UV),[103] electrochemical (EC),[104] and laser induced fluorescence (LIF)[105] detection. LIF provides the best mass sensitivity for coupling with

MD-CE,[106] however since most analytes in biochemical systems are not natively fluorescent, a derivatization scheme must be employed. Derivatization protocols focus on minimizing the limitations of labeling reactions such as the occurrence of fluorescent by-products and long derivatization times that delay recording a biological event in near real time.

Fluorescein-5-isothiocyanate (FITC),[107] naphthalene-2,3-dicarboxyaldehyde (NDA),[108] and opthalaldehyde (OPA)[44,98,109,110] have all been previously employed in MD-CE analysis. FITC's long reaction times made it an undesirable reaction scheme, particularly when conducting *in vivo* experiments.[48] NDA and OPA overcame reaction time limitations, with effective reactions in under 1 minute,[111] however their disadvantages made their repeated use in online MD-CE assays challenging. NDA required separate store from cyano ions due to interactions yielding cyanohydrin intermediates, which produce fluorescent degradation products[108] and OPA suffered from absorbance in the near UV[48], photo-bleaching, and instability.[112] Dr. Michael Bowser's lab sought to employ 4-fluoro-7-nitro-2,1,3-benzoxadiazole (NBDF) as a labeling reagent to overcome previously encountered limitations. Use of NBDF was investigated due to its labeling of primary and secondary amines, as well as its excitation wavelength being compatible with common 488 nm argon ion and diode-pumped solid state lasers.[48] Figure 1.7 demonstrates the reaction scheme of NBDF with primary and secondary amines.

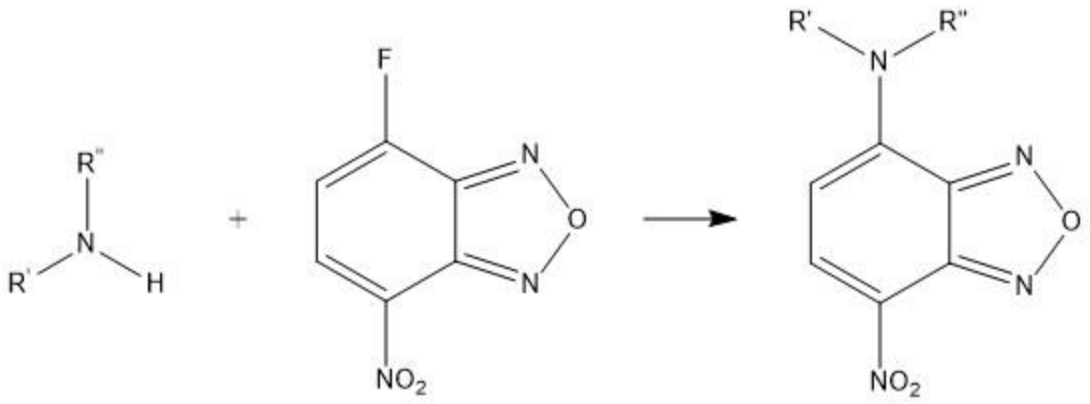

Figure 1.7. Derivatization reaction of NBDF with primary and secondary amines.

Although typical NBDF reaction times fluctuate around one hour at room temperature,[113] a complete reaction was achieved in 5 minutes by utilization of a water bath to heat the reaction capillary to 80 ºC during the online derivatization.[48] The primary limitation with the described derivatization scheme remains the hydrolysis by-product observed in CE-LIF separations.

In an effort to further increase the sensitivity of CE-LIF analysis, a sheath flow cuvette was introduced to the system. Buffer flows along the outside of the separation capillary as depicted in Figure 1.8. Streaming buffer pulls analytes into a laminar flow profile as they elute from the capillary.[114] Advantages of this system include no change in refractive index between the buffer and sample stream and reduced laser scatter, contributing to a reduced background and

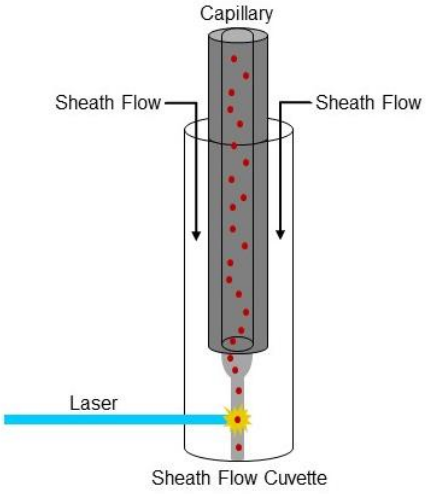

Figure 1.8. Schematic of a sheath flow cuvette design.

increased sensitivity. Sensitivity of the overall system was found to improve 15 fold through the implementation of a sheath flow cuvette.[98]

1.3 Scope of Thesis

The importance of adipose tissue and BCAAs in overall body metabolism and their potential use as biomarkers for metabolic dysregulation has only recently been realized. To elucidate their potential, their complete role in metabolism must be fully understood. Monitoring metabolism dynamics as they occur is the only way to comprehend the processes at play, however current research has been limited in its temporal resolution. In this work, we describe the development of an online MD-CE platform for the near real time analysis of BCAAs and their metabolites *in vivo.*

Chapter 2 describes the optimization of an online MD-CE assay for near real time monitoring of bioamines, particularly BCAAs and their metabolites. A temporal resolution of 22 seconds was able to be achieved, while still maintaining separation of leucine, isoleucine, and valine. An *in vivo* protocol for the sampling of adipose tissue and skeletal muscle was designed in Chapter 3. Parameters such as animal model, sampling locations, anesthetic regimes, surgical procedures, and euthanasia protocols were designed to allow for a variety of experiments to determine BCAAs' role in overall body metabolism. Chapter 4 presents the successful implantation of microdialysis probes in inguinal adipose tissue and quadriceps skeletal muscle. The amino acid signature and its reproducibility for each tissue is established. Chapter 5 describes the initial stimulation experiments in adipose tissue and skeletal muscle, utilizing both glucose and artificial

sweeteners. A summary of completed work and potential opportunities for future direction of the developed platform are outlined in Chapter 6.

Chapter 2

Characterization of Microdialysis – Capillary Electrophoresis Assay

Sections adapted from:

"Weisenberger, M.M and Bowser, M.T. *Anal. Chem.* **2017**, *89* (1), 1009-1014."

Reproduced with permission

2.1 Summary

In this work, a high-speed CE instrument coupled with online microdialysis sampling was optimized to yield the fastest temporal response possible while still providing separation of BCAAs and related metabolites. Parameters such as separation assay performance, reproducibility, LODs, temporal resolution, and relative recovery were assessed to ensure the assay's suitability for *in vivo* experimentation. The separation assay was able to separate and detect all bioamines of interest, with reproducibility established over time periods anticipated for *in vivo* studies. LODs were estimated to be 1.7 µM for glutamate, 1.3 µM for isoleucine, 2.5 µM for leucine, 690 nM for valine, 2.7 µM for taurine, and 6.5 µM for glutamine. Previous studies reported plasma BCAA levels to be significantly higher than the determined LODs in both mice and human subjects, therefore the separation assay was deemed sufficient for *in vivo* analysis. A 22 second temporal response was achieved for the system, a significant improvement over previous studies utilizing the current separation assay. This improvement allows for near real time analysis of dynamic changes occurring in *in vivo* amino acid metabolism. Microdialysis probe recovery was determined to be 16% for leucine, 18% for valine, 17% for alanine, 18% for taurine, and 14% for glutamate. Although the relative recovery percentages were not optimal, this only presents a challenge if amino acids are unable to be detected in biological dialysate. Given such high concentrations are expected in various tissues, it was decided to proceed with *in vivo* experiments with the current probe design, continuing optimization later on if recovery proved insufficient.

2.2 Introduction

Microdialysis sampling is the preferred sampling technique for *in vivo* measurements due to the small probe size yielding minimal disturbances to surrounding tissues, continuous monitoring of multiple analytes, and no net loss of surrounding fluid.[42,43] Microdialysis has been widely employed in neuroscience and pharmacological studies.[115] Coupling microdialysis probes to an online analytical technique greatly improves the temporal resolution of the assay.[49] Microdialysis sampling produces low mass recovery due to the small sample volumes involved,[64] and therefore high-speed CE is an excellent analytical separation method for online analysis due to its fast analysis time,[71,116] low volume requirements and high mass sensitivity.[64]

Online coupling of a microdialysis probe to an analytical system is possible due to the MWCO of the dialysis membrane acting as a purification step.[117] Direct coupling of microdialysis probes with high speed CE has been shown previously.[71,74,88] Microdialysis probes are constructed in-house using a side-by-side geometry as previously reported.[101] Sampling regions of probes varied from 3 mm to 1 cm in length, depending on use for *in vivo* versus *in vitro* applications. Bioamine derivatization has been optimized to produce a 5 minute reaction time with NBDF by heating portions of the reaction capillary.[48] High speed CE with online microdialysis sampling has been reported to achieve separations in under 5 seconds.[97] This online technique has been adapted to analyze various neurotransmitters in *in vivo* systems,[48,118] as well as online analysis of an astrocyte *in vitro* model.[45]

Microdialysis has been reported in tissues such as the dermis,[60,62] tumors,[1] muscle,[56] liver,[57,58] as well as intravenous sampling.[51,52] It has also been used to measure analytes such as inflammatory proteins,[119] glucose,[120] and pyruvate and lactate[121] in adipose tissue, but time points were only collected on the timescale of minutes to hours. A separation assay utilizing α-cyclodextrin was developed and optimized for the *in vitro* analysis of adipocytes.[122] BCAAs were resolved and their dynamics were analyzed as adipocytes were stimulated with glucose, insulin, and artificial sweeteners. This analysis however, was performed offline and had a temporal response of 60 – 90 seconds.

With the intention to implement this separation assay in an online analysis of BCAAs and their related metabolites from adipose tissue and skeletal muscle, instrumental parameters had to be examined to test this assay's suitability for *in vivo* studies. Near real time dynamic information regarding these bioamines is desired, and thus the temporal response of the system must be drastically improved. Optimization proceeded to improve the temporal resolution of the assay, sacrificing resolution where possible. The MD-CE assay was transitioned into an online analysis tool, optimized for separations under 20 seconds in adipose tissue and skeletal muscle.

2.3 Materials and Methods

2.3.1 Chemicals and Reagents

Chemicals. All amino acid standards were purchased from Sigma Aldrich (St. Louis, MO). D-glucose was purchased from Gibco (Life Technologies Corp., Grand Island, NY) and sodium tetraborate decahydrate was purchased from CHEM-IMPEX Int'l Inc. (Wood Dale, IL).

Buffers and Solutions. All solutions were prepared in deionized (DI) water (Milli-Q, 18.2 MΩ; Millipore, Bedford, MA) and filtered (0.22 μm). Ringer's solution was prepared with NaCl (123 mM), $CaCl_2$ (1.53 mM), KCl (4.96 mM) and 5 mM glucose with pH adjusted to 7.5. Artificial cerebral spinal fluid (aCSF) was comprised of NaCl (145 mM), KCl (2.7 mM), $MgSO_4$ (1.0 mM) and $CaCl_2$ (1.2 mM). The conditioning of microdialysis probes is the only instance in which aCSF was used during experimentation. Sheath flow buffer was comprised of 90 mM borate adjusted to pH 10 and CE separation buffer contained 90 mM borate/35 mM α-cyclodextrin (food grade, lot 010760F206, Cyclodextrin Technologies Development Inc., Alachua, FL) adjusted to pH 10. Derivatization solution was prepared by dissolving 40 mM NBDF (TCI America, Portland, OR) in methanol and mixing 1:1 with 500 μM HCl, producing a final concentration of 20 mM NBDF/250 μM HCl in 50% methanol. Derivatization solution was prepared daily and degassed under vacuum for 2 minutes prior to use.

2.3.2 Microdialysis

Microdialysis probes were constructed in-house using a side-by-side geometry as previously reported[101] (see Figure 2.1). Two 40 µm i.d. × 105 µm o.d. fused silica capillaries (Polymicro Technologies, Phoenix, AZ) were inserted into a 200 µm diameter hollow fiber, regenerated cellulose dialysis membrane (13 kD MWCO, Spectrum Laboratories, Rancho Dominquez, CA) and off-set by 3 mm to generate a sampling region. Capillaries were sealed in place using polyimide resin (Alltech, Deerfield, IL). Prior to use probes were conditioned with ethanol (55 µL/h for 25 minutes) followed by aCSF (55 µL/h for 25 minutes). During analysis probes were perfused with Ringer's solution at 25 µL/h.

2.3.3 Online CE-LIF Instrumentation

Online Derivatization. Dialysate was transferred to a 250 µm i.d. stainless steel cross (Valco Instruments Co. Inc., Houston, TX) in a 40 µm i.d. × 360 µm o.d. fused silica capillary (see Figure 2.1). Borate buffer and derivatization solution were introduced at the reaction cross at 5 µL/h each. The derivatization reaction proceeded through a 90 cm long, 75 µm i.d. × 360 µm o.d. fused silica capillary, of which a 66 cm portion was heated to 80 ºC, by running the capillary through flexible tubing containing water from a heating bath (NESLAB EX-7 Digital One heating bath circulator, Thermo, Newington, NH). Capillary dimensions and all flow rates produced a reaction time of 5 minutes.

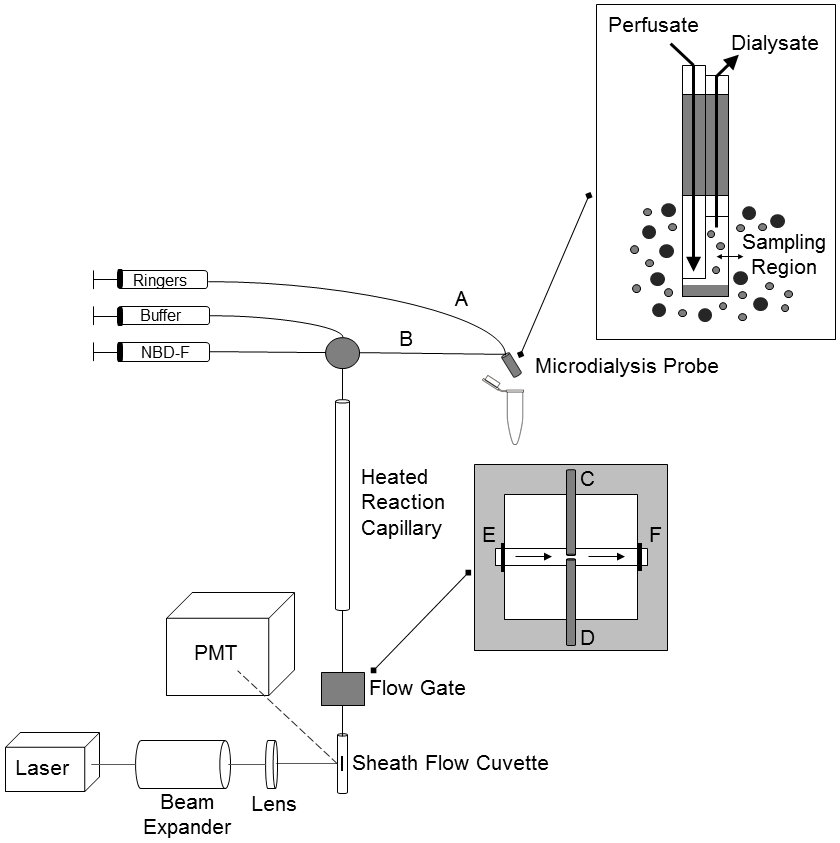

Figure 2.1. Schematic of the high-speed online MD-CE-LIF instrument. Probes are placed into an Eppendorf tube containing amino acid standards, and then perfused with Ringer's solution (A). Perfusate (B) mixes with borate buffer and NBDF through a heated reaction capillary prior to injection onto the CE separation capillary. A flow gated interface allows for the reaction capillary (C) and separation capillary (D) to be coaxially aligned across the separation buffer channel (E-F).

High-Speed CE. Discrete sample plugs from the reaction capillary were injected onto a 6.2-6.5 cm long, fused silica CE separation capillary (5 μm i.d. × 360 μm o.d.) using a flow gated interface.[96] The separation and reaction capillaries were coaxially

aligned leaving an approximately 50 μm gap in-between. Separation buffer was pumped through this spacing at 40 mL/h using a syringe pump (Pump 22 syringe pump, Harvard Apparatus, Holliston, MA). To perform an injection, buffer flow was stopped for 750 ms using a pneumatically actuated valve (C2-3000A 10 port valve, Valco Instruments Co. Inc., Houston, TX) controlled by an in-house developed LabView program. Following this delay, -19 to -21 kV of injection voltage was applied at the outlet of the separation capillary for 100 ms. Buffer crossflow was then resumed as the potential was increased to the separation voltage (-21 to -23 kV) over a period of 500 ms.

Detection Scheme. Laser-induced fluorescence (LIF) detection was performed using the 488 nm line of a 60 mW diode pumped solid-state laser (Coherent, Santa Clara, CA). The laser beam was expanded using a 10× beam expander (Edmund Optics Inc., Barrington, NJ) and focused directly beneath the outlet of the separation capillary, in a sheath flow cuvette,[123] using a 1× lens. A 60×, 0.7 NA long working distance objective (Universe Kogaku, Oyster Bay, NY) collected fluorescence at 90º. Collected emission was passed through spatial (~1 mm) and bandpass filters (543.5 ± 10 nm) and detected using a photomultiplier tube (PMT R1477, Hamamatsu Corp., Bridgewater, NJ). Current was filtered with a 10 ms rise time, amplified (Keithley Instruments Inc., Cleveland, OH) and recorded using a data acquisition card (National Instruments Corp., Austin, TX). Data was analyzed using Cutter Analysis 7.0.[124]

2.4 Results and Discussion

2.4.1 Separation of Standards

Prior to *in vivo* experiments, the performance of all instrumental components and the separation assay must be assessed. It is imperative that all analytes of interest be identified and separated reproducibly in standard solutions. A twenty four amino acid mixture was run on the MD-CE instrument to identify analytes and determine reproducibility. Addition of 35 mM α-cyclodextrin to the separation buffer (90 mM borate, pH = 10) aided in the separation of amine analytes.[122] As shown in Figure 2.2, fifteen amino acids were able to be separated and identified.

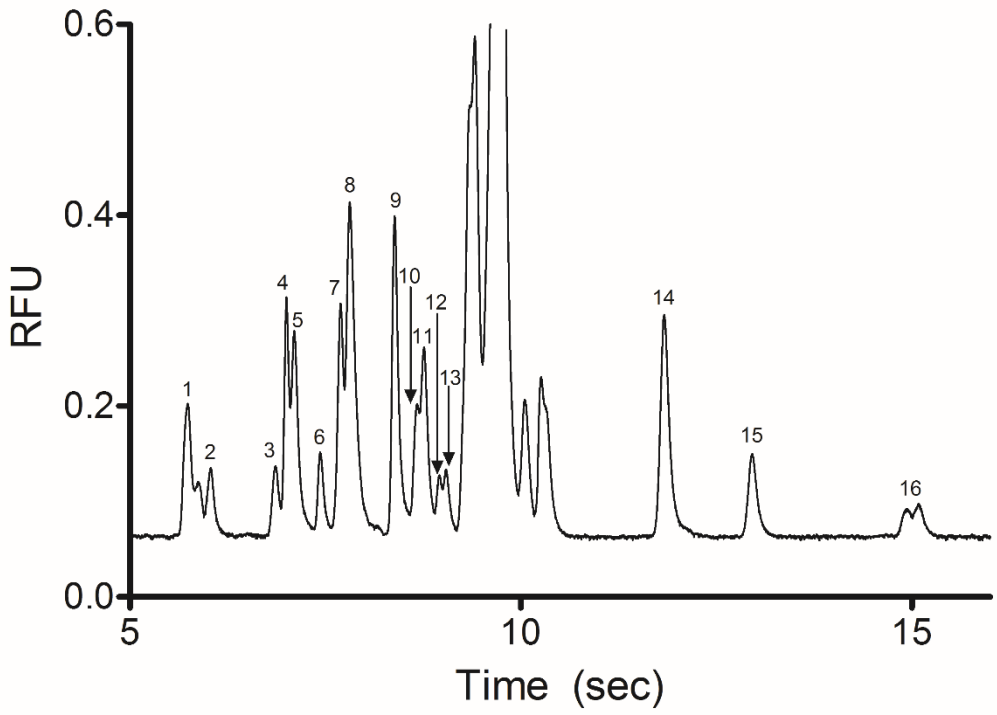

Figure 2.2. Online MD-CE analysis of small molecule amine standards in under 20 seconds. Peaks of interest were resolved from other analytes in the separation and identified as (1) arginine, (2) lysine, (3) lysine, (4) isoleucine, (5) leucine, (6) methionine, (7) phenylalanine, (8) valine, (9) GABA, (10) glutamine, (11) alanine, (12) DL-β-amino-n-butyric-acid (β-ABA), (13) glycine, (14) taurine, (15) glutamate and (16) D/L aspartate.

The separated standard mixture contained twenty four acids: D/L serine, L alanine, L tyrosine, L tryptophan, D asparagine, L arginine, L histidine, D/L aspartic acid, L leucine, D/L-β-amino-n-butyric-acid (β-ABA), L methionine, L glutamic acid, L valine, L cysteine, β alanine, L isoleucine, glycine, L glutamine, L phenylalanine, L citrulle, L threonine, taurine, γ-amino-n-butyric-acid (GABA), and L lysine. As shown above, sixteen peaks corresponding to fifteen different amino acids, were able to be identified in the separation window. The remaining amino acids were assumed to co-elute with the NBD-OH peak. This conclusion was reached after each amino acid was tested individually to determine migration times. NBD-OH is a byproduct of the NBDF derivatization reaction, which is currently unable to be eliminated. Adjustments to pH and borate concentration can be used to shift the NBD-OH peak in the electropherogram, to minimally interfere with analytes of interest. All amino acids of interest, BCAAs and downstream metabolites (alanine, glutamate, and glutamine), are able to be separated and identified with the described separation assay, and therefore the location of the NBD-OH peak was suitable for further experimentation.

Reproducibility of the separation is imperative for a lengthy period of time, as *in vivo* experiments are expected to proceed longer than one hour. Figure 2.3 displays full amino acid standard separations, with overlaid electropherograms collected at various time points during an hour long experiment. As shown, all fifteen amino acids are present with the same signal intensity and no peak drifting for the entire length of time. Therefore the separation was deemed reproducible.

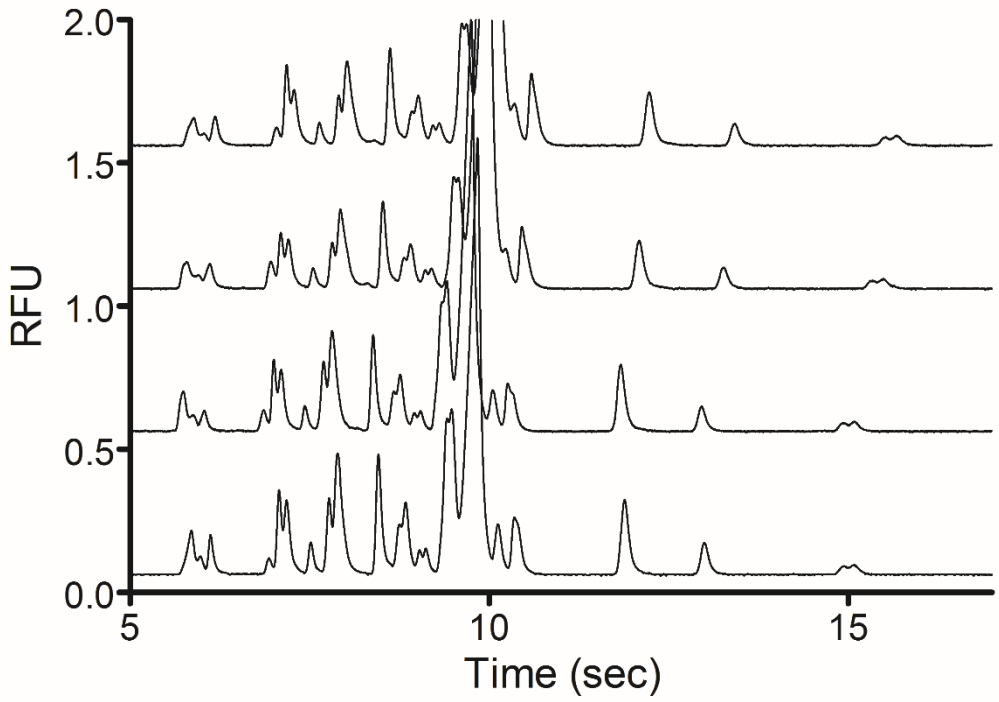

Figure 2.3. Overlaid electropherograms from a twenty four amino acid standard separation. Reproducibility of separation was able to be verified for an hour of instrument operation.

All amino acids were separated in under 15 seconds, a dramatic improvement in the resolution of the same separation assay in an offline MD-CE system. Improving the speed of separations was critical in this online MD-CE instrumentation, as it determined the temporal resolution of the assay. A modest reduction in the resolution of several amino acids occurred due to this temporal response decrease, however all analytes of interest can still be identified and separated from one another. This improvement in analysis time will be significantly beneficial for future dynamic *in vivo* experiments. A theoretical plate count was calculated to be 51,000 for this instrument.

2.4.2 Limits of Detection

It is crucial that the online MD-CE assay be capable of detecting biological concentrations of amino acids present in adipose tissue and skeletal muscle. Blomstrand et al. monitored the effects of amino acid supplements and exercise on plasma BCAA levels. Isoleucine levels ranged from 77 to 90 µM, leucine levels ranged from 150 to 188 µM, and valine spanned 298 to 330 µM.[125] Marchianti et al. examined plasma concentrations of amino acids in wild type and db mice, an animal model for type 2 diabetes. Isoleucine concentrations ranged from 74 to 219 µM, depending on experimental conditions. Leucine concentrations ranged from 109 to 349 µM and valine concentrations spanned 213 to 508 µM.[126] The LODs for the described assay were determined by 3 standard deviations above baseline noise. These LODs represent the concentration of analytes outside the microdialysis probe, prior to the labeling reaction. LODs for the online MD-CE assay were estimated to be 1.7 µM for glutamate, 1.3 µM for isoleucine, 2.5 µM for leucine, 690 nM for valine, 2.7 µM for taurine, and 6.5 µM for glutamine. Low concentrations of amino acids were measured in order to confirm the system's ability to detect small amounts of analyte. As demonstrated in Figure 2.4, concentrations as low as 5 µM are easily distinguished from baseline. In conjunction with the plasma concentrations of BCAAs from Marchianti and Blomstrand, this suggests that detection of BCAAs in adipose tissue and skeletal muscle using this assay will not be an issue.

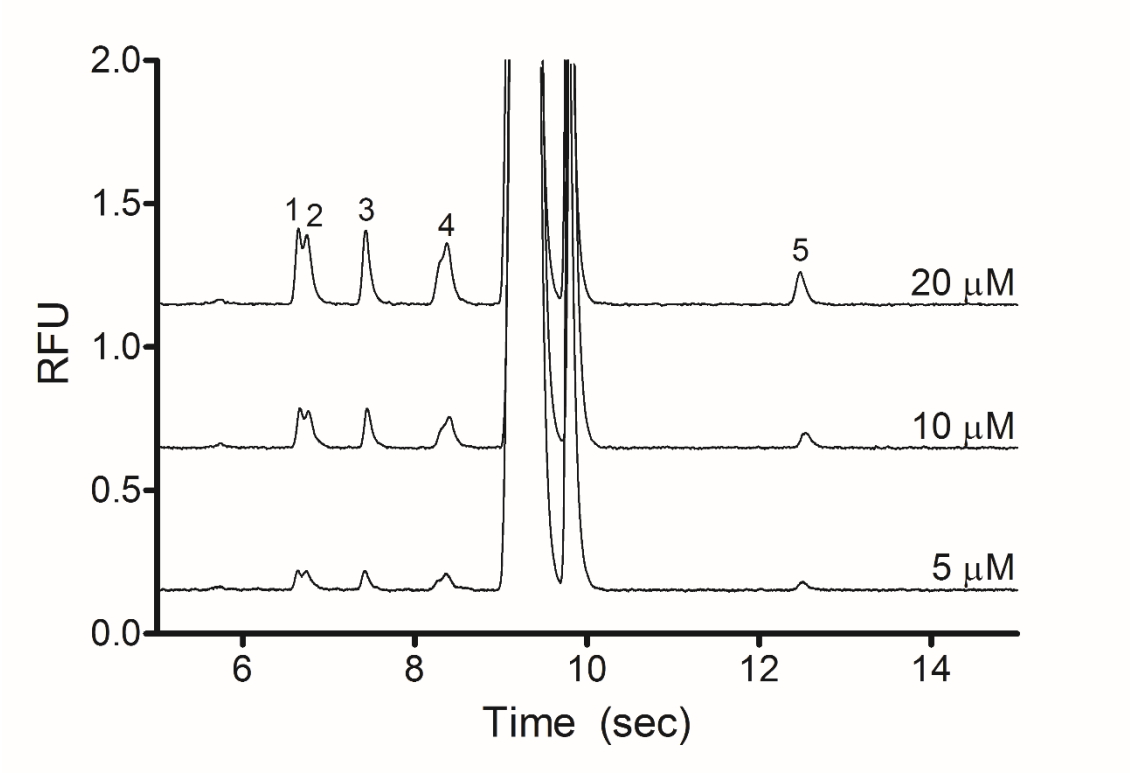

Figure 2.4. LOD studies using the online MD-CE system. Electropherograms from BCAA standards of varying concentrations. Peaks identified as (1) isoleucine, (2) leucine, (3) valine, (4) glutamine/alanine and (5) glutamate.

2.4.3 Temporal Resolution

Stimuli will be administered to adipose tissue and skeletal muscle *in vivo* with the goal to monitor changing amino acid levels. The temporal response of the assay must be as close to near real time as possible, in order to observe these changes as they are occurring. In order to assess the temporal response of the MD-CE assay, standards of varying leucine concentration were prepared. The microdialysis probe was transferred to a leucine standard for five minutes, then transferred to a blank Ringer's solution for three minutes, to a different leucine concentration for another five minutes, and then back to

blank Ringer's solution. This process was repeated for all concentrations of leucine standard, as shown in Figure 2.5.

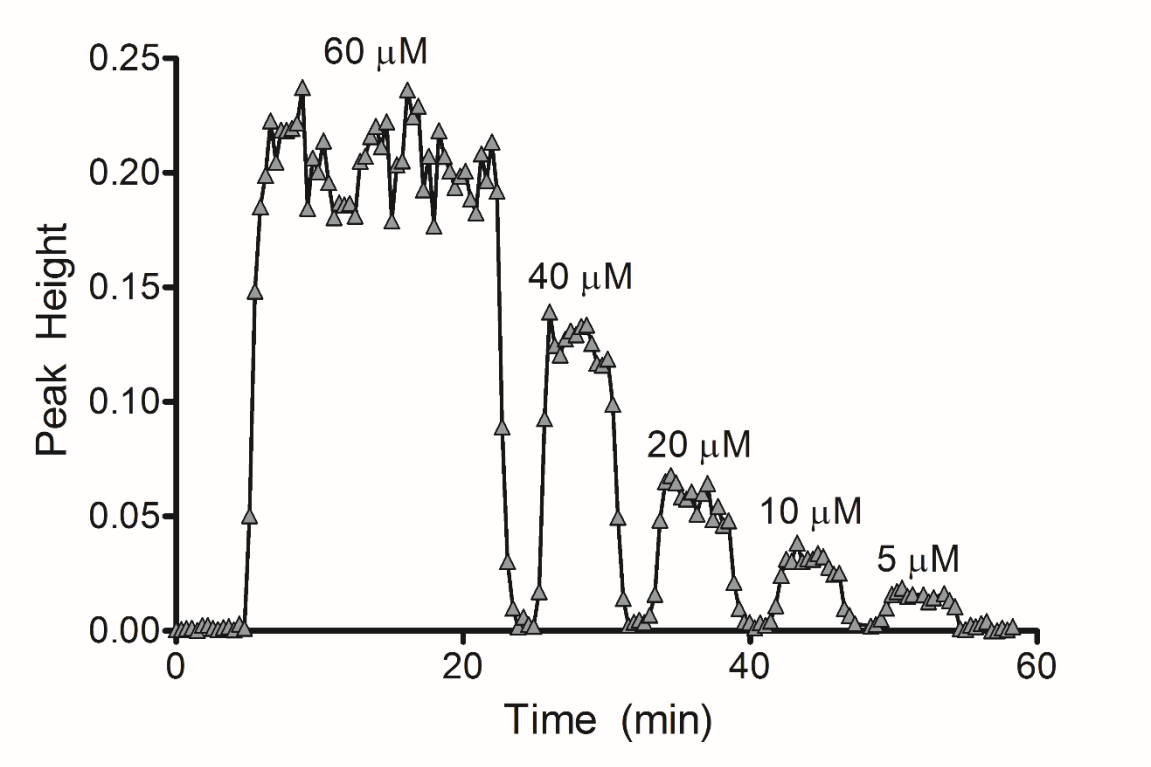

Figure 2.5. The temporal response of the online MD-CE assay. Probes were transferred from solutions of different concentrations of leucine, being placed in a solution of Ringer's (blank) in between each transfer. A full signal is achieved within 1-2 separations, yielding a temporal response of 22 seconds.

As demonstrated above, the signal for leucine plateaued within 1-2 separations, indicating a 22 second temporal resolution is achieved. Separation time is 20 seconds for each run, however factors such as injection and delay time also contribute to the overall temporal response of the system. A 22 second temporal resolution is a significant improvement over the 60-90 second temporal resolution of the previous offline MD-CE assay for BCAAs.[122] Hence, the modest sacrifice in resolution of amino acids serves to transform the MD-CE assay into a near real time method. The run to run reproducibility

was 8%, as determined by relative standard deviation. Analogous to LOD calculations, biological changes greater than 24% (i.e. 3 × rsd) can be observed with statistical significance.

2.4.4 Microdialysis Probe Recovery

One of the fundamental limitations of microdialysis sampling is that the fraction of analyte recovered in the dialysate is always less than the actual concentrations of analyte in the surrounding matrix about the probe. The ratio of these two concentrations is known as relative recovery. Relative recovery is affected by the size of the probe's sampling region, probe membrane material, and flow rate of the perfusate. Previous *in vitro* work utilized a sampling region of 1 cm, to maximize exposure to various cell models,[45,46] while previous *in vivo* studies employed a 3 mm sampling region to minimize damage to surrounding tissue upon probe implantation and more accurately target specific tissue locations.[48,101] Probe sampling regions were set at 3 mm for all described experiments and regenerated cellulose was chosen as the dialysis membrane material due to its successful use in the previous biological studies.

As perfusion rates into the probe increase, relative recovery of analytes is decreased; therefore slow perfusion rates are preferred, particularly *in vivo*. Perfusion rates were set at 25 µL/hr, which was optimized with the NBDF derivatization reaction to yield a complete labeling reaction within 5 minutes. Relative recovery of microdialysis probes constructed in house was determined to be 16.2% for leucine, 18.2% for valine, 17.1% for alanine, 17.8% for taurine, and 13.5% for glutamate. Probes constructed on

various days and from different batches were tested, and their results averaged, to determine a representative recovery across all probes utilized. All analytes displayed similar recoveries, which was encouraging as it demonstrates that no one analyte diffuses more favorably across the dialysis membrane as compared to others. Although the recovery percentages are not optimal, the only requirement is that amino acids levels are able to be detected *in vivo*, with dynamic changes observed in near real time. Experiments proceeded towards *in vivo* studies, with adjustments to perfusion flow rate and/or sampling region size kept as options for future optimization should probe recovery prove to be an issue *in vivo*.

2.5 Conclusions

We have developed an analytical platform to analyze the *in vivo* dynamics of BCAAs and related metabolites within adipose tissue and skeletal muscle. BCAAs and related metabolites were separated and identified to test the separation assay's performance, with LODs determined to be suitable for expected biological concentrations. The MD-CE assay achieves a 22 second temporal resolution, making this system a near real time analysis method for small molecule bioamine dynamics. Future studies will focus on applying a variety of stimulations to adipose tissue both locally and systemically. It is our goal through these experiments, to determine the full role BCAAs play in overall body metabolism.

Chapter 3

Design and Development of an *In Vivo* Protocol for the Sampling of Adipose and Skeletal Muscle Tissue

3.1 Summary

In this work, an *in vivo* protocol was designed, developed and subsequently approved by the Institutional Animal Care and Use Committee (IACUC) at the University of Minnesota. The protocol was designed to be comprehensive, allowing for multiple generations of research to complete a full scale study of BCAA metabolism in adipose tissue and skeletal muscle induced by various stimuli.

The animal model selected was C57BL6 male mice, due to their frequent use in obesity research. Sampling locations were chosen based on their involvement in metabolically-related functions and providing an easily accessible site for microdialysis probe insertion. Therefore the quadriceps of the hind limb and the inguinal adipose tissue depot were selected for skeletal muscle and adipose tissue. Anesthetic regimes and euthanasia methods were designed based on available equipment, personnel safety, and safety and ease for the animal model. Isoflurane anesthesia is the chosen technique, with initial induction allowing mice to remain free-moving in an induction chamber, and maintenance of surgical levels occurring via a nose cone in close proximity to the high speed MD-CE instrument. An intracardiac shot of potassium chloride (KCl) under increased isoflurane was chosen as the prominent euthanasia method, with a thoracotomy utilized as a secondary verification procedure. Stimuli chosen for administration included insulin, glucose, BCAAs, and twelve artificial sweeteners.

Finally, a detailed standard operating procedure (SOP) is provided. Much of the animal handling protocol was designed through practical experience, and thus should be

provided to the next generation of research to aide in their *in vivo* experimentation progress.

3.2 *In Vivo* Protocol Design

3.2.1 Model and Tissue Selection

The aim of the proposed research is to study the induced metabolism of bioamines, particularly BCAAs, by various stimuli *in vivo*. Adipose tissue and skeletal muscle are the desired sampling locations, as it has been shown that adipose tissue plays a significant role in regulating BCAAs[30,31] and skeletal muscle plays an important role in overall body metabolism.[3] With this research providing key insights into the metabolism dynamics of adipose tissue under various metabolic conditions, an animal model that will allow for comparisons to current metabolism and obesity literature is desired.

C57BL6 male mice were chosen as the animal model due to their frequent use in obesity research.[127,128] This strain of mouse is the most commonly used inbred strain,[129] and the progression of their metabolism dysfunction mimics that of the progression of human obesity.[41] Male mice will be used exclusively to avoid unintended pregnancies in females, and most importantly, to avoid the complications caused by the presence of mammary tissue. Female mice have five pairs of mammary glands, all situated within adipose tissue depots (See Figure 3.1).[130,131] Once fully developed, mammary tissue can extend through almost all of the subcutaneous areas,[132] therefore probe insertion into solely adipose tissue would be extremely challenging.

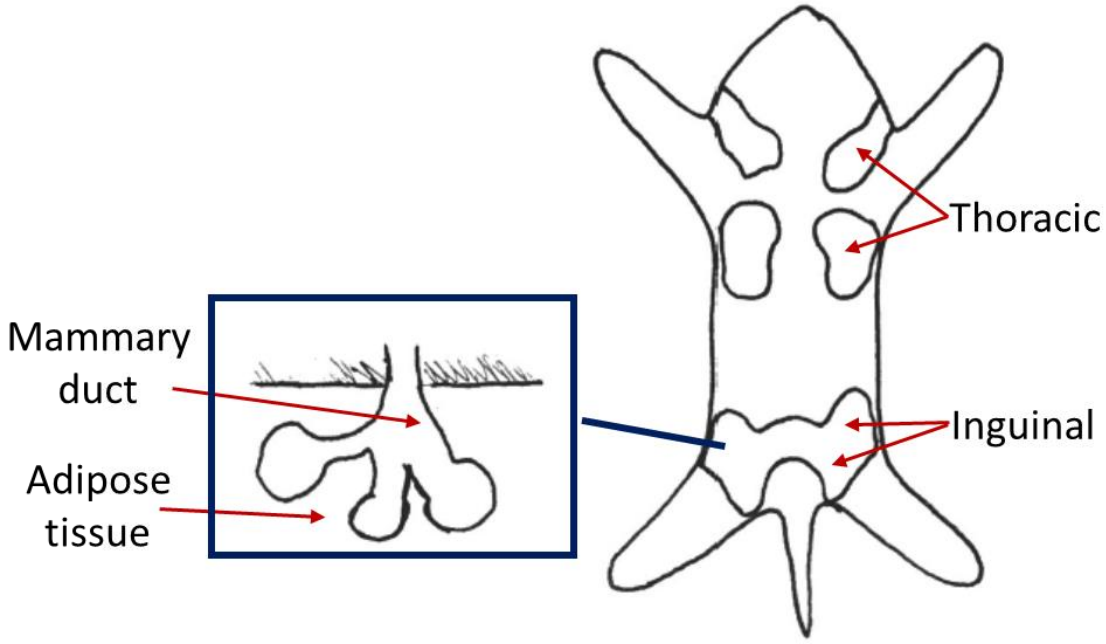

Figure 3.1. Locations of mammary glands in a female mouse.

Metabolic research frequently targets adipose tissue in the epididymal, subscapular, and inguinal depots (See Figure 3.2).[133] The epididymal depot is located deep in the abdominal cavity, attached to the testes and epididymis. Microdialysis probes will be inserted into the desired tissue for sampling, with as minimal disturbances to the surrounding tissue as possible. The location of epididymal adipose tissue causes reproducible probe implantation with minimal damage to be extremely difficult. The subscapular adipose tissue depot is located between the scapulae, underneath the subcutaneous layer. This depot contains BAT however, which is primarily involved in thermogenesis.[134] Since the described research is focused on BCAA regulation and

metabolic function, WAT is required. Therefore all adipose tissue sampling will occur in the inguinal adipose tissue depot, located in the joint region where the hind limb attaches to the abdomen. Its subcutaneous nature will allow for microdialysis probe insertion with minimal damage to both surrounding tissues and the probe itself.

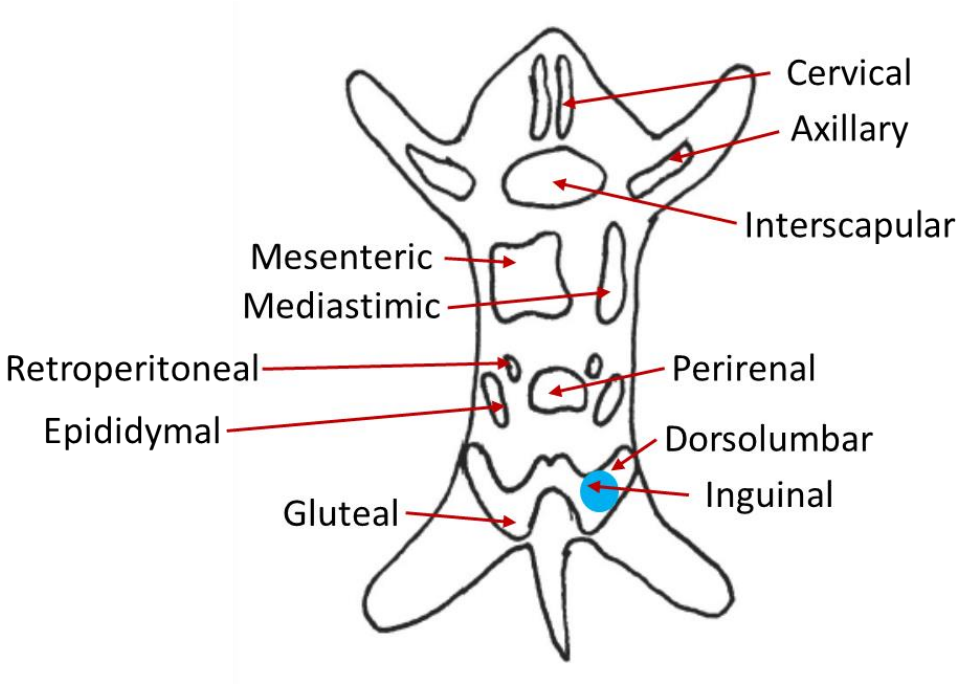

Figure 3.2. Adipose tissue depots in a mouse. The inguinal depot selected for sampling is highlighted.

The skeletal muscle location chosen for sampling was the quadriceps of the hind limb (See Figure 3.3).[135] The quadriceps were selected due to their ease of accessibility, particularly in regards to the orientation of the mouse during anesthesia. The mouse must be positioned on its back in order to access the inguinal adipose tissue depot with a microdialysis probe, making the quadriceps also easily accessible. This selection allows for dialysate collection to proceed from both tissue locations in the same mouse, if simultaneous samples from various locations were ever desired.

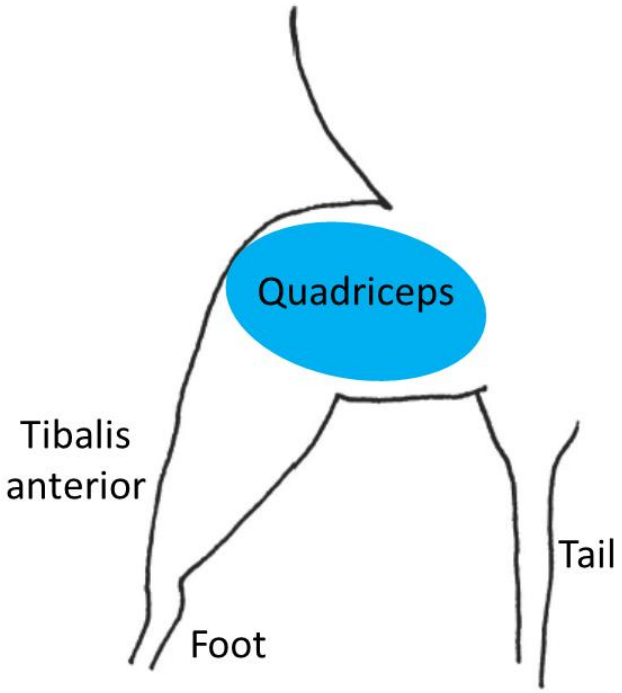

Figure 3.3. Skeletal muscle locations in a mouse hind limb, with the sampling location highlighted.

3.2.2 Anesthesia

Mice must be anesthetized throughout the procedure, prior to microdialysis probe insertion and through the entirety of all data collection. Anesthetic regimes can utilize either injectable or inhalant anesthetics, with inhalant methods offering the advantages of rapid recovery, a more steady-state dosing, and quick adjustment of anesthetic concentration based on the animal's needs.[136] This allows for a more steady anesthetic depth throughout the entire experiment. Inhalation anesthesia has also been shown to have a reduced effect on kidney and liver functions in mice, as well as causes less cardiovascular depression. Disadvantages of inhalant methods include hypotension, vasodilation, myocardial depression and respiratory depression.[137]

Common inhalant anesthetics include nitrous oxide, methoxyflurane, halothane, sevoflurane, and isoflurane. Nitrous oxide displays positive analgesic properties, however its use as the only source of anesthesia in rodents is discouraged as it is not a complete anesthetic.[138] Methoxyflurane releases inorganic fluoride ion once metabolized, which causes renal damage. Therefore an elaborate scavenging system is recommended for personnel safety.[139] Halothane has demonstrated hepatotoxic and mutagenic effects in humans following repeated exposure, and sevoflurane is often cost prohibitive for use in animal studies.[137] Isoflurane is the recommended anesthetic for Swiss, CD-1, and C57BL6 mice strains,[140] and it exhibits rapid induction and recovery times. Disadvantages include delayed growth and cleft palates in newborns with mothers exposed to isoflurane and decreased immune systems.[141,142]

C57BL6 male mice are initially induced using an induction chamber. An induction chamber is utilized in order to minimize stress on the animal prior to anesthesia. Physical restraint of mice can cause increases to epinephrine and corticosteroid levels, increase to glucose levels, and stimulate respiratory and cardiovascular functioning.[143] By allowing mice to be free-moving during initial induction, stress from the animal can be minimized. Induction levels in mice using isoflurane are recommended to be 3.5 - 4.5% according to Flecknell[144] and 4 – 5% in 0.8 – 1.0 L/min according to Gargiulo.[137] The approved IACUC protocol allows for a range of 0.5 – 5.0% isoflurane in 1 L/min oxygen, adjusting based on each individual mouse's response. Prior to anesthetic induction, all mice experience a four hour daytime fast. Brief fasting prior to anesthesia has been shown to help normalize animal to animal variability

in several imaging studies.[143] Daytime fasting, while still allowing free access to water, is anticipated to help normalize glucose and insulin levels across mice.

Post induction, mice are transferred to a nose cone situated on top of a heating pad. Hypothermia in mice is one of the most common causes of anesthetic death[136] and the core body temperature of a mouse will begin to rapidly diminish immediately following induction.[137] The heating pad, and occasional use of a warm blanket, are utilized as necessary in order to maintain an acceptable core body temperature. Isoflurane is delivered in 1 L/min oxygen at the nose cone at a concentration of 0.5 – 2.5%, depending on individual mouse reflexes. Recommended dosages of isoflurane for surgical maintenance range from 1 - 3% in 0.8 – 1.0 L/min.[136,137] Anesthetic depth is continuously verified during the experiment by testing pedal, hind-limb and tail-pinch reflexes. Isoflurane concentration is adjusted as necessary to ensure proper anesthetic depth. Ophthalmic ointment is also applied to the eyes during maintenance of surgical anesthesia levels to prevent corneal desiccation.[137]

3.2.3 Microdialysis Probe Insertion and Stimuli Administration

BCAA metabolism will be monitored in adipose tissue and skeletal muscle as it is induced by various stimuli. BCAAs regulate protein synthesis,[12] insulin sensitivity,[21,28] insulin secretion,[10] and appetite control.[11] It has also been shown that circulating levels of BCAAs are elevated in obese patients and those with type 2 diabetes,[21,26-28] and that these circulating levels deceased upon weight loss. This demonstrates adipose tissue's role in regulating BCAA concentrations.[20,30,31] Recent studies have also shown that artificial

sweeteners alter the gut microbiota of mice,[145] prompting the need for further analysis of artificial sweeteners, and their potential effects on BCAA metabolism.

It was desired that the IACUC protocol be designed to allow for a full scale study into the metabolism dynamics of BCAAs over multiple generations of research. Bioamine levels were to be monitored in the inguinal adipose tissue depot and the hind limb quadriceps of mice. Microdialysis probes were the sampling method chosen, and it was determined that they would be inserted into the tissue of interest through the use of a hollow needle. The preliminary design hypothesized that the microdialysis probe would be threaded through a hollow needle, and once flush with the outlet tip, both the needle and microdialysis probe would be inserted into the tissue. The needle would then be pulled back over the probe, leaving the probe in place in the tissue of interest. The proposed implantation procedure prevents damage to the probe membrane, and is theoretically feasible for both types of tissue. Hands-on experimentation will confirm this method's viability.

As a comprehensive study examining adipose tissue's role on BCAA metabolism, multiple dosing methods were desired. Stimuli were to be administered via reverse microdialysis, such that only the tissue of interest would be initially exposed to the stimuli. In this way, the sole response of the tissue could be examined. Systemic methods of tail vein injection and oral gavage were also to be administered so that the stimuli would be carried through the bloodstream and adsorbed through the gastrointestinal tract, respectively, prior to affecting the tissue of interest. In this way, the tissue's response of BCAA metabolism will be captured after it has been affected by the stimuli and all interworking bodily systems.

Stimuli to be studied include glucose, insulin, BCAAs and twelve artificial sweeteners. The artificial sweeteners include stevioside, steviol, sucralose, aspartame, saccharin, acesulfame K (ace K), sucrose, fructose, aspartate, phenylalanine, neotame, and neotame de-ester. While saccharin, sucralose, aspartame, ace K, and neotame are recognized as commercially available artificial sweeteners,[146,147] the other metabolites are included in order to analyze all components possible post-digestion. Aspartate and phenylalanine are the resulting compounds once aspartame has been digested,[148,149] and glucose and fructose result from sucrose's metabolism. Neotame undergoes a de-esterification process to form neotame de-ester,[150] and stevioside is metabolized to steviol.[151] Insulin and BCAAs will also be examined as interesting components related to overall body metabolism. Maximum concentrations of each stimuli were set as twice the acceptable daily intake (ADI) for each metabolite,[152-161] with multiple concentrations of each metabolite expected to be provided to tissues in order to yield pharmacological kinetics. Maximum concentrations for each stimuli in the protocol are listed as: 10 mg/kg stevioside, 8 mg/kg steviol, 10 mg/kg sucralose, 100 mg/kg aspartame, 10 mg/kg saccharin, 30 mg/kg ace K, 2 g/kg glucose, 2 g/kg fructose, 2 g/kg sucrose, 100 mg/kg aspartate, 100 mg/kg phenylalanine, 4 mg/kg neotame, 4 mg/kg neotame de-ester, 2 U/kg insulin, 140 mg/kg valine, 260 mg/kg leucine, and 120 mg/kg isoleucine.

3.2.4 Euthanasia

Following each experiment, mice must be euthanized due to risk of infection. All experiments, anesthesia, and probe implantation occur in the laboratory of Dr. Michael Bowser, and while associated benchtops and instruments are routinely cleaned and

sterilized, other areas in the laboratory following non-sterile protocols increase the risk of post-surgery infection. Euthanasia methods are chosen based on their reliability, ability to be painless, irreversibility, yielding rapid unconsciousness, and safety and ease of personnel to perform.[162] The absence of respiratory function and heartbeat are good indicators of a complete euthanasia procedure. It is often recommended however, that a verification procedure be performed after confirmed death, such as exsanguination or a thoracotomy.[163]

Recommended euthanasia methods for small rodents include, but are not limited to, barbiturates, carbon dioxide, potassium chloride, decapitation, and cervical dislocation. Barbiturates, such as sodium pentobarbital, are delivered intravenously and are considered both safe and humane. They are one of the more common euthanasia methods employed,[164] but their storage and use in a laboratory requires a DEA license to be held and maintained by all relevant personnel. Carbon dioxide is another commonly used euthanasia technique, particularly for laboratories euthanizing multiple rodents at once. Death occurs within 5-6 minutes,[164] however the University of Minnesota's IACUC and Research Animal Resources (RAR) staff require a secondary procedure, such as cervical dislocation, for complete verification. KCl euthanasia is performed by administering an intracardiac dose of 1-2 mEq/kg. This procedure must be performed while the animal is still under anesthesia. Decapitation utilizes a guillotine to sever the rodent's head from the body at the atlanto-occipital joint. This procedure is most commonly employed in pharmacological studies when the histology of brain slices are desired. Finally, cervical dislocation separates the skull and spinal cord by applying

pressure to the base of the skull while simultaneously pulling on the tail.[164] This technique can only be performed in small rodents.

Due to the extra complications introduced by the requirement of a DEA license, and the lack of need for brain slices and risk to personnel safety through guillotine operation, barbiturates and decapitation are not utilized in the described protocol. Carbon dioxide, while commonly employed, would require the purchasing of carbon dioxide tanks and euthanasia chamber. Since only one animal is used for each experiment, the benefit of being able to euthanize multiple mice simultaneously does not offset the purchasing of new equipment. Cervical dislocation is arguably the most advantageous method, requiring no purchased equipment and feasible when experimenting with only one mouse at a time, however personnel ease and comfort at performing the technique did not make this a desirable method. Personnel have been trained on proper cervical dislocation techniques, in the event an emergency required its use, but the euthanasia method chosen for the described protocol is an intracardiac dose of KCl under anesthesia, followed by a thoracotomy.

At the conclusion of each experiment, isoflurane is increased to 5.0% in 1 L/min oxygen at the nose cone for a minimum of 3 minutes. KCl (1 – 3 mEq/kg) is prepared in 0.5 mL DI water. The KCl solution is delivered through an intracardiac shot with a 1 mL syringe, and death is confirmed by the cessation of heartbeat and respiratory function. Following death confirmation, the mouse is removed from the nose cone and a thoracotomy is preformed to create a pneumothorax as a secondary procedure.

3.3 Standard Operating Procedure

Currently I am the sole researcher trained and practiced in all animal handling and *in vivo* experimental procedures. A portion of my research responsibility during graduate school was to design and establish a functioning *in vivo* protocol that would allow for experimentation for an extended period of time. The protocol designed, submitted and approved by IACUC is valid until February 2019, and thus there is a high probability that a future student will engage in *in vivo* experiments after my departure. This section serves as my attempt to pass along the practical knowledge and experience I have gained over the last several years. It is my hope that the next researcher will be able to continue where I left off, and utilize the preliminary work completed.

3.3.1 Picking up Mice

Mice are housed by RAR in Jackson Hall. RAR veterinary staff will accept animal deliveries, feed mice, and clean the cage bedding for a daily fee. Housing is located in a Specific Pathogen Free (SPF) zone and therefore all personnel entering animal housing must have completed microisolator training and follow all protocols described therein. Bring a black cloth to the facilities so the cage can be covered when traveling back to Nils Hasselmo (cage covering is required when transporting animals so the contents of the cage remain unknown in public). In the Jackson Hall facilities, retrieve a pink carcass bag from the supply closet. These will be needed to return all animal waste at the conclusion of the experiment.

Retrieve the animal cage containing a single mouse. Mice are housed individually so only the animal to be used for an experiment leaves the SPF facilities. Cover the cage with the black cloth and use the underground tunnels and skyways free from students to transport the cage back to the laboratory, avoiding class pass-periods whenever possible. Once back in the laboratory, remove the cover from the cage. If the experiment calls for a 4 hour daytime fast, remove the food from the cage but leave the mouse free access to water.

3.3.2 Initial Induction of Anesthesia

The anesthesia equipment utilized for experiments includes an isoflurane vaporizer, switching manifold, nose cone, oxygen tank, induction chamber and waste scavenging pump. The isoflurane vaporizer must be calibrated annually as per IACUC instructions. Prior to each experiment, ensure the vaporizer is filled with isoflurane. See Figure 3.4 for vaporizer details.

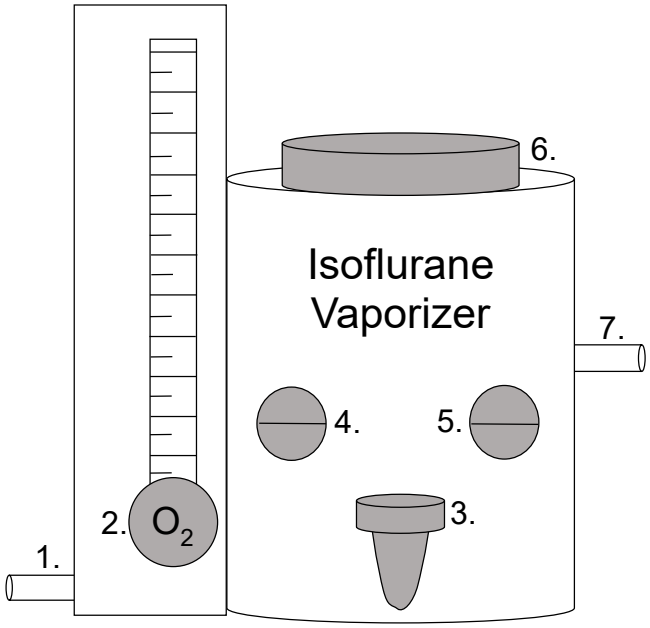

Figure 3.4. Isoflurane vaporizer schematic. Oxygen lines attach to vaporizer at (1) and the oxygen rate during anesthesia is adjusted at (2). Isoflurane is refilled through the chamber at (3), with a full tank being denoted by the liquid level reaching the line at (4). The tank must never be allowed to drop below the line denotation at (5). Isoflurane concentration is adjusted at (6) and the isoflurane gas lines attach at (7) to deliver anesthesia gas to the switching manifold.

Attach the gas anesthetic waste line to the scavenging pump (located in the fume hood). Make sure all gas lines to the oxygen tank, vaporizer, induction chamber, and nose cone are securely fastened. Above the nose cone there is a scavenging line venting system; open the scavenging line and turn on the heating pad prior to initial induction (heating pad is usually set at 50-75% power to begin; adjust as necessary throughout the experiment). Transfer the mouse from the cage to the induction chamber. Techniques to pick up and maneuver mice are taught in the Mouse Basics class, hosted through RAR. Once the mouse is placed gently inside the induction chamber, place the lid on the chamber and pull the fume hood sash down (as the induction chamber waste gas vents into the fume hood). Switch the manifold to select only the induction chamber.

Open the oxygen tank and set the regulator to 40 psi. Turn on the oxygen supply at the vaporizer to be 1 L/min and turn on the isoflurane supply. The protocol approved by IACUC allows for 0.5-5.0% isoflurane during induction, however 5.0% has been the concentration most frequently used. Within one minute, the mouse should begin to experience the anesthetic. Typical responses include curious smelling and increased movement around the chamber. Mice (20-25g, 6-8 weeks of age) are usually under an appropriate depth of anesthesia to be transferred to the nose cone in 6 minutes (changes in breathing rate are the visual indicators of deep anesthesia).

Once the mouse is at the correct depth of anesthesia for transfer, turn down the isoflurane to 2.5% (current protocol allows for 0.5-2.5% isoflurane at nose cone). Adjust the manifold: induction chamber valve – OFF, nose cone valve – ON, waste line valve – ON. Remove the lid from the induction chamber and transfer the mouse to the nose cone. Pull the fume hood sash back down when finished, as the waste line from the nose cone vents into the hood.

3.3.3 Anesthetic at Nose Cone

Place the nose of the mouse firmly inside the nose cone, holding in this position for several moments, to ensure depth of anesthesia is still sufficient. After several minutes, remove the mouse from the nose cone and quickly apply ophthalmic eye cream using a cotton swab. Immediately place the mouse back into the nose cone, positioned on its back with its nose firmly in the nose cone. Adjust the nose cone height to allow for comfortable positioning of mouse (neck should be aligned straight with body and not bent back). Perform pedal, hind limb and tail reflex testing. Pedal reflex testing involves

pinching between the toes, hind limb reflex testing pinches the limb above where the foot attaches, and tail reflex testing pinches the tail just below where it attaches to the body. Pinch firmly, and if the mouse is under sufficient levels of anesthesia, no twitching or movement will be observed in either hind limb or the tail. If no responses are observed, secure the mouse to the heating pad to avoid movement of any tissue during the experiment. If responses are present, adjust the isoflurane until no reflexes are observed.

Reflex testing must be performed and recorded every 5-15 minutes to ensure anesthetic depth is sufficiently maintained. Ideally, the isoflurane concentration will be just enough to maintain anesthesia, and no more. Typically the nose cone is set at 2.5% for the initial transfer, and then reduced to 2.0-2.25% for the remainder of the experiment, depending on the reflex responses of individual mice. Throughout the experiment, the temperature of the mouse must be carefully monitored as well. Mice are extremely susceptible to hypothermia under anesthesia, and therefore if the limbs ever feel cool, increase the heating pad power. Be careful not to overheat the mouse. Once anesthetic depth has been successfully maintained at the nose cone for approximately 30 minutes, the microdialysis probe can be inserted into the tissue of interest.

3.3.4 Microdialysis Probe Insertion

Microdialysis probes should already be connected to the instrument and sampling from Eppendorf tubes containing standards in Ringer's solution. Remove the microdialysis probe from the sample vial and thread it through a 19 gauge needle. Be sure to thread the probe without bending or damaging the membrane of the sampling region. The probe tip should be slightly less than flush with the end of the needle. Push the

needle into the tissue of interest, and once at the desired depth, hold the capillary in place and pull the needle back over the probe. The microdialysis probe should have remained in the tissue, however slight adjustments to its depth can be achieved by grasping the probe close to the tissue with tweezers and pulling the probe either further in or out. The precise implantation procedure for inguinal adipose tissue and quadriceps muscle is described in Chapter 4, however this general procedure can be adapted to most sampling locations. In the instance of hind limb or inguinal adipose tissue sampling, once the probe is implanted, secure the limb and needle in place to prevent any movement during data collection.

3.3.5 Euthanasia

Once the experiment is complete, detach the capillary connecting the reaction tee to the microdialysis probe. The probe should remain in the tissue for verification of location during dissection, however the mouse must be disconnected from the instrument for euthanasia. Increase the isoflurane to 5.0% for approximately 3 minutes and then deliver an intracardiac shot of KCl. The KCl solution should be previously prepared at 3 mEq and contained in a 1 mL syringe.

To find the heart, place an index finger and thumb on opposite sides of the thoracic cavity and move up or down along the cavity until the heartbeat is felt between the fingers. Mice have an extremely fast heartbeat, so do not confuse feeling your own heartbeat between your fingers with theirs. Once the lateral position of the heart has been located, insert the needle into the center of the thoracic cavity at this location, being sure

to go underneath the sternum (the needle may need to be inserted at a slight angle). Push the KCl solution into the heart slowly. Breathing and heartbeat should cease immediately.

Turn off the isoflurane and oxygen at the vaporizer. Remove the deceased mouse from the nose cone and place on the bench to perform a thoracotomy. Insert scalpel into chest cavity and create an incision opening the chest. This creates a pneumothorax and is a confirmation of the euthanasia procedure. Post thoracotomy, dissect the tissue surrounding the probe to ensure successful implantation of probe into the desired sampling region. For sampling from the inguinal adipose tissue depot or the hind limb muscle, dissections typically begin in the upper abdominal region. Using a scalpel and scissors, the subcutaneous layer can be separated from the abdominal cavity, without puncturing through the abdominal wall. The subcutaneous layer is then carefully separated all the way down to the hind limb. Here the inguinal adipose tissue depot can be separated from the underlying muscle tissue to verify probe location. After visually confirming the microdialysis probe placement, remove the probe from the tissue and weigh the mouse for records.

3.3.6 Returning Animal Waste and Cleaning

Place the carcass into the pink waste bag. If any paper based materials were contaminated with blood (paper towels, cotton swabs, etc.), they will need to be taken separately to RAR and disposed of in the proper containers. Cover the cage and pink bag with the black cloth and return to Jackson Hall using the tunnels/skyways avoiding student traffic. Place the pink carcass bag into RAR's animal waste fridge and place the

cage on the shelves designated for dirty cages. Turn in the white card located on the front of the animal cage to the outbox at the entrance to the facilities.

All needles, syringes and scalpels used during the experiment should be disposed of in the proper sharps container. All capillary, including the microdialysis probe, should be disposed of in the proper broken glass container. The heating pad, benchtop, and surgical scissors and scalpel (non-disposable) must be sterilized with 70% ethanol. Set all valves to OFF in the manifold and verify that the isoflurane and oxygen in the vaporizer are turned off. Close the oxygen tank, turn off the heating pad, and close the scavenging vent line. Disconnect the scavenging gas waste line from the scavenging pump and store all gas lines appropriately.

3.4 Conclusion

This work allows for *in vivo* experimentation within Dr. Michael Bowser's lab through February 2019. Full anesthetic and euthanasia regimes are permitted to be conducted within the lab, alongside microdialysis probe implantation procedures. Male C57BL6 mice undergo isoflurane anesthesia prior to microdialysis probe implantation in either the inguinal adipose tissue depot or the hind limb quadriceps. Tissue is stimulated through reverse microdialysis, tail vein injection, or oral gavage by insulin, glucose, BCAAs, or a variety of artificial sweeteners. Risk of infection requires this procedure be non-survival, and thus an intracardiac dose of KCl followed by a thoracotomy is performed for euthanasia. Full procedural details are outlined for future *in vivo* experiments.

3.5 Acknowledgements

I'd like to thank all of RAR's veterinary staff for their incredible work in caring for all mice, as well their training on the handling, anesthesia and euthanasia of rodents. I'd also like to thank Dr. David Bernlohr, for his assistance in developing a protocol suitable for obesity experiments, Dave Osborn, owner of The Anesthesia Repair Guy, Inc., for his isoflurane vaporizer calibration and instructions on the operation of anesthetic equipment, and Haley Phillips, a graduate student in Dr. Theresa Reineke's lab, for instructions on tail vein injections.

Chapter 4

In Vivo Monitoring of Amino Acid Biomarkers from Inguinal Adipose Tissue and Skeletal Muscle Using Online Microdialysis-Capillary Electrophoresis

Sections adapted from:

"Weisenberger, M.M and Bowser, M.T. *Anal. Chem.* **2017**, *89* (1), 1009-1014."

Reproduced with permission

4.1 Summary

In this work, sampling procedures were developed and optimized for a C57BL6 mouse. Microdialysis probes were successfully implanted into inguinal adipose tissue reproducibly. Placement of the probe was visually verified following each experiment with a full dissection. Measurements made in the adipose tissue of four mice generated similar basal recordings, including the presence of arginine, lysine, isoleucine, leucine, methionine, phenylalanine, valine, GABA, glutamine, alanine, glycine, and taurine. A successful and reproducible implantation procedure was also developed for quadriceps skeletal muscle, with placement visually verified as well. Basal recordings in muscle across three mice found similar traces, with arginine, lysine, isoleucine, leucine, methionine, phenylalanine, valine, GABA, glutamine, alanine, glycine, taurine, and glutamate detected.

To demonstrate the high speed microdialysis-CE assay's ability to monitor metabolism dynamics in near real time, a tail vein stimulation of insulin was administered. Bioamine levels were recorded in inguinal adipose tissue prior to, during, and post stimulation. Valine, alanine, and taurine levels all drastically increased following the initial stimulus, and their levels remained elevated post stimulation. Valine levels increased 40% initially before returning to an elevated baseline of 34%. Alanine increased by 46% with an elevated baseline of 16%, while taurine increased by 37% with an elevated baseline of 21%. All post stimulation levels were found to be significantly different than original basal levels ($p < 0.001$). It can therefore be determined that the

developed assay has the ability to monitor dynamics as they occur in near real time as a response to administered stimuli.

4.2 Introduction

Current metabolism and obesity research utilizes *in vitro, in vivo,* and *ex vivo* models, however *in vivo* experiments allow for interworking body systems to be examined. This is an important aspect for metabolism research, given that metabolic dynamics occurring in adipose tissue are part of a signaling network that includes the pancreas, liver, muscle, and brain.[10-12] Current studies are limited in their time response, with typical measurements occurring on the timescale of minutes to hours.[119-121] The developed online high-speed MD-CE assay has a temporal resolution of 22 seconds, allowing for near real time measurements of metabolism dynamics.

Microdialysis probes have been successfully implanted in the dermis,[60-62] liver,[57-59] muscle,[54,56] tumor,[54,55] and brain[50] tissues. In order to record metabolic dynamics in near real time, microdialysis probes must be implanted directly into adipose tissue and skeletal muscle. This will allow for bioamine levels to be monitored prior to, during, and post stimulus administration. Implantation procedures must allow for reproducible implantation directly into the tissue of interest, with minimal damage to the surrounding tissues and no damage to the probe membrane.

C57BL6 mice have been selected as the model for *in vivo* experiments due to the progression of their metabolic dysregulation mimicking that of human's metabolic dyregulation.[41] The inguinal adipose tissue was selected as the adipose sampling depot

due to its composition of white adipose tissue and its subcutaneous location allowing for easier probe insertion.[133,134] The quadriceps skeletal muscle was selected as the sampling location for muscle due to ease of insertion with the mouse positioning under anesethesia.[135] Reproducibility between mice for adipose tissue and skeletal muscle amino acid signatures will also need to be established in order to draw general conclusions regarding induced metabolism dynamics due to administered stimuli.

4.3 Materials and Methods

4.3.1 Chemicals and Reagents

Chemicals. Insulin (human recombinant, lot 15L255-B) and all amino acid standards were purchased from Sigma Aldrich (St. Louis, MO). D-glucose was purchased from Gibco (Life Technologies Corp., Grand Island, NY) and sodium tetraborate decahydrate was purchased from CHEM-IMPEX Int'l Inc. (Wood Dale, IL).

Buffers and Solutions. All solutions were prepared in DI water (Milli-Q, 18.2 MΩ; Millipore, Bedford, MA) and filtered (0.22 μm). Ringer's solution was prepared with NaCl (123 mM), $CaCl_2$ (1.53 mM), KCl (4.96 mM) and 5 mM glucose with pH adjusted to 7.5. aCSF was comprised of NaCl (145 mM), KCl (2.7 mM), $MgSO_4$ (1.0 mM) and $CaCl_2$ (1.2 mM). The conditioning of microdialysis probes is the only instance in which aCSF was used during experimentation. Sheath flow buffer was comprised of 90 mM borate adjusted to pH 10 and CE separation buffer contained 90 mM borate/35 mM α-cyclodextrin (food grade, lot 010760F206, Cyclodextrin Technologies Development Inc., Alachua, FL) adjusted to pH 10. Insulin stimulation solution was prepared by

dissolving 2U/kg insulin in 0.1 mL Ringer's solution. Derivatization solution was prepared by dissolving 40 mM NBDF (TCI America, Portland, OR) in methanol and mixing 1:1 with 500 µM HCl, producing a final concentration of 20 mM NBDF/250 µM HCl in 50% methanol. Derivatization solution was prepared daily and degassed under vacuum for 2 minutes prior to use.

4.3.2 Microdialysis

Microdialysis probes were constructed in-house using a side-by-side geometry as previously reported[101] (see Figure 4.1). Two 40 µm i.d. × 105 µm o.d. fused silica capillaries (Polymicro Technologies, Phoenix, AZ) were inserted into a 200 µm diameter hollow fiber, regenerated cellulose dialysis membrane (13 kD MWCO, Spectrum Laboratories, Rancho Dominquez, CA) and off-set by 3 mm to generate a sampling region. Capillaries were sealed in place using polyimide resin (Alltech, Deerfield, IL). Prior to use probes were conditioned with ethanol (55 µL/h for 25 minutes) followed by aCSF (55 µL/h for 25 minutes). During analysis probes were perfused with Ringer's solution at 25 µL/h.

4.3.3 Online CE-LIF Instrumentation

Online Derivatization. Dialysate was transferred to a 250 µm i.d. stainless steel cross (Valco Instruments Co. Inc., Houston, TX) in a 40 µm i.d. × 360 µm o.d. fused silica capillary (see Figure 4.1). Borate buffer and derivatization solution were introduced at the reaction cross at 5 µL/h each. The derivatization reaction proceeded through a 90

cm long, 75 µm i.d. × 360 µm o.d. fused silica capillary, of which a 66 cm portion was heated to 80ºC, by running the capillary through flexible tubing containing water from a heating bath (NESLAB EX-7 Digital One heating bath circulator, Thermo, Newington, NH). Capillary dimensions and all flow rates produced a reaction time of 5 minutes.

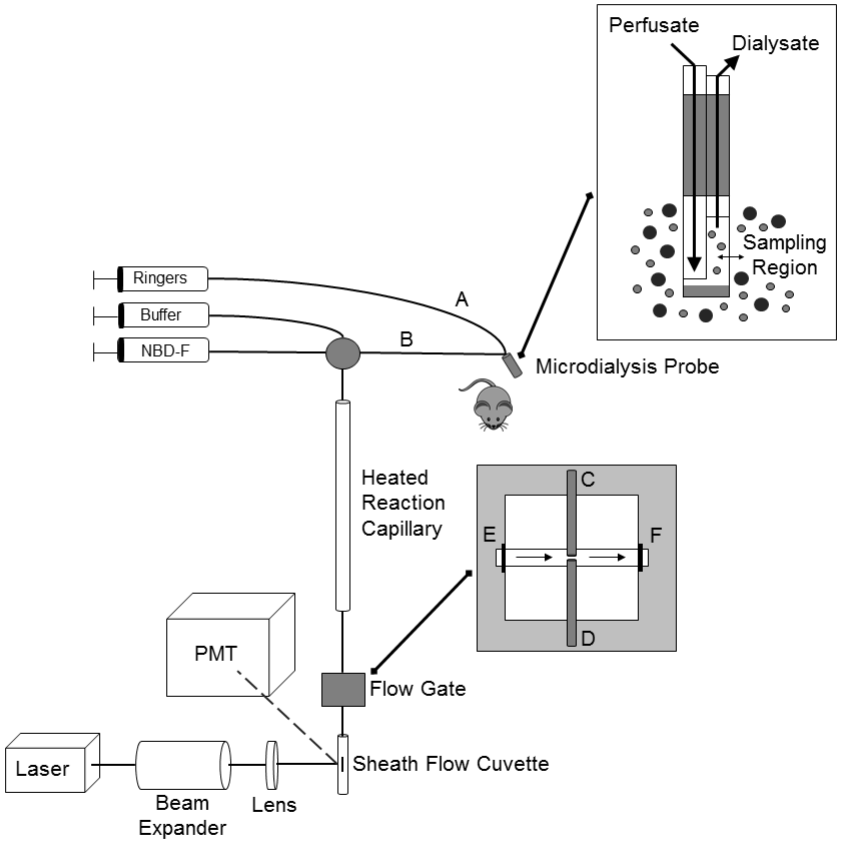

Figure 4.1. Schematic of the high-speed online MD-CE-LIF instrument. Probes are implanted into inguinal adipose tissue or quadriceps skeletal muscle, and then perfused with Ringer's solution (A). Perfusate (B) mixes with borate buffer and NBDF through a heated reaction capillary prior to injection onto the CE separation capillary. A flow gated interface allows for the reaction capillary (C) and separation capillary (D) to be coaxially aligned across the separation buffer channel (E-F).

High-Speed CE. Discrete sample plugs from the reaction capillary were injected onto a 6.2-6.5 cm long, fused silica CE separation capillary (5 μm i.d. × 360 μm o.d.) using a flow gated interface.[96] The separation and reaction capillaries were coaxially aligned leaving an approximately 50 μm gap in-between. Separation buffer was pumped through this spacing at 40 mL/h using a syringe pump (Pump 22 syringe pump, Harvard Apparatus, Holliston, MA). To perform an injection, buffer flow was stopped for 750 ms using a pneumatically actuated valve (C2-3000A 10 port valve, Valco Instruments Co. Inc., Houston, TX) controlled by an in-house developed LabView program. Following this delay, -19 to -21 kV of injection voltage was applied at the outlet of the separation capillary for 100 ms. Buffer crossflow was then resumed as the potential was increased to the separation voltage (-21 to -23 kV) over a period of 500 ms.

Detection Scheme. Laser-induced fluorescence (LIF) detection was performed using the 488 nm line of a 60 mW diode pumped solid-state laser (Coherent, Santa Clara, CA). The laser beam was expanded using a 10× beam expander (Edmund Optics Inc., Barrington, NJ) and focused directly beneath the outlet of the separation capillary, in a sheath flow cuvette,[123] using a 1× lens. A 60×, 0.7 NA long working distance objective (Universe Kogaku, Oyster Bay, NY) collected fluorescence at 90º. Collected emission was passed through spatial (~1 mm) and bandpass filters (543.5 ± 10 nm) and detected using a photomultiplier tube (PMT R1477, Hamamatsu Corp., Bridgewater, NJ). Current was filtered with a 10 ms rise time, amplified (Keithley Instruments Inc., Cleveland, OH) and recorded using a data acquisition card (National Instruments Corp., Austin, TX). Data was analyzed using Cutter Analysis 7.0.[124]

4.3.4 *In Vivo* Characterization

All animal experiments were performed in strict compliance to the protocol approved by IACUC at the University of Minnesota. Mice were housed in RAR facilities and fed a standard chow diet. Prior to all experiments, mice experienced a 4 hour daytime fast. Male C57BL6 mice (20-25 g, 6-7 weeks of age; Envigo, Indianapolis, IN) were initially anesthetized in an induction chamber (Harvard Apparatus, Holliston, MA) using isoflurane (5% in 1 L/min medical grade oxygen; Piramal Critical Care Inc., Bethlehem, PA). After sedation mice were fitted with an anesthesia mask (Scivena Scientific, Clackamas, OR) for maintenance of surgical anesthesia levels (2.5% isoflurane in 1 L/min oxygen). Microdialysis probes were implanted into the tissue of interest once the mouse was unresponsive to pedal and hind limb reflex testing. After insertion, the needle was pulled out of the tissue carefully, leaving the microdialysis probe in place. The probe was then secured and allowed to equilibrate for 15-30 minutes before basal concentrations were recorded. CE separations were performed every 22 s. Following 15-20 minutes of basal recordings, insulin stimulations were administered intravenously through the tail vein (0.1 mL of 2U/kg insulin).

4.4 Results and Discussion

4.4.1 Microdialysis Probe Implantation into Inguinal Adipose Tissue

Once the inguinal adipose tissue depot was selected as the sampling location for WAT, a protocol was developed to allow for reproducible implantation of the microdialysis probe with no damage to the probe membrane and minimal disturbances to

surrounding tissues. The initial concept was to use a hollow needle in an approach similar to a guide cannula. A microdialysis probe, with its fairly flexible sampling region, might deviate from the intended path if inserted directly into the soft tissue on its own. There is also risk of damage to the dialysis membrane if the probe tip is forced through the skin and various tissues unprotected. Guiding a hollow needle into the tissue of interest first would ensure that the desired position was achieved, and subsequent threading of the probe through the needle would allow the probe to remain protected. In order to minimize tissue disturbances, the smallest needle possible needed to be utilized.

Needles ranging from 16G to 22G were tested for their ease in microdialysis probe threading. The sampling region of the probe is only 200 µm in diameter, and therefore it could theoretically be threaded through all selected gauges. However, the probe must be threaded precisely through the needle, it cannot "miss" the needle opening and hit the inner walls, as damage to the membrane would be a likely outcome. Since threading the probe would be done at the benchtop during an experiment, a microscope would be unable to be utilized. Therefore a minimum of 18G allowed for reproducible threading. The needle must then be retracted over the probe, once insertion is complete, to leave only the probe in place within the tissue. The probe has a "jacket" above the membrane to keep the inlet and outlet capillaries securely in place. Needle selections must also be able to accommodate this encasement as well. A 19G needle was therefore determined the needle insertion choice due to it being the smallest size which would easily and comfortably be threaded back over the probe.

Implantation into inguinal adipose tissue was initially attempted by inserting the needle directly down into the tissue with the mouse positioned on its back. The needle

was inserted perpendicularly while the skin around the hind limb joint was stretched taut to ease insertion through the skin. Implantation into solely adipose tissue utilizing this technique proved exceedingly difficult. The inguinal adipose tissue depot is extremely thin and subcutaneous. The needle and microdialysis probe were frequently inserted too deep, sampling instead from the underlying skeletal muscle beneath the adipose tissue.

A successful and reproducible implantation protocol was developed by inserting the needle while maintaining a parallel approach to the abdominal cavity. The mouse was positioned on its back and the left hind limb was gently stretched outwards to create taut skin above the inguinal adipose tissue depot. The microdialysis probe was threaded through the 19G hollow needle until the tip of the probe was flush with the needle outlet. Keeping the needle and probe parallel to the abdomen, implantation began slightly inferior to the hind limb joint, and proceeded until approximately 0.3-0.7 cm of the needle had been inserted. The probe's inlet and outlet capillaries were then grasped securely behind the needle to prevent the probe from shifting, while the needle was retracted carefully over the probe. Once complete needle retraction was accomplished, the probe was secured in place to prevent movement in the tissue for the remainder of the experiment.

Figure 4.2 displays an image of the microdialysis probe within the inguinal depot. The adipose tissue has been dissected away from the abdominal cavity and the hind limb muscle (located dorsally to inguinal adipose tissue). The location of the probe in inguinal adipose tissue was visually verified following each *in vivo* experiment by full dissection. Probes were also removed from adipose tissue post dissection to examine the dialysis membrane for damage.

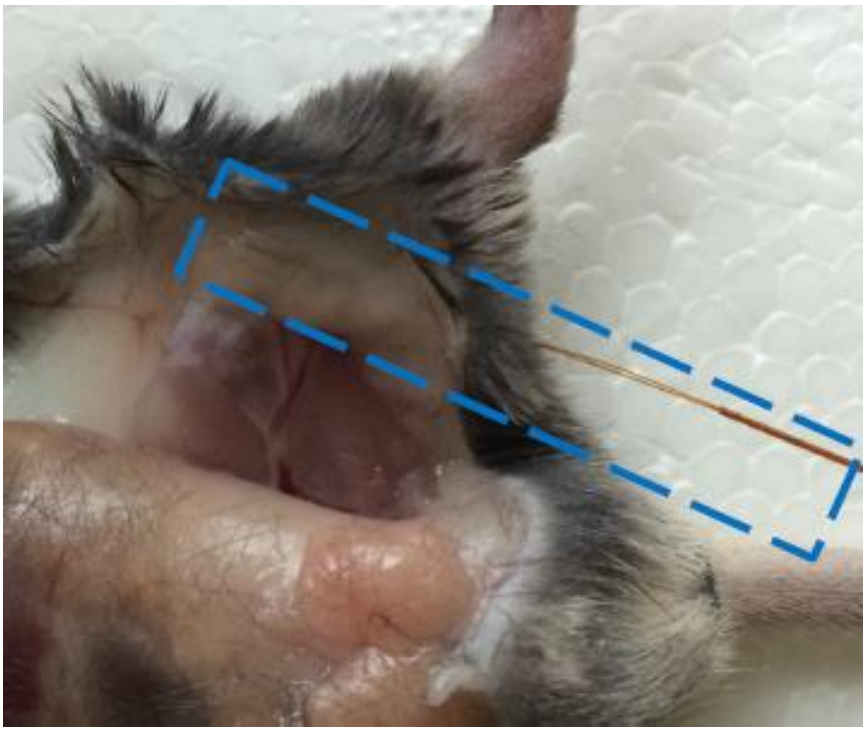

Figure 4.2. Verification of microdialysis probe placement in the inguinal adipose tissue. After completion of the MD-CE experiments, the mouse was euthanized and dissected to expose the inguinal fat depot. The microdialysis probe has been outlined. It can be visually verified that the sampling region of the probe is located within adipose tissue.

A reproducible implantation protocol was developed to insert microdialysis probes with minimal tissue disturbances and no damage to the probe membrane within inguinal adipose tissue. Once probes had equilibrated in the tissue for 15-30 minutes, bioamine basal recordings were collected.

4.4.2. Amino Acid Signature of Adipose Tissue

CE separations were performed every 22 seconds on dialysate collected from inguinal adipose tissue. A total of twelve amines were able to be resolved and detected in adipose tissue at concentrations significantly higher than the LOD as shown in Figure

5.3A. The separation time was set at 20 seconds, however all detectable amines were separated within 15 seconds. Figure 5.3A displays an electropherogram collected under basal conditions, with the unlabeled peaks in the electropherogram corresponding to by-products of the derivatization reaction. Analytes of interest, including isoleucine, leucine, valine, glutamine, and alanine, were able to be detected in adipose tissue. Isoleucine and leucine were able to be separated and individually identified, despite the sacrifices in resolution to improve the temporal response.

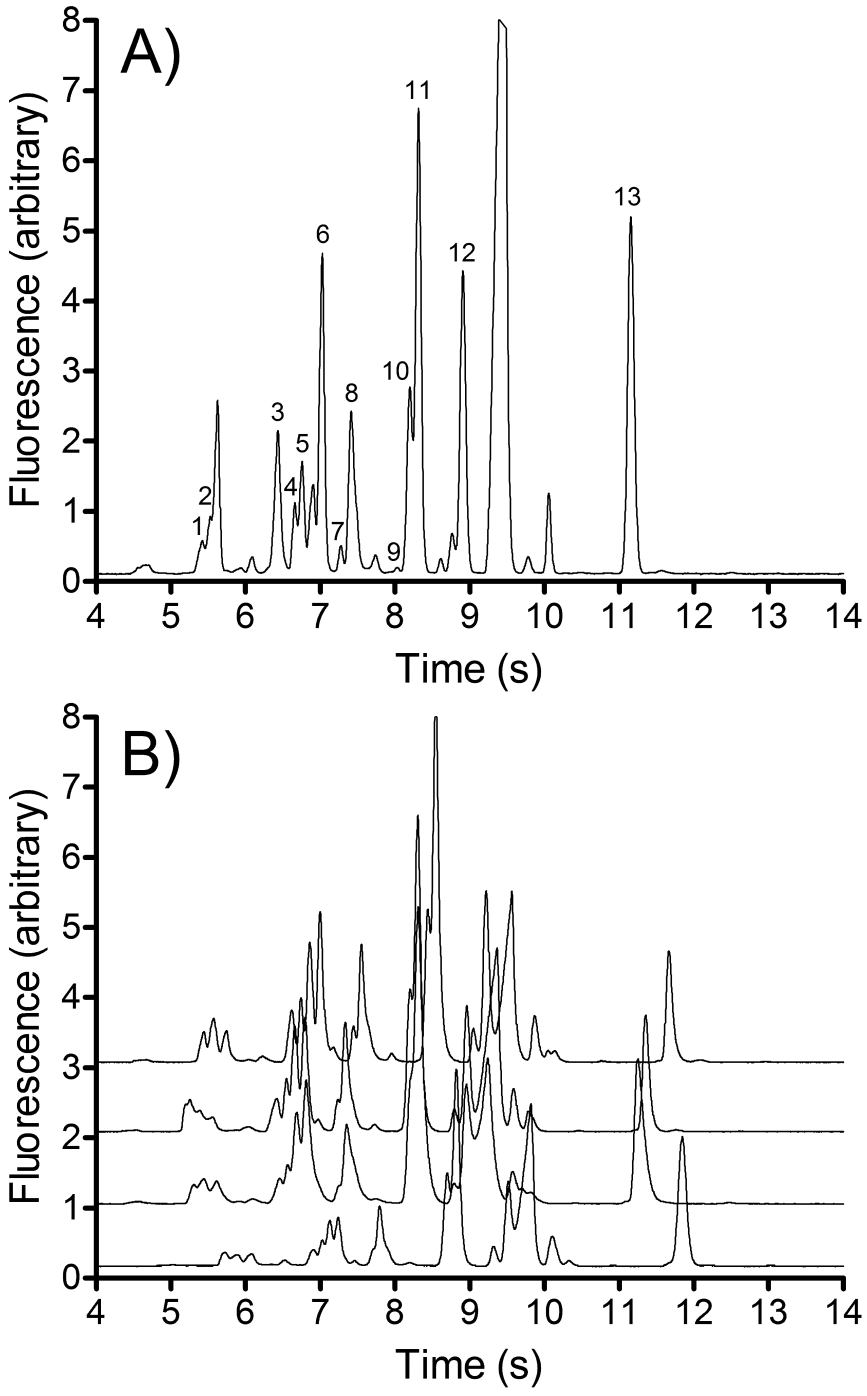

Figure 4.3. (A) Electropherogram of amino acids at basal levels in inguinal adipose tissue. Peaks identified as (1) arginine, (2-3) lysine, (4) isoleucine, (5) leucine, (6) methionine, (7) phenylalanine, (8) valine, (9) GABA, (10) glutamine, (11) alanine, (12) glycine, (13) taurine. (B) Electropherograms of basal amino acids from adipose tissue of four different mice.

In order to ensure the amino acid profile of adipose tissue was reproducible between mice, basal recordings were examined across four different subjects. Figure 5.3B displays the amino acid profiles of different mice. As shown, the amino acid signature of adipose tissue was found to be remarkably reproducible. An interesting discovery was the absence of glutamate in all mice examined. This finding was unexpected, given the anticipated concentrations of BCAAs[125,126] and due to the known ability of adipose tissue to regulate BCAA metabolism,[30,31] the presence of downstream metabolism products was expected. It is possible for some glutamate to be present in the examined adipose tissue, just at concentrations below the LOD. One hypothesis is that within adipose tissue, glutamine is preferred to be present and therefore glutamate is converted to glutamine. Studies have shown that the activity of the phosphate-dependent glutaminase, which requires glutamine, to be greater in adipose tissue than in the liver. It has also been discovered that when tricylglycerol formation and lipogenesis are preferred, adipose tissue converts glutamine to glutamate, and then metabolizes glutamate to acetyl-CoA products for lipogenesis.[165]

4.4.3 Microdialysis Probe Implantation into Skeletal Muscle

Amino acid metabolism in skeletal muscle was a desired point of comparison with adipose tissue due to muscle's known role in protein metabolism. Skeletal muscle's protein synthesis and degradation act as the supply of plasma amino acids during fasting states.[166] Therefore an implantation protocol for skeletal muscle had to be developed.

The inguinal adipose tissue depot chosen for microdialysis probe implantation was located near the left hind limb. The left inguinal depot was selected due to ease of

orientation with the mouse positioned on its back for the probe in relation to the CE instrument. Although currently only one probe is anticipated to be inserted into tissue at a time, future experiments may desire bioamine dynamics from both skeletal muscle and adipose tissue simultaneously. The insertion procedure developed for skeletal muscle was designed to allow for future collections of dialysate from skeletal muscle while sampling was occurring in adipose tissue, and vice versa. Skeletal muscle from the right quadriceps was chosen as the probe sampling location.

Microdialysis probe implantation into skeletal muscle proceeded with the same hollow needle approach as outlined for adipose tissue. The probe was threaded through a 19G hollow needle until the tip of the probe was flush with the needle outlet. The skin above the right hind limb quadriceps was pulled taut to ease insertion. Once the needle and probe were in the desired sampling location, the outlet and inlet capillaries of the probe were firmly grasped while the needle was retraced to prevent any deviation of the probe in muscle. After the needle was fully retracted, the microdialysis probe was secured in place. Verification of the probe's placement in quadriceps skeletal muscle can be visualized in Figure 4.4.

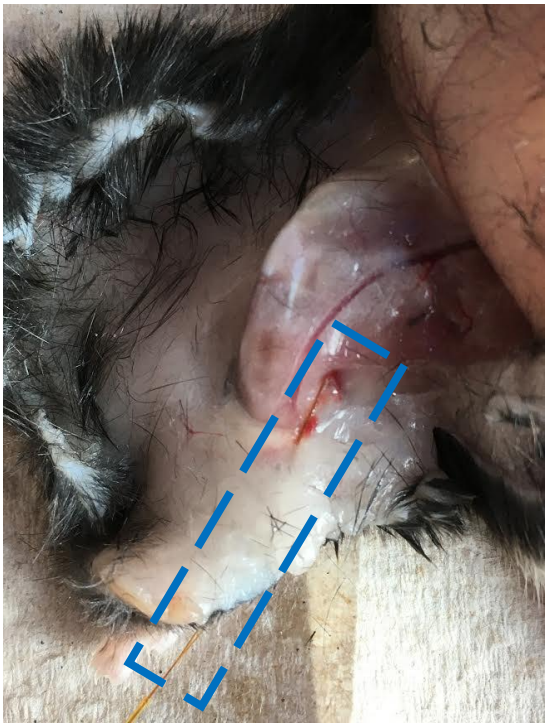

Figure 4.4. Verification of microdialysis probe placement in the right quadriceps skeletal muscle. After completion of the MD-CE experiments, the mouse was euthanized and dissected to expose the tissue. The microdialysis probe has been outlined. It can be visually verified that the sampling region of the probe is located within skeletal muscle.

Initially, probe implantation into skeletal muscle utilized the parallel approach which was successful for adipose tissue. The needle and probe were kept parallel to the abdomen, beginning insertion slightly inferior to the joint area of the right hind limb, and proceeding until 0.3-0.7 cm of the needle was inserted into tissue. Instead of keeping the needle subcutaneous, insertion began at a more dorsal location on the hind limb, with the mouse still positioned on its back. This procedure did not prove to be reproducible however, with varying depths into skeletal muscle attained each time. Several insertions also resulted in partial insertion into adipose tissue as well.

A successful insertion approach into skeletal muscle was achieved by keeping the needle and probe at a 45º angle instead of parallel during implantation. Insertion began

slightly inferior to the right hind limb joint, and proceeded at a 45º angle towards the patella joint. Once the needle had entered the tissue approximately 0.3-0.7 cm, the needle was retracted to leave only the microdialysis probe in skeletal muscle. Probes were visually verified for their successful insertion into skeletal muscle following each *in vivo* experiment by full dissection, and probes were removed and examined post dissection to verify no membrane damage was incurred. Once probes had been allowed to equilibrate in skeletal muscle for 15-30 minutes, basal recordings were collected.

4.4.4 Amino Acid Signature of Skeletal Muscle

CE separations were performed every 22 seconds in skeletal muscle. Thirteen amines were able to be detected and identified in skeletal muscle, as shown in Figure 4.5A. As in adipose tissue, all amines were separated in under 15 seconds, with unlabeled peaks in the electropherograms corresponding to by-products of the derivatization reaction. Isoleucine and leucine were still able to be separated and individually identified, however their resolutions were significantly decreased. In fact, all resolutions were reduced in basal skeletal muscle traces as compared to adipose tissue. No separation conditions were altered to potentially cause this change. It would be expected that the change in tissue density would affect the tortuosity of amine diffusion for microdialysis sampling. This would affect solely relative recovery of the probe between these tissues. It can be postulated at this time that the differences in the sampled chemical matrix between adipose tissue and skeletal muscle are responsible for the diminished resolution observed, as that is the only changing variable in the separations.

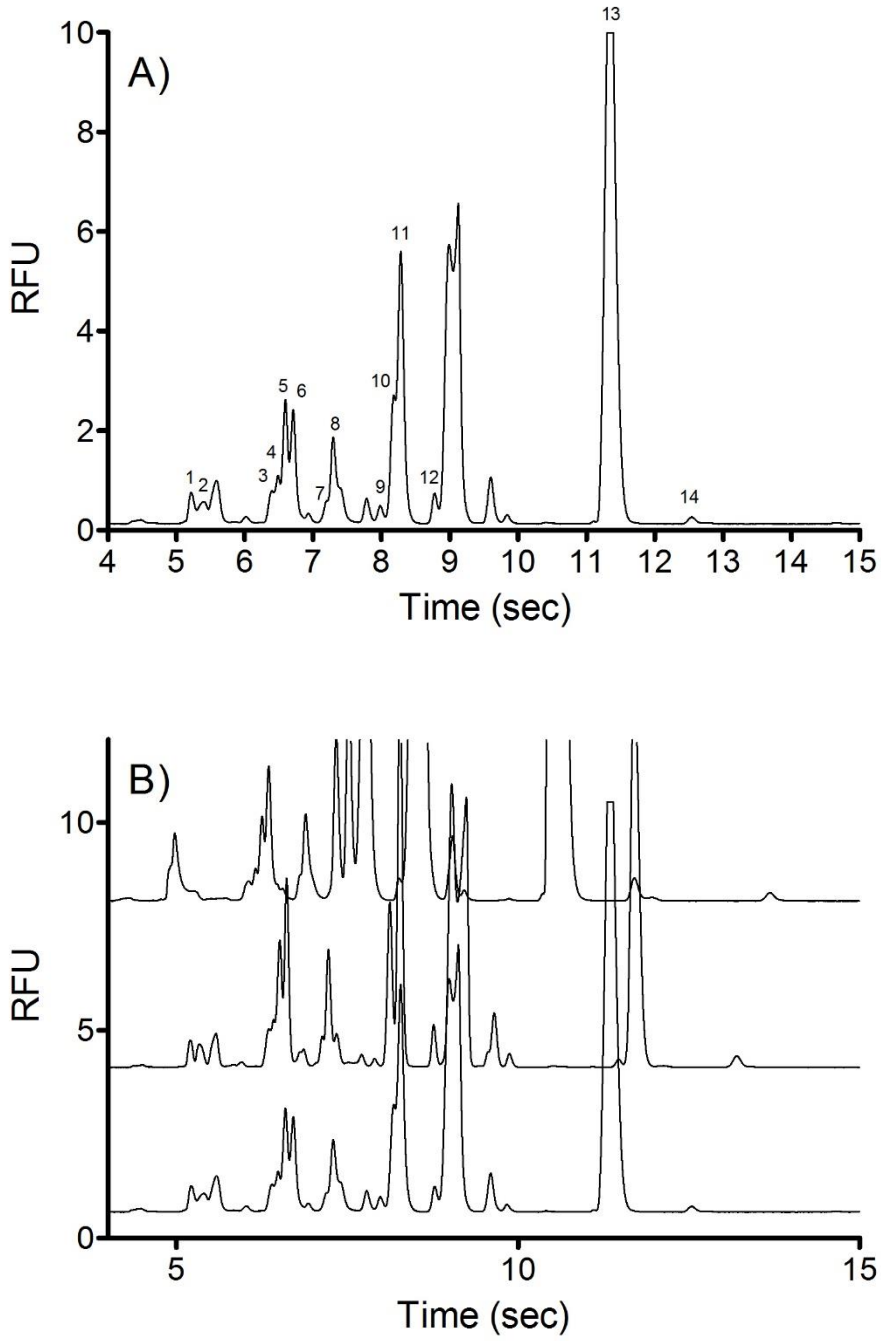

Figure 4.5. (A) Electropherogram of amino acids at basal levels in skeletal muscle. Peaks identified as (1) arginine, (2-3) lysine, (4) isoleucine, (5) leucine, (6) methionine, (7) phenylalanine, (8) valine, (9) GABA, (10) glutamine, (11) alanine, (12) glycine, (13) taurine, (14) glutamate. (B) Electropherograms of basal amino acids from skeletal muscle of three different mice.

Reproducibility of skeletal muscle's amino acid signature was verified in Figure 4.5B. As shown, the presence of the same amino acids is reproducible in three mice. Decreased resolution can be visualized in all electropherograms, supporting the hypothesis that a change found in the chemical matrix of skeletal muscle as compared to adipose tissue is responsible. Another interesting discovery was the presence of glutamate in all skeletal muscle basal recordings. Although present in significantly less quantities than isoleucine, leucine, valine, glutamine, and alanine, it is easily identifiable above baseline.

4.4.5 MD-CE Analysis of Bioamine Dynamics in Adipose Tissue

In order to fully understand the roles BCAAs play in overall body metabolism, their dynamics must be characterized as they respond to various metabolic stimuli. The online MD-CE assay is able to perform an analysis every 22 seconds, allowing dynamic changes to be recorded in near real time. As a demonstration, an intravenous injection of 2 U/kg insulin into the tail vein was given to a mouse. The microdialysis probe was implanted in inguinal adipose tissue, to record fat tissue's response to this systemic stimuli. The MD-CE assay was able to record basal measurements before the injection, during the initial stimulus, and through the refractory period as analyte concentrations re-stabilized. Basal levels recorded before stimulation allow relative changes to be assessed, with each mouse acting as its own control. Relative changes in analyte concentrations are commonly reported in microdialysis assays as compared to absolute concentrations since they do not depend on the validity of *in vitro* calibration, which may or may not accurately predict *in vivo* recovery.

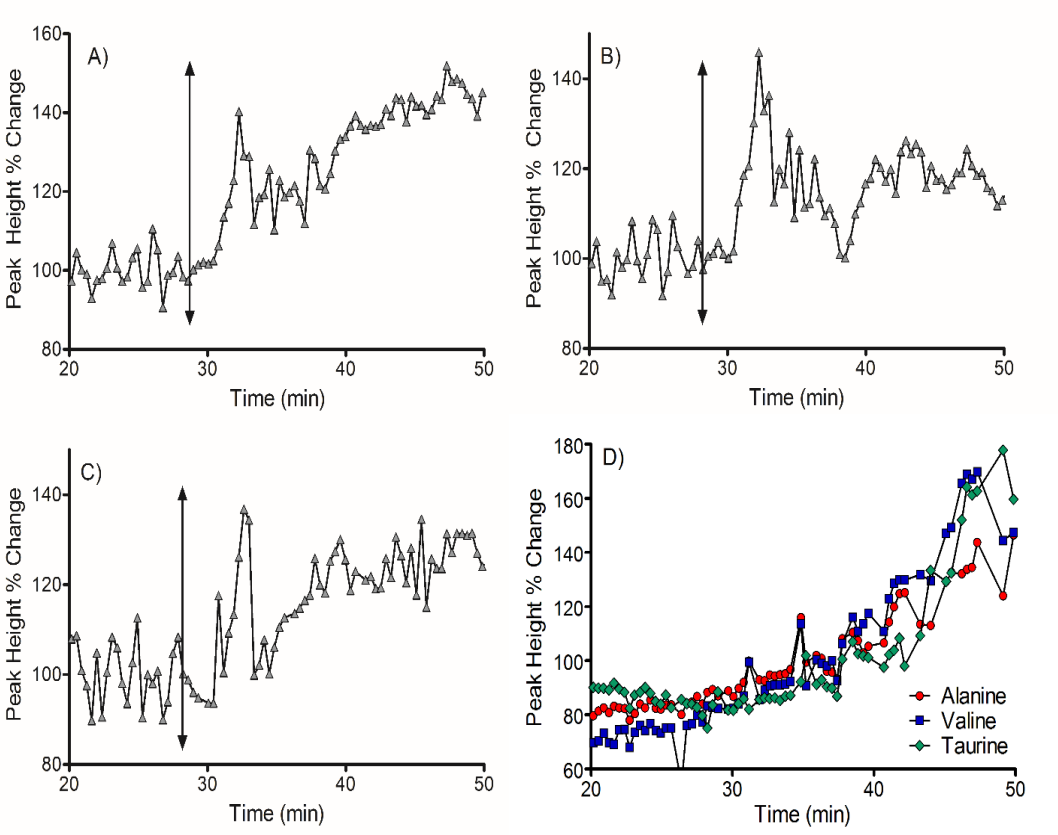

Figure 4.6. Valine (A), alanine (B) and taurine (C) traces in adipose tissue as insulin stimulation is applied. The time of stimulation is denoted on each graph by the drawn arrow. Amino acids responded with an increase within 5 minutes, before returning to an elevated baseline. Controls for each amino acid are displayed in (D).

Figure 4.6 displays the resulting dynamics induced via a systemic insulin stimulation. As shown in Figure 5.6A-C, basal levels of each amino acid were recorded for approximately eight minutes following a 20 minute probe equilibration period. The vertical line on each graph denotes the time at which the insulin stimulation was injected. Valine, alanine, and taurine levels increased markedly in adipose tissue within 5 minutes of the insulin injection before returning to an elevated baseline. Valine's peak height

increased 40% during the initial response before returning to a baseline elevated by 34% over original basal levels. Alanine's peak height initially increased by 46% with average levels post stimulation remaining elevated by 16%. Taurine's peak height increased by 37% during the initial stimulus before returning to an elevated baseline, 21% higher than the original basal levels. Average post stimulation levels for all three amino acids were significantly different than the original basal levels ($p < 0.001$). Figure 5.6D displays the negative control for each amino acid, in which their levels were monitored in inguinal adipose tissue without any stimulus. As shown, the levels of each amino acid do not drastically spike in the control data. Due to the negative control and individual bioamine results which showed initial spikes to varying degrees, it can be determined with confidence that the observed changes in Figures 5.6A-C are the result of induced biological dynamics from the insulin stimulation and not instrumental fluctuations.

In the same manner with which valine, alanine, and taurine were monitored every 22 seconds throughout a stimulation event, all other bioamines separated and identified in adipose tissue could be monitored as well. These three amino acids displayed the most significant changes due an insulin stimulation, and they all are of interest due to the metabolism-related goal of this research. Valine, as a BCAA, acts as a nutrient signal to the peripheral nervous system, regulates energy balance and appetite, and promotes protein synthesis and degradation.[19,22] Alanine is derived from BCAA metabolism and the degradation of pyruvate, and is linked to metabolic pathways such as the citric acid cycle, gluconeogenesis, and glycolysis. Taurine has also been shown to improve metabolism in animal studies, suggesting that supplementation could aide in the treatment of type 2 diabetes.[167]

4.5 Conclusion

This work integrated an online MD-CE assay capable of 22 second temporal resolution with *in vivo* sampling from inguinal adipose tissue and quadriceps skeletal muscle. An implantation procedure was developed for both tissues, utilizing a 19G hollow needle to minimize disturbances to surrounding tissue and providing precise probe placement. Following each experiment, probe placement and an intact probe membrane were visually verified by a full dissection. The presence of 12 and 13 bioamines were identified in adipose tissue and skeletal muscle, respectively. Both tissues demonstrated reproducible amino acid signatures between mice. To demonstrate the ability of the developed implantation procedure and online MD-CE assay for monitoring induced biological dynamics, an insulin stimulation was administered. Valine, alanine, and taurine levels were found to spike within 5 minutes, and post-stimulation levels remained significantly elevated compared to original basal levels in adipose tissue. This proved the ability of this assay to monitor *in vivo* dynamics on a 22 second timescale. Future studies will focus on applying a variety of stimulations to aide in determining the full role of BCAAs in adipose tissue's metabolism and energy regulation.

Chapter 5

In Vivo Monitoring of Induced Metabolism Dynamics in Adipose Tissue and Skeletal Muscle

5.1 Summary

Bioamines were monitored in adipose tissue and skeletal muscle while biologically relevant stimuli were administered to mice under anesthesia. Amino acid levels were recorded prior to, during, and post stimulation. All stimulations were administered through retrodialysis, directly into the tissue of interest, for a total of five minutes.

A 20 mM glucose stimulation was administered to four mice, with bioamine levels recorded in inguinal adipose tissue, and to three mice with results recorded in quadriceps skeletal muscle. In both tissues, no reproducible dynamics were observed for alanine, leucine, valine, or taurine. It was initially hypothesized that glucose wasn't evoking a strong response in the tissue due to its ability to be easily metabolized through glycolysis. Therefore the next stimuli chosen were artificial sweeteners, to compare their elicited response to that of glucose.

Saccharin (10 mg/kg) and ace K (2.4 mg/kg) were administered to three and two mice, respectively, with bioamines monitored in adipose tissue. For both stimulations, no reproducible trend emerged for alanine, leucine, valine, or taurine. The random responses observed from different mice appears to indicate that while the stimulation was administered directly to the tissue, it most likely is being immediately dispersed throughout the body, carried by plasma. This would cause the stimulus to be quickly diluted below the effective concentration administered. All body systems would also then be affected by this stimulus, and therefore responses recorded in adipose tissue do not

exhibit a dramatic and reproducible change, due to other tissues metabolizing the stimulus instead.

5.2 Introduction

Plasma BCAA levels have been found to be elevated in obese individuals as well as those with type 2 diabetes.[21,28,29] BCAA levels have also been found to be one of the best indicators of metabolic dysregulation, often appearing in advance of increased fasting glucose levels.[21,28] Adipose tissue is known to regulate BCAA levels,[30,31] as well as participate in the metabolism signaling network with the brain, liver, muscle, and pancreas.[10-12] In order to fully establish these bioamines as biomarkers for metabolic dysregulation, their dynamics under various metabolic conditions must be fully understood. Current research is limited in its time response for monitoring these bioamines, with typical analysis times ranging from minutes to hours.[119-121] Metabolism dynamics occur on a much faster timescale, and thus they must be monitored in as close to near real time as possible.

The body metabolizes glucose through glycolysis, to produce pyruvate, ATP, and NADH. ATP provides the necessary energy for the body to perform a variety of functions, and NADH is a coenzyme involved in the release of energy.[168] Induced bioamine metabolism dynamics will therefore be monitored as a response to glucose in near real time. In this way, it will be possible to examine these bioamines as adipose tissue is actively involved in metabolism. Glucose stimulations will also be administered to skeletal muscle to observe dynamics occurring in this tissue. Skeletal muscle, with its

protein synthesis and degradation supplying plasma amino acids during fasting states,[166] is an interesting point of comparison for adipose tissue's metabolism.

Initial FDA studies have found artificial sweeteners to be safe for human consumption, however recent findings have demonstrated saccharin and ace K to promote new adipocyte growth.[169] Preliminary studies conducted *in vitro* have displayed differences in amino acid metabolism in adipocytes – varying degrees of BCAA uptake and presence of downstream metabolites – when incubated with artificial sweeteners as compared to glucose.[170] With a high prevalence of artificial sweeteners in food and beverages consumed, the metabolic dynamics induced by artificial sweeteners should be examined as well. By comparing these dynamics with those induced by glucose, it can be determined whether or not the consumption of artificial sweeteners yields differing metabolic dynamics in adipose tissue on the timescale of seconds. This could explain why the increased use of artificial sweeteners throughout the years also corresponds to an increase in obesity within the United States.[2]

5.3 Materials and Methods

5.3.1 Chemicals and Reagents

Chemicals. Insulin (human recombinant, lot 15L255-B), saccharin, ace K, and all amino acid standards were purchased from Sigma Aldrich (St. Louis, MO). D-glucose was purchased from Gibco (Life Technologies Corp., Grand Island, NY) and sodium tetraborate decahydrate was purchased from CHEM-IMPEX Int'l Inc. (Wood Dale, IL).

Buffers and Solutions. All solutions were prepared in DI water (Milli-Q, 18.2 MΩ; Millipore, Bedford, MA) and filtered (0.22 μm). Ringer's solution was prepared with NaCl (123 mM), $CaCl_2$ (1.53 mM), KCl (4.96 mM) and 5 mM glucose with pH adjusted to 7.5. aCSF was comprised of NaCl (145 mM), KCl (2.7 mM), $MgSO_4$ (1.0 mM) and $CaCl_2$ (1.2 mM). The conditioning of microdialysis probes is the only instance in which aCSF was used during experimentation. Sheath flow buffer was comprised of 90 mM borate adjusted to pH 10 and CE separation buffer contained 90 mM borate/35 mM α-cyclodextrin (food grade, lot 010760F206, Cyclodextrin Technologies Development Inc., Alachua, FL) adjusted to pH 10. Insulin stimulation solution was prepared by dissolving 2U/kg insulin in 0.1 mL Ringer's solution. 20 mM glucose and 0.853 M ace K solutions were prepared in Ringer's solution. Saccharin stimulation solution was prepared by dissolving 10 mg of saccharin per kg of mouse in 1.0 mL Ringer's solution (approximately 1.36 mM saccharin solution). Derivatization solution was prepared by dissolving 40 mM NBDF (TCI America, Portland, OR) in methanol and mixing 1:1 with 500 μM HCl, producing a final concentration of 20 mM NBDF/250 μM HCl in 50% methanol. Derivatization solution was prepared daily and degassed under vacuum for 2 minutes prior to use.

5.3.2 Microdialysis

Microdialysis probes were constructed in-house using a side-by-side geometry as previously reported[101] (see Figure 4.1). Two 40 μm i.d. × 105 μm o.d. fused silica capillaries (Polymicro Technologies, Phoenix, AZ) were inserted into a 200 μm diameter

hollow fiber, regenerated cellulose dialysis membrane (13 kD MWCO, Spectrum Laboratories, Rancho Dominquez, CA) and off-set by 3 mm to generate a sampling region. Capillaries were sealed in place using polyimide resin (Alltech, Deerfield, IL). Prior to use probes were conditioned with ethanol (55 µL/h for 25 minutes) followed by aCSF (55 µL/h for 25 minutes). During analysis probes were perfused with Ringer's solution at 25 µL/h.

5.3.3 Online CE-LIF Instrumentation

Online Derivatization. Dialysate was transferred to a 250 µm i.d. stainless steel cross (Valco Instruments Co. Inc., Houston, TX) in a 40 µm i.d. × 360 µm o.d. fused silica capillary (see Figure 4.1). Borate buffer and derivatization solution were introduced at the reaction cross at 5 µL/h each. The derivatization reaction proceeded through a 90 cm long, 75 µm i.d. × 360 µm o.d. fused silica capillary, of which a 66 cm portion was heated to 80ºC, by running the capillary through flexible tubing containing water from a heating bath (NESLAB EX-7 Digital One heating bath circulator, Thermo, Newington, NH). Capillary dimensions and all flow rates produced a reaction time of 5 minutes.

High-Speed CE. Discrete sample plugs from the reaction capillary were injected onto a 6.2-6.5 cm long, fused silica CE separation capillary (5 µm i.d. × 360 µm o.d.) using a flow gated interface.[96] The separation and reaction capillaries were coaxially aligned leaving an approximately 50 µm gap in-between. Separation buffer was pumped through this spacing at 40 mL/h using a syringe pump (Pump 22 syringe pump, Harvard Apparatus, Holliston, MA). To perform an injection, buffer flow was stopped for 750 ms

using a pneumatically actuated valve (C2-3000A 10 port valve, Valco Instruments Co. Inc., Houston, TX) controlled by an in-house developed LabView program. Following this delay, -19 to -21 kV of injection voltage was applied at the outlet of the separation capillary for 100 ms. Buffer crossflow was then resumed as the potential was increased to the separation voltage (-21 to -23 kV) over a period of 500 ms.

Detection Scheme. Laser-induced fluorescence (LIF) detection was performed using the 488 nm line of a 60 mW diode pumped solid-state laser (Coherent, Santa Clara, CA). The laser beam was expanded using a 10× beam expander (Edmund Optics Inc., Barrington, NJ) and focused directly beneath the outlet of the separation capillary, in a sheath flow cuvette,[123] using a 1× lens. A 60×, 0.7 NA long working distance objective (Universe Kogaku, Oyster Bay, NY) collected fluorescence at 90º. Collected emission was passed through spatial (~1 mm) and bandpass filters (543.5 ± 10 nm) and detected using a photomultiplier tube (PMT R1477, Hamamatsu Corp., Bridgewater, NJ). Current was filtered with a 10 ms rise time, amplified (Keithley Instruments Inc., Cleveland, OH) and recorded using a data acquisition card (National Instruments Corp., Austin, TX). Data was analyzed using Cutter Analysis 7.0.[124]

5.3.4 *In Vivo* Characterization

All animal experiments were performed in strict compliance to the protocol approved by IACUC at the University of Minnesota. Mice were housed in RAR facilities and fed a standard chow diet. Prior to all experiments, mice experienced a 4 hour daytime fast. Male C57BL6 mice (20-25 g, 6-7 weeks of age; Envigo, Indianapolis, IN) were

initially anesthetized in an induction chamber (Harvard Apparatus, Holliston, MA) using isoflurane (5% in 1 L/min medical grade oxygen; Piramal Critical Care Inc., Bethlehem, PA). After sedation mice were fitted with an anesthesia mask (Scivena Scientific, Clackamas, OR) for maintenance of surgical anesthesia levels (2.5% isoflurane in 1 L/min oxygen). Microdialysis probes were implanted into the tissue of interest once the mouse was unresponsive to pedal and hind limb reflex testing. After insertion, the needle was pulled out of the tissue carefully, leaving the microdialysis probe in place. The probe was then secured and allowed to equilibrate for 15-30 minutes before basal concentrations were recorded. CE separations were performed every 22 seconds. Following basal recordings, stimulations were administered through retrodialysis for a period of five minutes.

5.4 Results and Discussion

5.4.1. Glucose Stimulation in Adipose Tissue

Initial stimulus experiments sought to expand on previous *in vitro* work done by Dr. Rachel Harstad, a former Bowser group researcher.[46] Dr. Harstad cultured 3T3-L1 adipocytes, which were then exposed to glucose and excess BCAAs. *In vitro* analysis concluded that in the presence of glucose, BCAAs were uptaken by adipocytes. Various concentrations of glucose were examined for their effect on adipocyte uptake. Glucose was selected as the first stimulation to be administered to adipose tissue with the intention of comparing the *in vitro* and *in vivo* assays.

Microdialysis probes were successfully implanted into inguinal adipose tissue of four different mice. A 20 mM glucose stimulation was provided via retrodialysis for five minutes, with bioamine levels monitored prior to, during, and post stimulation. Figure 5.1 displays the resulting traces for alanine, leucine, valine, and taurine (A → D respectively). Each bioamine's level was recorded every 22 seconds. The traces are expressed as time post stimulation, with the time of administered stimulus being denoted as 0 minutes, and levels recorded for 50 to 90 minutes post stimulation. The bar on each graph denotes the time at which an induced change would be expected to reach the detector. Dynamic changes were assessed as the percentage of peak height change compared to average basal levels. By assessing dynamics as relative changes, as opposed to absolute concentrations, each animal is able to act as its own control.

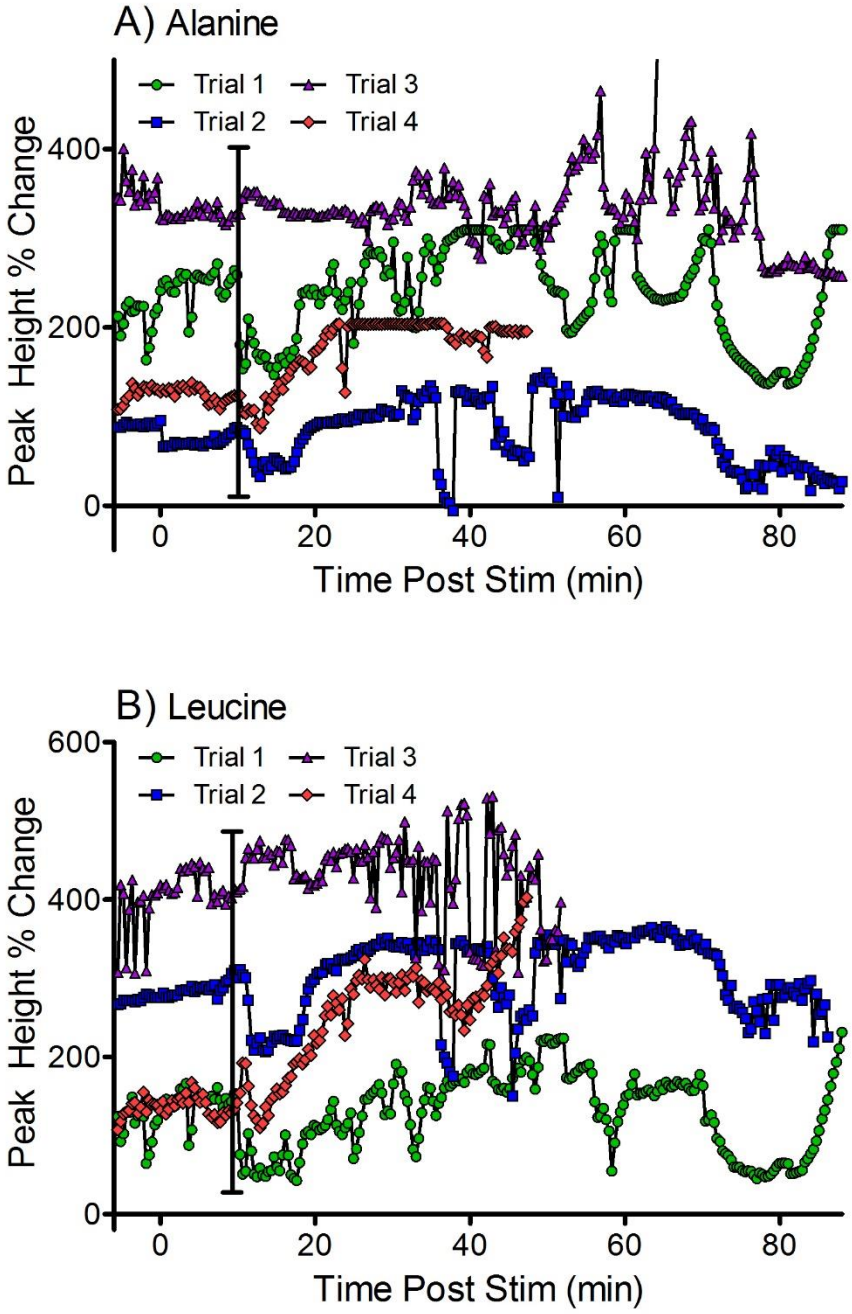

Figure 5.1. (A) Alanine, (B) leucine, (C) valine, and (D) taurine traces in adipose tissue of four mice during a 20 mM glucose stimulation. Bioamines were monitored prior to, during, and post stimulation. Administration of the stimulus occurred at time 0 on the recorded traces, and proceeded for 5 minutes. The bar indicates when induced dynamics are expected to reach the detector.

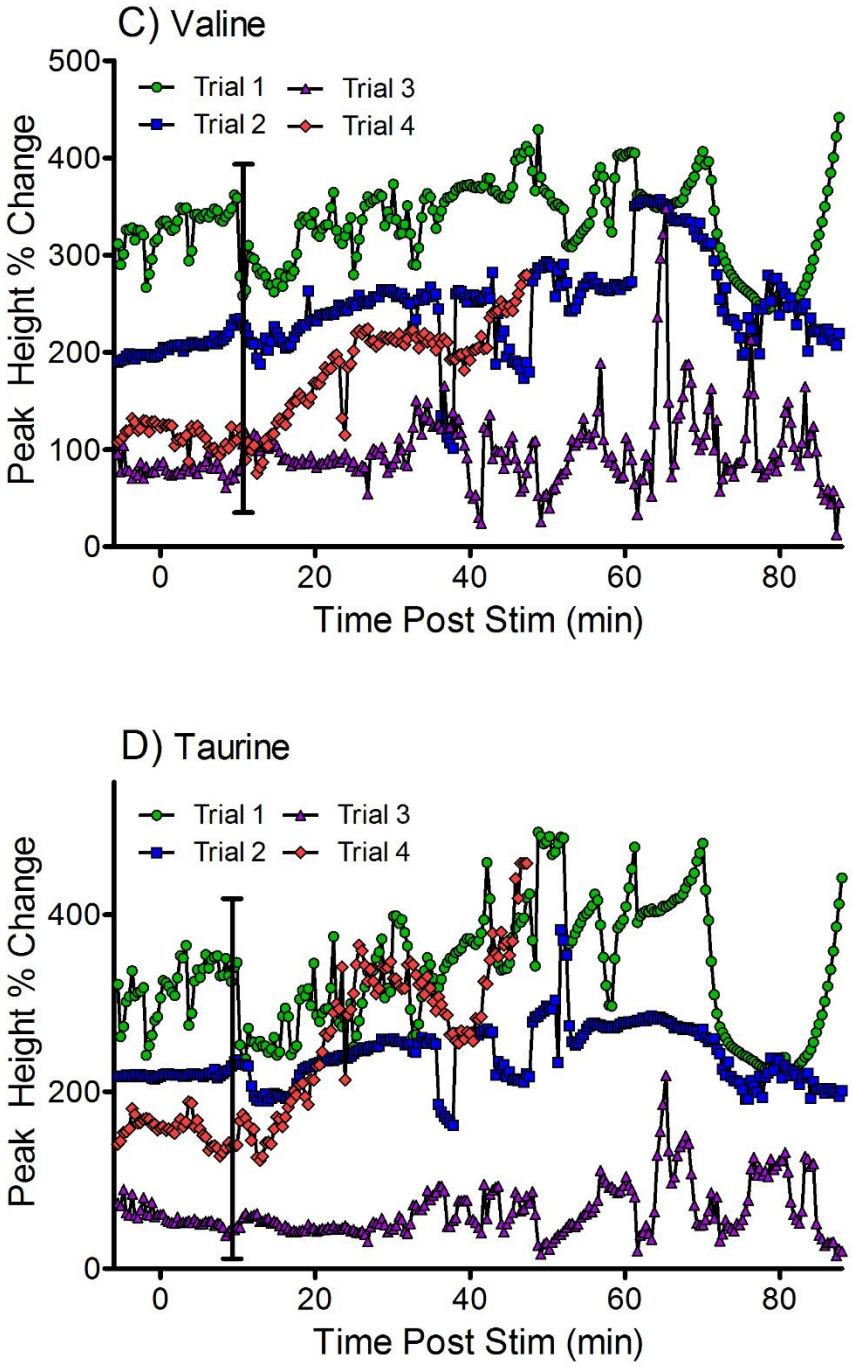

Figure 5.1. (A) Alanine, (B) leucine, (C) valine, and (D) taurine traces in adipose tissue of four mice during a 20 mM glucose stimulation. Bioamines were monitored prior to, during, and post stimulation. Administration of the stimulus occurred at time 0 on the recorded traces, and proceeded for 5 minutes. The bar indicates when induced dynamics are expected to reach detector.

As shown in Figures 5.1A-D, no reproducible dynamic changes were observed in adipose tissue for alanine, leucine, valine, or taurine due to a 20 mM glucose stimulation. Each trace initially fluctuates around 100% change in percentage peak height (100% being equivalent to the average basal peak height, with any deviation representing a change from basal levels). The traces have been manually offset from one another for ease of visualization. Some dramatic changes are observed, such as the decrease in peak height from trial 1 around 70 minutes post stimulation, however that exact change was observed in all bioamine traces. This is therefore hypothesized to be the result of instrumental fluctuations and not due to metabolism dynamics. The same principle holds true for the sharp declines in trial 2 at 37 and 45 minutes. Regardless, no bioamine traces demonstrated reproducible fluctuations with other trials, and therefore glucose was determined to induce no reproducible metabolism dynamics in adipose tissue at 20 mM delivered through retrodialysis.

It was hypothesized that no dynamics were established for glucose stimulations due to the body's ability to readily regulate circulating glucose. The next stimulation utilized an artificial sweetener, as a means to test whether the mouse's metabolism reacted differently to saccharin and ace K as compared to glucose.

5.4.2. Saccharin Stimulation in Adipose Tissue

Saccharin was administered via retrodialysis to inguinal adipose tissue for five minutes. The saccharin stimulation was set at 10 mg/kg (10 mg of saccharin per 1 kg of mouse), or twice the ADI, and was dissolved in 1 mL of Ringers' solution. The mice

utilized in the previous glucose study weighed an average of 25 g, and thus the saccharin stimulation solution was prepared for this dosage. Therefore the approximate concentration of stimulus was 1.36 mM saccharin. Figure 5.2 displays the traces of alanine, leucine, valine, and taurine (A→D respectively) with levels monitored prior to, during, and post stimulation. The time of stimulus administration is denoted by 0 minutes on the traces, with the bar on each graph representing the time of an expected induced dynamic change reaching the detector.

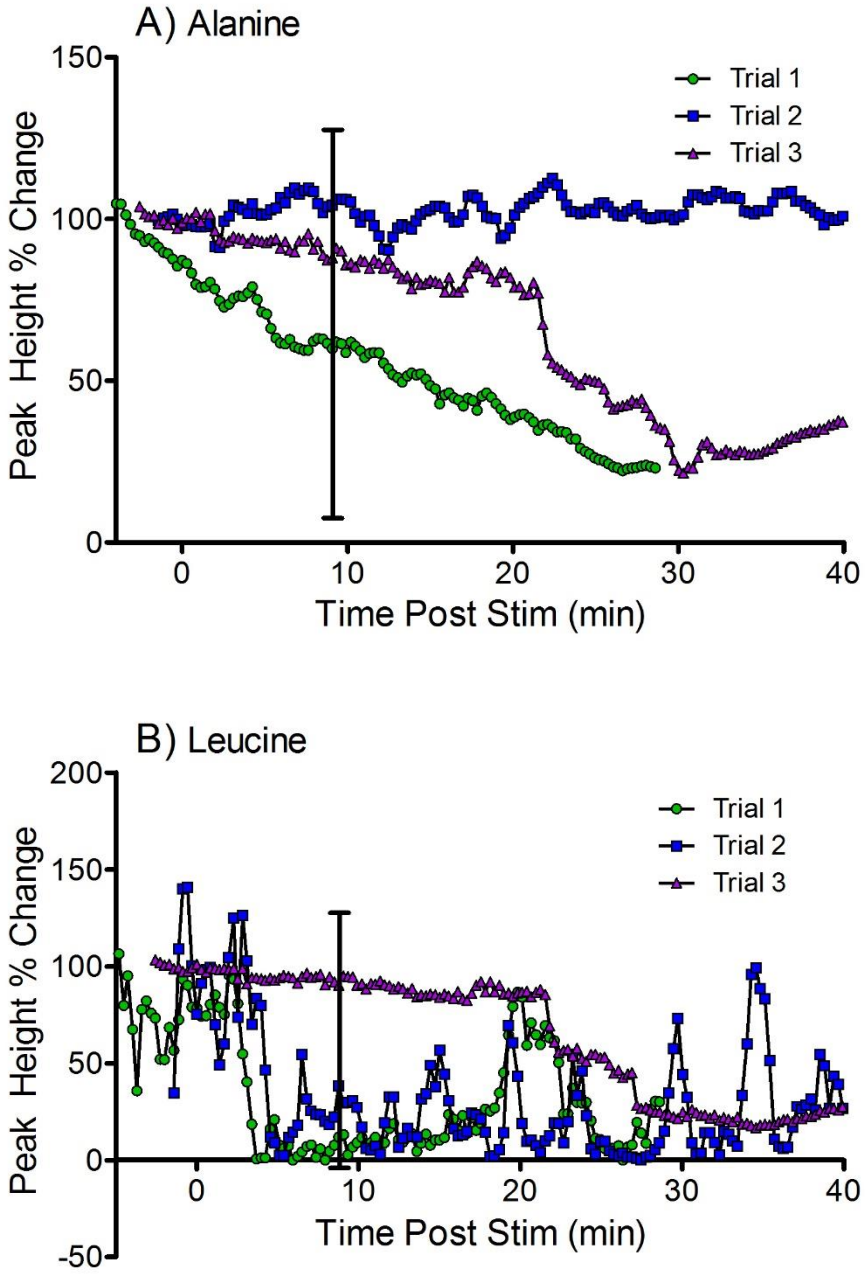

Figure 5.2. (A) Alanine, (B) leucine, (C) valine, and (D) taurine traces in adipose tissue of three mice during a 10 mg/kg saccharin stimulation. Bioamines were monitored prior to, during, and post stimulation. Administration of the stimulus occurred at time 0 on the recorded traces, and proceeded for 5 minutes. The bar indicates when the induced dynamics are expected to reach the detector.

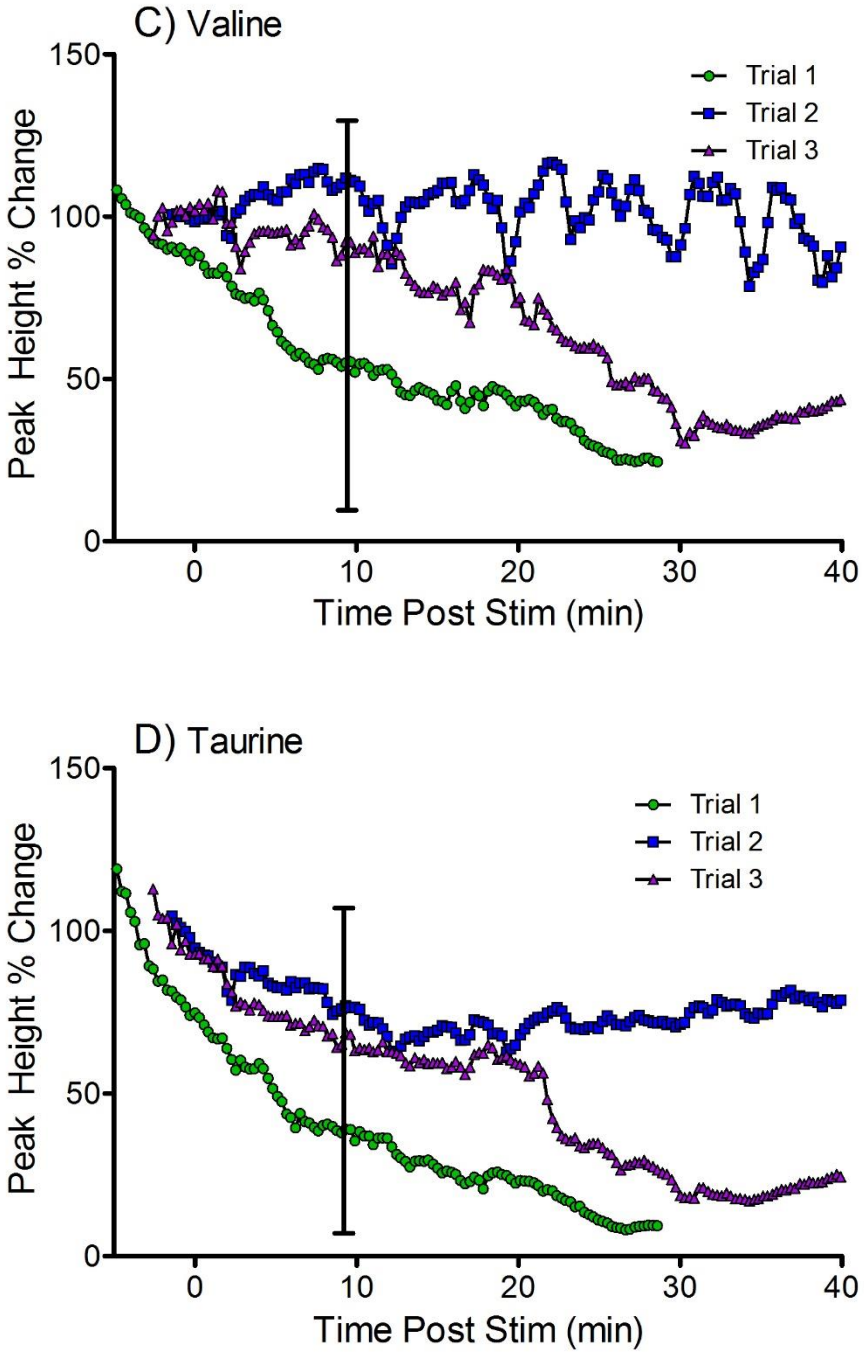

Figure 5.2. (A) Alanine, (B) leucine, (C) valine, and (D) taurine traces in adipose tissue of three mice during a 10 mg/kg saccharin stimulation. Bioamines were monitored prior to, during, and post stimulation. Administration of the stimulus occurred at time 0 on the recorded traces, and proceeded for 5 minutes. The bar indicates when the induced dynamics are expected to reach the detector.

In Figure 5.2A-D, the traces have not been manually offset. In the case of saccharin stimulations, each trial yielded such varying results, that a manual offset was not required to view the full trace. A total of three mice were examined for saccharin studies, and similar to glucose, no reproducible dynamics were observed for all bioamines.

Although the saccharin stimulation solution was prepared at twice the ADI (10 mg/kg), the tissue did not experience the full potency of this solution. As prepared, the entire 1 mL represented twice the ADI, but with the stimulation only administered for five minutes, that entire volume was not delivered to the tissue. Also, the recovery of the microdialysis probe (as determined in Chapter 2.4.4.), was determined to be approximately 17% for all analytes of interest. Relative recovery represents the fraction of analyte recovered from the tissue, but also signifies the fraction of perfusate, or stimulation, that is delivered to the tissue. Based on the amount of volume delivered through the probe in five minutes, and accounting for 17% relative recovery, it is estimated that the tissue only experienced 0.0035 mg/kg of the intended 10 mg/kg saccharin dose. For the next serious of stimulations, the maximum dosage of ace K was ensured to be delivered to the tissue, to determine whether a higher concentration of stimulus was required to elicit metabolism dynamics *in vivo*.

5.4.3. Ace K Stimulation in Adipose Tissue

The maximum allowed dosage for ace K as per our IACUC protocol is 30 mg/kg, or twice the ADI. In order to ensure that this maximum concentration is delivered to the

tissue of interest, factors such as total volume delivered and the recovery of the probe must be taken into account.

The perfusion flow rate through the probe is set at 25 µL/hr. This flow rate is optimized for the NBDF derivatization reaction, and thus is consistent throughout all experiments. Stimulations are administered for five minutes, which indicates that a total volume of 2.083 µL of stimulation solution is delivered through the probe in this time. The relative recovery of the microdialysis probe is 17%, which also approximates the fraction of stimulant, or ace K, which will be administered to the tissue from the stimulation solution.

Assuming a 25 g mouse, as was the average for all adipose tissue glucose experiments, 30 mg/kg of ace K stimulation would require a total of 0.75 mg, or 3.73×10^{-6} moles of ace K to be delivered to adipose tissue within five minutes. To deliver 3.73×10^{-6} moles of ace K, in 2.083 µL of stimulation solution, while accounting 17% recovery/delivery, the stimulation solution perfused through the probe must be 10.52 M ace K.

A sugar solution of 10.52 M is not able to be perfused through the microdialysis probe, as its viscosity could negatively impact the flow of solution through the derivatization capillary. Thus a solution of 0.853 M was prepared instead, which corresponds to approximately 2.4 mg/kg ace K. Figure 5.3 displays the traces of alanine, leucine, valine, and taurine prior to, during, and post stimulation. The stimulation start time is denoted by 0 minutes on the traces below, and the bar represents the time at which any induced dynamics reach the detector.

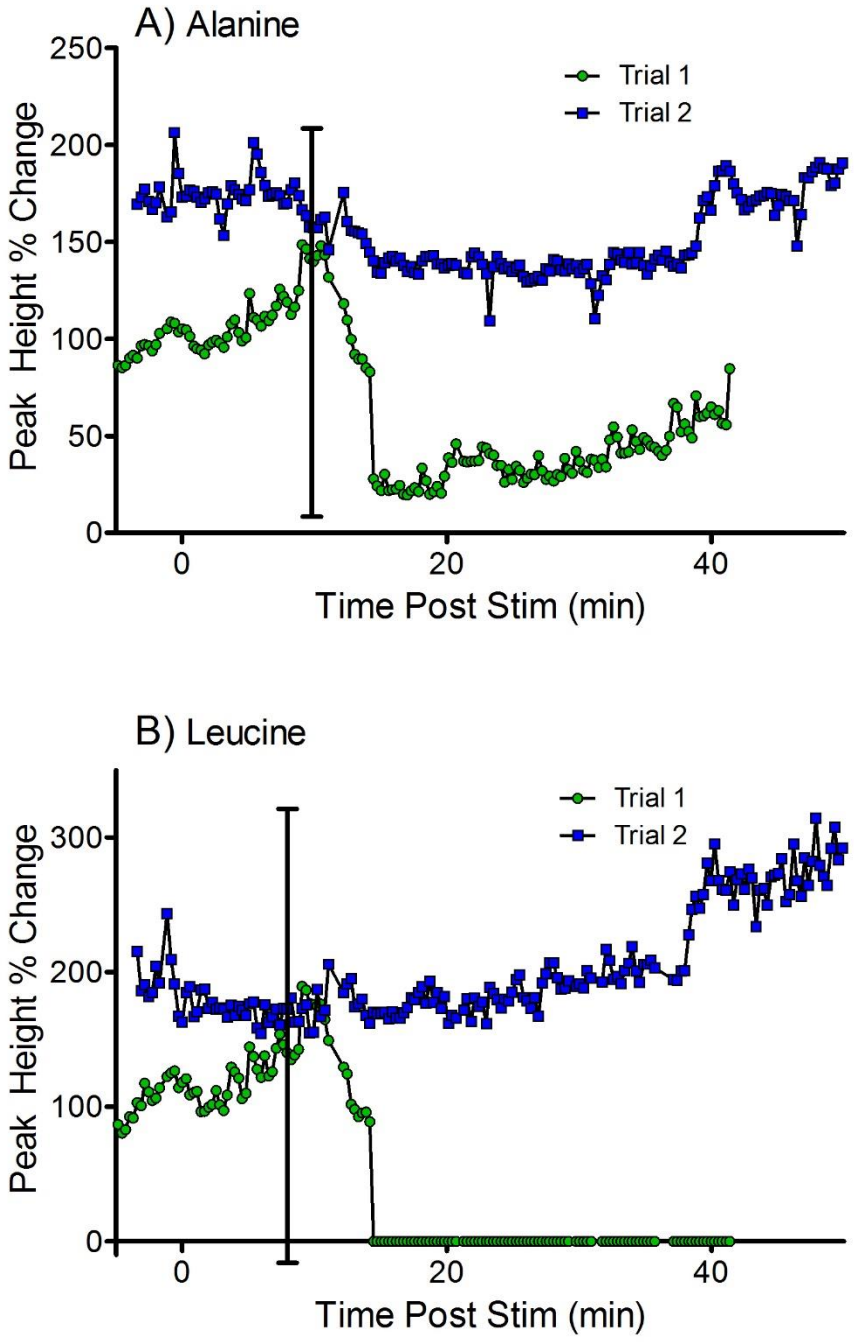

Figure 5.3. (A) Alanine, (B) leucine, (C) valine, and (D) taurine traces in adipose tissue of two mice during a 2.4 mg/kg ace K stimulation. Bioamines were monitored prior to, during, and post stimulation. Administration of the stimulus occurred at time 0 on the recorded traces, and proceeded for 5 minutes. The bar indicates when induced dynamics are expected to reach the detector.

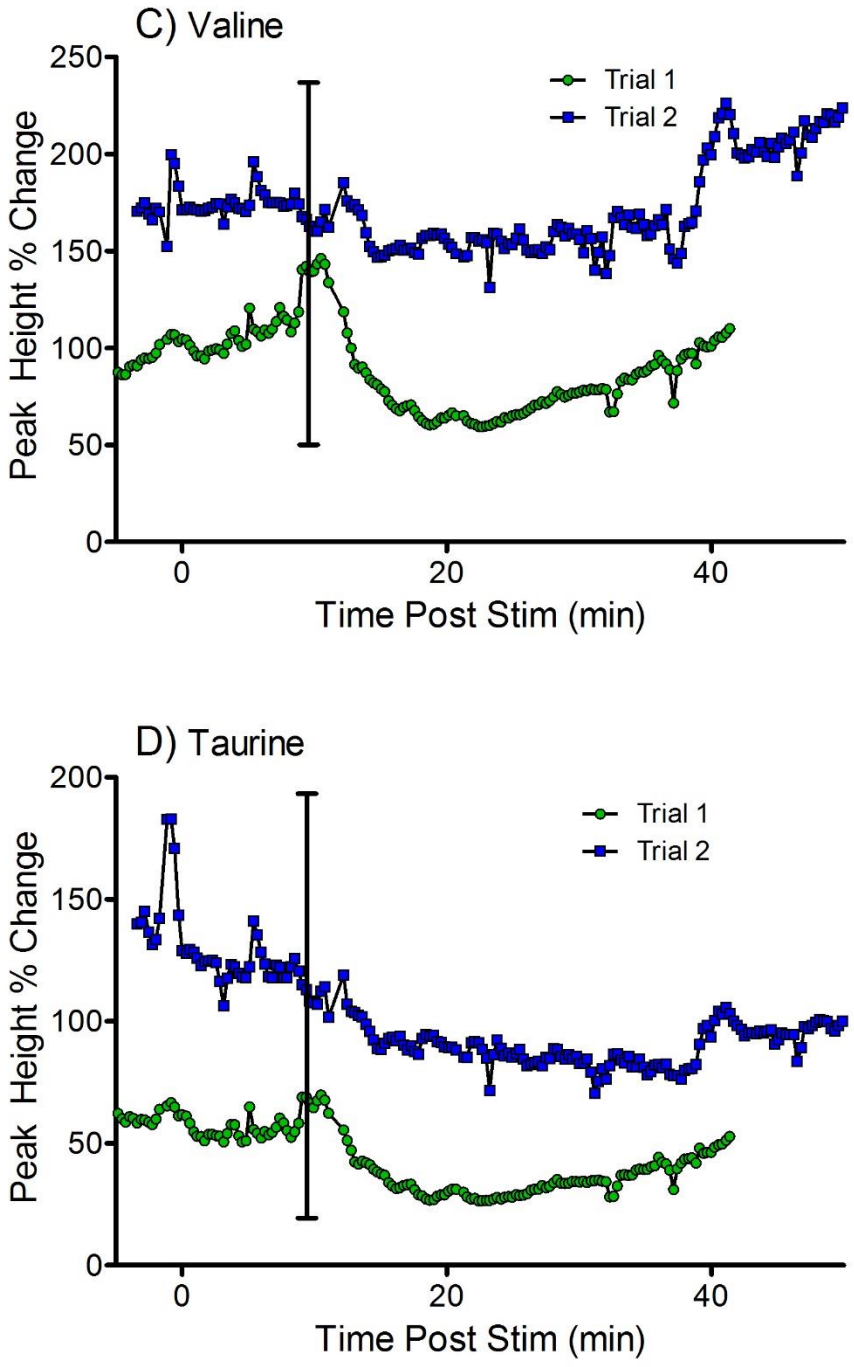

Figure 5.3. (A) Alanine, (B) leucine, (C) valine, and (D) taurine traces in adipose tissue of two mice during a 2.4 mg/kg ace K stimulation. Bioamines were monitored prior to, during, and post stimulation. Administration of the stimulus occurred at time 0 on the recorded traces, and proceeded for 5 minutes. The bar indicates when induced dynamics are expected to reach the detector.

Traces in Figure 5.3 have been manually offset for ease of visualization. Leucine in trial 1 decreased below the LOD following the stimulus, and therefore the system was unable to monitor any induced dynamics. It appears that the examined bioamines demonstrate a slight increase in peak height around 10 minutes, which is the first time at which an induced dynamic would be expected to reach the detector. However, following the slight initial increase, trial 1 bioamines decrease throughout the remainder of the experiment. Taurine exhibits a similar trace for trial 2, however alanine, leucine, and valine in trial 2 remain fairly consistent. The general decrease in trial 1 bioamines could be due to a decline in the animal due to anesthesia, however more trials are necessary to conclude whether or not this is an induced dynamic. These results appear to show an induced dynamic immediately following stimulus administration. This preliminary evidence supports the idea that a more concentrated dose of stimulus is required to elicit a biological response when administered via retrodialysis. Further studies are required to conclude if the responses observed in these trials are induced by ace K.

5.4.4. Glucose Stimulation in Skeletal Muscle

With glucose, saccharin, and ace K all yielding no reproducible response in induced metabolism dynamics in adipose tissue, it was decided to administer glucose stimulation in skeletal muscle. Skeletal muscle is actively involved in protein synthesis and degradation, and thus its induced metabolism dynamics are an interesting point of comparison against adipose tissue. A 20 mM glucose stimulation was administered to quadriceps skeletal muscle for five minutes via retrodialysis. This concentration of

glucose was selected due to its previous utilization in adipose tissue studies providing a direct line of comparison between the two tissues.

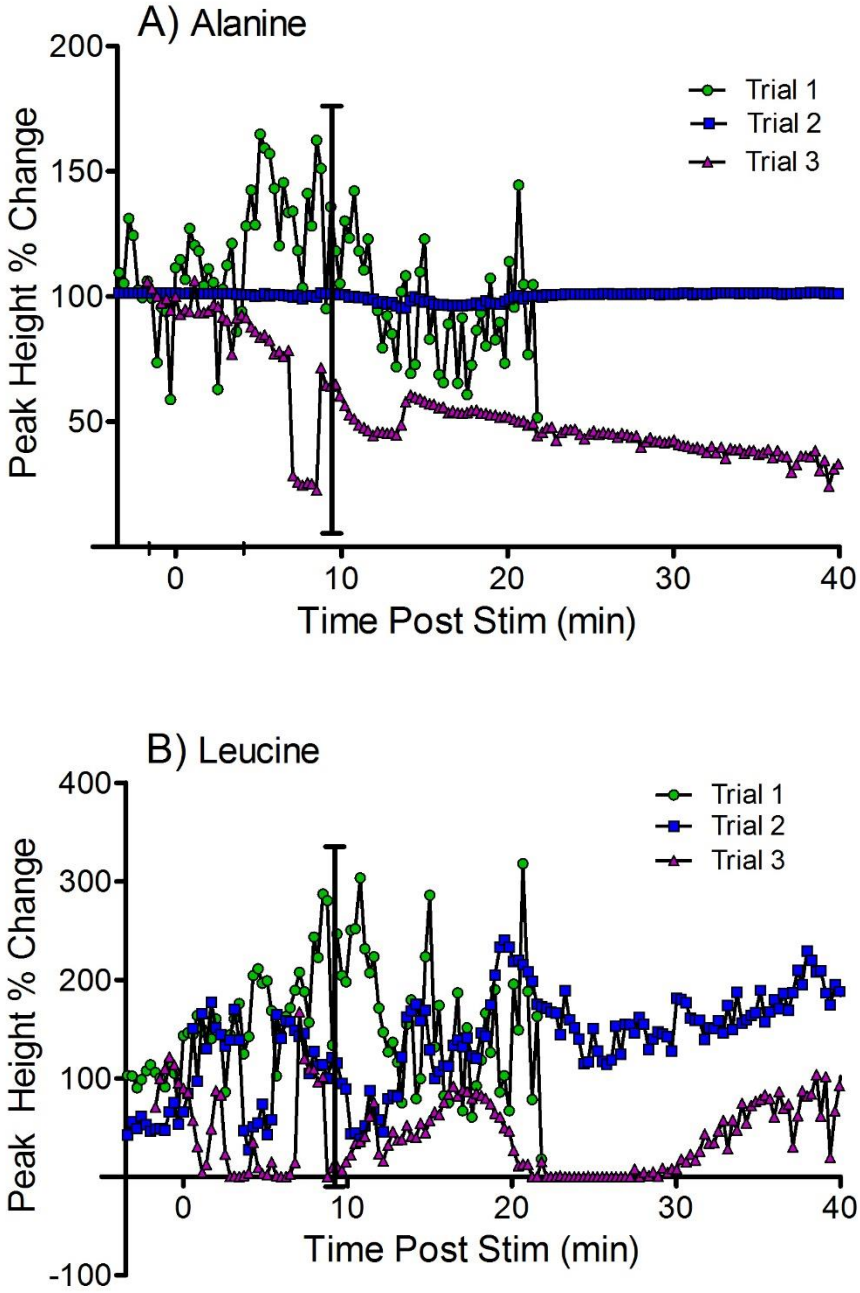

Figure 5.4. (A) Alanine, (B) leucine, (C) valine, and (D) taurine traces in skeletal muscle of three mice during a 20 mM glucose stimulation. Bioamines were monitored prior to, during, and post stimulation. Administration of the stimulus occurred at time 0 on the recorded traces, and proceeded for 5 minutes. The bar indicates when induced dynamics are expected to reach the detector.

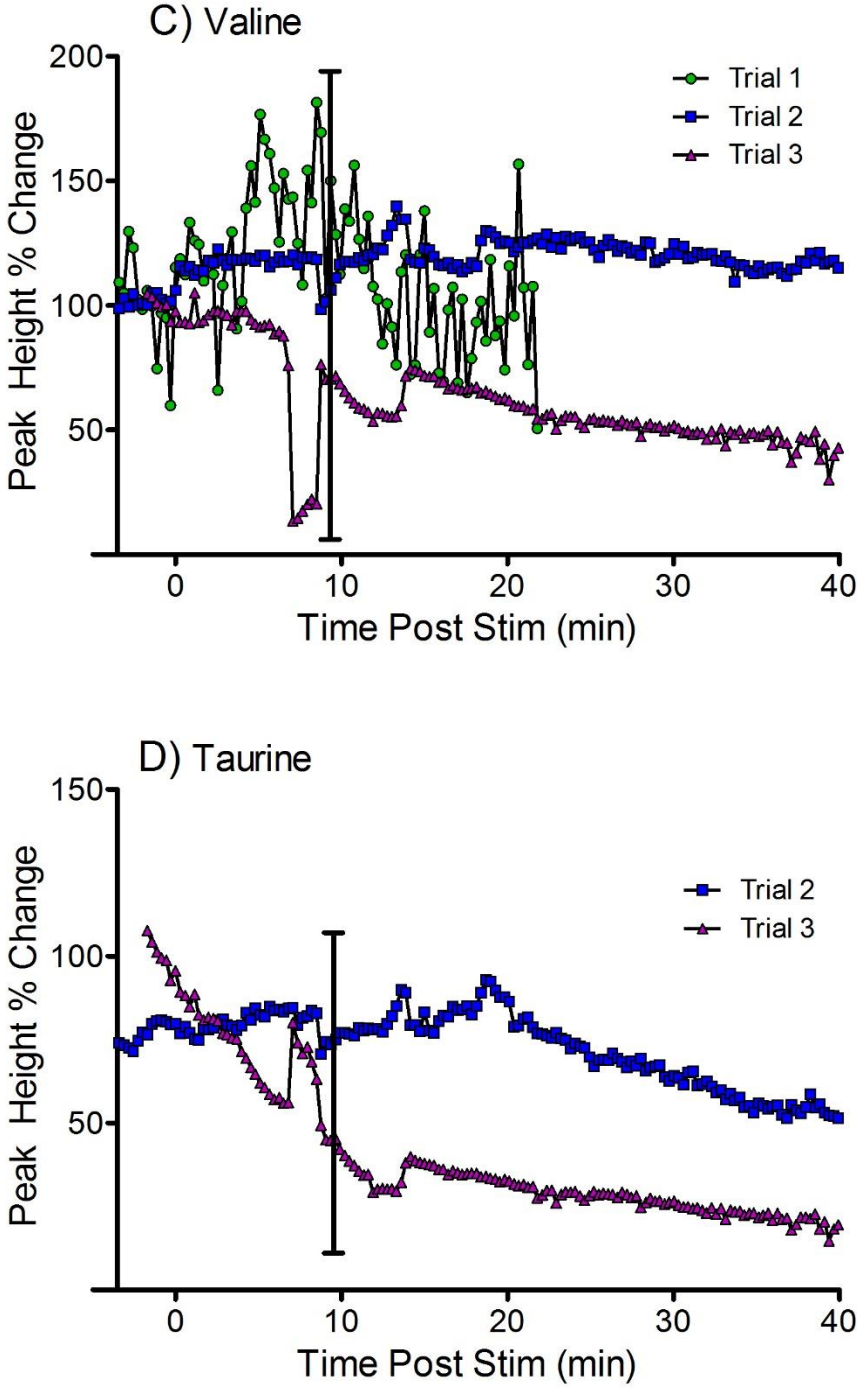

Figure 5.4. (A) Alanine, (B) leucine, (C) valine, and (D) taurine traces in skeletal muscle of three mice during a 20 mM glucose stimulation. Bioamines were monitored prior to, during, and post stimulation. Administration of the stimulus occurred at time 0 on the recorded traces, and proceeded for 5 minutes. The bar indicates when induced dynamics are expected to reach the detector.

The time of stimulus administration is denoted by 0 minutes on each trace, with the bar representing when an induced dynamic would reach the detector. Alanine, valine, and taurine (Figure 5.4A, C, and D respectively) have not been manually offset. The bioamine levels from each trial yielded varying traces that are easily visualized. Leucine, displayed in Figure 5.4B, has been manually offset to allow for easier visualization of each trace. All traces initially fluctuate around 100% peak height change, which is representative of the average basal level. Taurine was only able to be examined in two trials, as during the first trial, its signal maxed out the detector for the entire experiment. Any efforts to reduce amplification of signal to better examine taurine, resulted in all other bioamines not generating enough signal to be monitored. Therefore, no changes were able to be assessed in taurine's signal from trial 1.

No reproducible dynamics were observed in skeletal muscle for alanine, leucine, valine, or taurine due to a glucose stimulation. It is hypothesized that due to all stimulations being administered via retrodialysis, they are in fact not entering and affecting the tissue of interest. Instead the stimuli are being quickly diluted and distributed through the body to affect all tissues. A higher concentration of stimulus is likely required to elicit a biological response from tissues *in vivo* when administered through retrodialysis.

Examining bioamine traces, throughout all administered stimuli, induced dynamics appear to be potentially present. Several trials in each administered stimuli exhibit sharp changes in bioamine peak height around 10 minutes, which is when the initial stimulus is expected to reach the detector. With only several trials in each stimulus, it is not possible to confidently conclude whether or not the dynamics occurring are due

to the stimulus provided. More trials in each study could produce a pattern of bioamine responses that due to animal to animal variability, are not immediately evident after several preliminary trials.

5.5 Conclusion

Biologically relevant stimulations of glucose, saccharin, and ace K were administered through retrodialysis to inguinal adipose tissue and quadriceps skeletal muscle. Bioamine traces of alanine, leucine, valine, and taurine were monitored prior to, during, and post stimulation, with dynamic changes assessed as the percentage of peak height change as compared to the average basal levels. No reproducible dynamics were observed as a result of any stimulation administered, even when the stimulation was ensured to deliver the maximum dosage directly to the tissue. This is believed to be due to the stimulation being diffused throughout the entire body upon delivery, and thus not solely affecting the tissue as anticipated. It is also plausible that more trials in each study would produce a pattern of induced dynamics.

Chapter 6

Summary and Future Outlook

6.1 Summary

The described work outlines the development and application of an analytical platform capable of monitoring amino acid metabolism dynamics *in vivo* in near real time. The online high-speed CE instrument coupled with microdialysis sampling was optimized for near real time analysis of BCAAs and their related metabolites in chapter 2. Addition of 35 mM α-cyclodextrin to the separation buffer (90 mM borate, pH=10) allowed for the separation of all BCAAs and their downstream metabolites (glutamine, alanine, and glutamate).[122] All amino acids of interest were able to be identified in a standard separation, with modest sacrifices made in resolution to achieve the fastest time response possible. LODs ranged from 690 nM to 6.5 µM depending on the analyte examined. These calculated LODs were significantly lower than the anticipated biological concentrations in adipose tissue and skeletal muscle, and therefore deemed sufficient to proceed towards *in vivo* studies. Microdialysis probe recovery was calculated to be between 14% and 18% for all analytes of interest. The temporal response of the system was determined to be 22 seconds, a vast improvement over previous utilization of this separation assay.[122]

In chapter 3, an entire *in vivo* protocol was designed and developed to allow for a variety of future *in vivo* experiments. C57BL6 male mice were selected as the model due to their frequent use in obesity research.[127,128] Male mice were chosen exclusively in order to avoid the complexities of mammary glands within adipose tissue depots as found in female mice.[130,131] The inguinal adipose tissue depot and quadriceps of the hind limb were selected as the tissue locations due to their metabolic properties[133] and ease of

accessibility for microdialysis probe insertion.[135] Microdialysis probes were to be inserted into tissue locations using a hollow needle, which would be subsequently pulled back over the probe to leave only the dialysis membrane in the tissue for sampling. Probe insertion was to begin once the mouse was under surgical levels of anesthesia.

Isoflurane inhalant anesthetic was chosen for its rapid induction[136] and recommended use on C57BL6 strains.[140] Initial induction was designed to take place in an induction chamber, with surgical levels of anesthesia maintained throughout the experiment at a nose cone. Euthanasia was set to conclude each experiment by means of an intracardiac dose of KCl under anesthesia, followed by a thoracotomy as a secondary procedure. A complete and detailed SOP is provided at the conclusion of chapter 3, in the attempt to pass along developed animal handling knowledge to potential future researchers joining the project.

Initial biological experiments were outlined in chapter 4, both in inguinal adipose tissue and quadriceps hind-limb muscle. Reproducible microdialysis probe insertion into both types of tissue was developed and verified by full tissue dissection following each experiment. Probes were also examined post-dissection to ensure the dialysis membrane was not damaged during implantation. All amino acids of interest were separated and identified within a 15 second separation window. In adipose tissue, 12 amines were detected at concentrations significantly higher than the LOD while 13 amines were detected in skeletal muscle. Glutamate was not found in adipose tissue in any detectable quantity, however its presence was able to be monitored in skeletal muscle. The amino acid signature of both tissues was found to be reproducible between different mice.

An insulin stimulation was provided via the tail vein to induce metabolism dynamics in adipose tissue. Dynamic changes were able to be observed in several bioamines, indicating the developed analytical platform was in fact able to monitor induced biological dynamics. Chapter 5 focused on various stimulations provided to adipose tissue and skeletal muscle. A glucose stimulation did not yield reproducible induced dynamics when provided to either adipose tissue or skeletal muscle. Saccharin and ace K stimulations were administered to adipose tissue, both yielding no reproducible induced metabolism dynamics. Glucose, saccharin, and ace K stimulations were administered to adipose tissue through retrodialysis, and therefore it is possible that the stimulations were cleared from the adipose tissue and circulated through the body before any noticeable effect on adipose tissue was able to take place. Sampling from various other tissue locations (i.e. skeletal muscle), while administering the stimulation still in adipose tissue, would allow for determination as to whether other tissues were being affected by the stimulation. If metabolism was induced in skeletal muscle from a stimulation provided through retrodialysis in adipose tissue, it would indicate the stimulation is being cleared from adipose tissue, and circulated throughout the body.

6.2 Future Outlook

An analytical platform capable of near real time analysis of metabolism dynamics in adipose tissue and skeletal muscle has been fully developed. The separation assay's performance has been characterized and optimized to allow for a 22 second temporal resolution, and the reproducible implantation of microdialysis probes into adipose tissue

and skeletal muscle was designed and verified. Initial biological stimulations focused on induced metabolism dynamics in the inguinal adipose tissue of C57BL6 male mice by glucose and artificial sweeteners. Adipose tissue was the predominant tissue of interest due to its active role in the signaling network to maintain energy balance[13,14] and its regulation of circulating BCAA levels.[30,31] BCAAs are known to be actively involved in insulin secretion,[10] protein synthesis and degradation,[12] and appetite control,[11] as well as acting as one of the best predictors of metabolic disorders such as diabetes.[21,28]

Previous *in vitro* work utilizing adipocytes in an offline analysis demonstrated altered metabolism when adipocytes were incubated with glucose and fructose, ace K, stevioside, or saccharin. Dr. Rachel Harstad, a former graduate student in Dr. Bowser's lab, discovered that adipocyte incubation with 5 mM glucose and 30 mM fructose diminished BCAA uptake as compared to incubation with 5 mM glucose. Incubation with 5 mM glucose and 64.5 µM stevioside did not further induce BCAA uptake as compared to controls, however glutamate release was promoted.[170] With these preliminary *in vitro* results, further analysis of metabolism dynamics was desired *in vivo*, where the result of interworking bodily systems could be examined. Glucose, saccharin, and ace K were administered as stimuli, however results indicated that no noticeable metabolism dynamics were induced. This most likely indicated that at the concentrations provided, circulating blood was able to clear the stimulus and diffuse it through the entire body. The research thus far indicates that in an *in vivo* system, at the tested concentrations, metabolism did not respond any differently to artificial sweeteners as compared to glucose.

The next step in this project would be to examine a variety of concentrations for each stimuli, in order to gain pharmacokinetic information. In this way, it could be determined if there is a specific concentration of artificial sweeteners and/or glucose in which the body begins to experience altered metabolism. The near real time aspect to data collection will not only demonstrate at what concentration the stimuli begins inducing different metabolism dynamics, but also how the metabolism dynamics are altered. Information as to how metabolism dynamics are altered under varying conditions of artificial sweetener stimuli would provide key insights into their nutritional use for preventing and combating obesity.

Another direction for the future of this project would be to reproduce all preliminary stimuli and corresponding pharmacokinetic experiments in the inguinal adipose tissue depot of ob/ob mice. The ob/ob mouse has a genetic knockout that prevents the hormone leptin from being produced.[171] Leptin plays a significant role in appetite signaling to the brain,[172] and thus without it, mice consume food excessively. Mice then gain an extreme amount of weight and frequently develop high blood sugar. This mouse phenotype is frequently used in metabolism, obesity, and type 2 diabetes studies. Reproducing these stimuli experiments in this model would provide insight into potential altered metabolism dynamics in adipose tissue when in an obese or type 2 diabetic state.

A final alternative direction for the future of this project would involve switching focus from adipose tissue to skeletal muscle as the predominant tissue of interest. Skeletal muscle constitutes approximately 40-50% of total body mass in the average adult male,[173] and with its significant role in glucose regulation[174] and protein storage,[175] changes in its

metabolism would have an immense impact on the body's overall metabolism and energy regulation.[176] While muscle metabolism is well understood, the complete effects of artificial sweeteners on induced metabolic dynamics have yet to be fully realized. Recent findings have demonstrated saccharin and ace K to promote new adipocyte growth,[169] and preliminary studies in adipocytes displayed differences in amino acid metabolism when they were incubated with artificial sweeteners as compared to glucose.[170] If metabolic dynamics in adipocytes are altered when induced by artificial sweeteners, it could be assumed that skeletal muscle cells would experience similar changes.

To examine altered metabolism dynamics induced by artificial sweeteners in skeletal muscle, an *in vitro* assay should be employed initially. This would avoid the complex responses due to interworking bodily systems often seen in *in vivo* experiments, and thus skeletal muscle cell's sole response to all stimuli could be examined. The biological model proposed would be an immortal mouse skeletal myoblast cell line, C2C12. This cell line was derived from a C3H mouse donor's satellite cells in the thigh muscle.[177] These myoblasts are frequently used for the studies of muscle development and differentiation,[178] and are commercially available.

The culture and passaging of C2C12 myoblasts has been well documented.[179] Briefly, cells can be grown in an incubator at 37 ºC with 5% CO_2. Their growth medium contains DMEM (Dulbecco's Modified Eagle Medium), FBS (fetal bovine serum) and P/S (penicillin/streptomycin) solution. Myogenic differentiation begins immediately once cells reach confluency; therefore additional collections of myoblasts can be regenerated from the immortal cell line by passaging cells into new culture dishes prior to reaching confluency. The original immortal line and new passages can be stored long term by

freezing in liquid nitrogen. Cell viability can be determined by fluorescein diacetate (FDA) staining. FDA is a non-fluorescent compound that generates a fluorescent signal only once it is taken up by mammalian cells and has the acetate groups removed by active intracellular enzymes.[180] This is an excellent method to verify cell viability as cells must be active in order to generate a fluorescent signal under confocal microscopy.

After verification of cell viability, skeletal muscle metabolism would be characterized. By examining the amino acid uptake/release of cells in the presence of either glucose or artificial sweeteners, the differences these stimuli have on the overall metabolism of skeletal muscle cells can be determined. Upon reaching confluency, the cells can be incubated in an excess of glucose for 30 minutes. Post incubation, the incubation medium will be collected and transferred to an Eppendorf tube. A microdialysis probe will be placed in the Eppendorf tube to sample small molecule analytes for offline analysis by high-speed CE. This entire procedure would then be repeated, incubating muscle cells with a variety of artificial sweeteners (ace K, saccharin, aspartame, fructose, steviol), testing all stimuli at varying concentrations. These offline studies will then allow for the determination of overall amino acid metabolism from muscle cells as a result of incubation with artificial sweeteners versus glucose.

Following the characterization of skeletal muscle cell's overall amino acid uptake/release induced by glucose or artificial sweeteners, dynamic changes can monitored using online high-speed CE. By monitoring the dynamic changes in amino acid uptake/release, their rate of metabolism can be studied. Changes to this metabolic rate and overall outcome will provide valuable insight into how these sweeteners behave differently in muscle tissue.

Skeletal muscle cells would be grown to confluency on the surface of a microdialysis probe as previously described.[45] Dr. Amy Stading, a previous Bowser researcher, was able to successfully grow astrocyte cells on the surface of a microdialysis probe and monitor their response to stimuli by inclusion of the stimuli into the perfusate. Dr. Harstad was unable to repeat this protocol with adipocytes however, presumable due to adipocyte cell size being so large compared to the surface area of the probe (average adipocyte cells are >100 µm in diameter[181]). This online technique would be dependent on myoblasts adhering to the microdialysis probe. The length of a C2C12 myotube was found to be 130-520 µm.[182] Adjustments could be made to the probe size to make adhesion more attainable. If optimization of this *in vitro* protocol was unsuccessful, online analysis would have to proceed with myoblasts cultured in a cell flask, and sample of cell media collected at specific time-points post incubation. Currently assuming that myoblast adhesion is feasible with protocol optimization, the microdialysis probe would collect dialysate to monitor the basal uptake/release of skeletal muscle cells. After several basal recordings have been completed to establish a baseline, a stimulation will be administered to the cells by inclusion into the perfusate flown through the probe. Stimuli will include glucose, ace K, saccharin, aspartame, fructose and steviol. This dynamic information will provide insight into the rate of metabolism and metabolic changes that occur within skeletal muscle when exposed to artificial sweeteners as opposed to glucose.

Following analysis of the *in vitro* assay, experiments would be reproduced *in vivo* in the skeletal muscle of the hind-limb quadriceps. This future direction will provide fundamental information regarding the metabolism dynamics of skeletal muscle exposed to artificial sweeteners. Complete understanding of skeletal muscle metabolism when

exposed to artificial sweeteners, as is common during a caloric-restricted diet, is critical for capitalizing on the prominent role of skeletal muscle in resting energy expenditure for combating obesity. This work will provide valuable information regarding the dynamics and overall metabolism of amino acids by skeletal muscle induced by artificial sweeteners as compared to glucose.

References

(1) Devineni, D.; KleinSzanto, A.; Gallo, J. M. *Cancer Research* **1996**, *56*, 1983-1987.
(2) Statistics, N. C. f. H.; Library of Congress Catalog Number 76-641496: Hyattsville, MD, 2016.
(3) Wolfe, R. R. *American Journal of Clinical Nutrition* **2006**, *84*, 475-482.
(4) Tam, C. S.; Lecoultre, V.; Ravussin, E. *Circulation* **2012**, *125*, 2782-2791.
(5) Enerback, S. *New England Journal of Medicine* **2009**, *360*, 2021-2023.
(6) Harms, M.; Seale, P. *Nature Medicine* **2013**, *19*, 1252-1263.
(7) Carter, E. A.; Bonab, A. A.; Hamrahi, V.; Pitman, J.; Winter, D.; Macintosh, L. J.; Cyr, E. M.; Paul, K.; Yerxa, J.; Jung, W.; Tompkins, R. G.; Fischman, A. J. *Life Sciences* **2011**, *89*, 78-85.
(8) Trayhurn, P. *Obesity Reviews* **2007**, *8*, 41-44.
(9) Fantuzzi, G. *Journal of Allergy and Clinical Immunology* **2005**, *115*, 911-919.
(10) Yang, J. C.; Chi, Y. J.; Burkhardt, B. R.; Guan, Y. F.; Wolf, B. A. *Nutrition Reviews* **2010**, *68*, 270-279.
(11) Howell, J. J.; Manning, B. D. *Trends in Endocrinology and Metabolism* **2011**, *22*, 94-102.
(12) Dodd, K. M.; Tee, A. R. *American Journal of Physiology-Endocrinology and Metabolism* **2012**, *302*, E1329-E1342.
(13) Romacho, T.; Elsen, M.; Rohrborn, D.; Eckel, J. *Acta Physiologica* **2014**, *210*, 733-753.
(14) Cao, H. M. *Journal of Endocrinology* **2014**, *220*, T47-T59.
(15) Vitali, A.; Murano, I.; Zingaretti, M. C.; Frontini, A.; Ricquier, D.; Cinti, S. *Journal of Lipid Research* **2012**, *53*, 619-629.
(16) Gregoire, F. M.; Smas, C. M.; Sul, H. S. *Physiological Reviews* **1998**, *78*, 783-809.
(17) Asterholm, I. W.; Tao, C.; Morley, T. S.; Wang, Q. A.; Delgado-Lopez, F.; Wang, Z. V.; Scherer, P. E. *Cell Metabolism* **2014**, *20*, 103-118.
(18) Ogden, C. L.; Carroll, M. D.; Kit, B. K.; Flegal, K. M.; National Center for Health Statistics: US Dept. of Health and Human Services, CDC.
(19) Wang, C. X.; Guo, F. F. *Chinese Science Bulletin* **2013**, *58*, 1228-1235.
(20) Herman, M. A.; She, P.; Peroni, O. D.; Lynch, C. J.; Kahn, B. B. *Journal of Biological Chemistry* **2010**, *285*, 11348-11356.
(21) Newgard, C. B. *Cell Metabolism* **2012**, *15*, 606-614.
(22) Herman, M. A.; She, P. X.; Peroni, O. D.; Lynch, C. J.; Kahn, B. B. *Journal of Biological Chemistry* **2010**, *285*, 11348-11356.
(23) Shimomura, Y.; Murakami, T.; Nakai, N.; Nagasaki, M.; Harris, R. A. *Journal of Nutrition* **2004**, *134*, 1583S-1587S.
(24) Chen, L. X.; Li, P.; Wang, J. J.; Li, X. L.; Gao, H. J.; Yin, Y. L.; Hou, Y. Q.; Wu, G. Y. *Amino Acids* **2009**, *37*, 143-152.
(25) Block, K. P.; Harper, A. E. *Journal of Nutrition* **1991**, *121*, 663-671.
(26) Lackey, D. E.; Lynch, C. J.; Olson, K. C.; Mostaedi, R.; Ali, M.; Smith, W. H.; Karpe, F.; Humphreys, S.; Bedinger, D. H.; Dunn, T. N.; Thomas, A. P.; Oort, P. J.; Kieffer, D. A.; Amin, R.; Bettaieb, A.; Haj, F. G.; Permana, P.; Anthony, T. G.; Adams, S. H. *American Journal of Physiology-Endocrinology and Metabolism* **2013**, *304*, E1175-E1187.
(27) Newgard, C. B.; An, J.; Bain, J. R.; Muehlbauer, M. J.; Stevens, R. D.; Lien, L. F.; Haqq, A. M.; Shah, S. H.; Arlotto, M.; Slentz, C. A.; Rochon, J.; Gallup, D.; Ilkayeva, O.; Wenner, B. R.; Yancy, W. S., Jr.; Eisenson, H.; Musante, G.; Surwit, R. S.; Millington, D. S.; Butler, M. D., et al. *Cell Metabolism* **2009**, *9*, 311-326.
(28) Adeva, M. M.; Calvino, J.; Souto, G.; Donapetry, C. *Amino Acids* **2012**, *43*, 171-181.

(29) Herr, J. K.; Smith, J. E.; Medley, C. D.; Shangguan, D. H.; Tan, W. H. *Analytical Chemistry* **2006**, *78*, 2918-2924.
(30) She, P. X.; Van Horn, C.; Reid, T.; Hutson, S. M.; Cooney, R. N.; Lynch, C. J. *American Journal of Physiology-Endocrinology and Metabolism* **2007**, *293*, E1552-E1563.
(31) Shah, S. H.; Crosslin, D. R.; Haynes, C. S.; Nelson, S.; Turer, C. B.; Stevens, R. D.; Muehlbauer, M. J.; Wenner, B. R.; Bain, J. R.; Laferrere, B.; Gorroochurn, P.; Teixeira, J.; Brantley, P. J.; Stevens, V. J.; Hollis, J. F.; Appel, L. J.; Lien, L. F.; Batch, B.; Newgard, C. B.; Svetkey, L. P. *Diabetologia* **2012**, *55*, 321-330.
(32) Green, H.; Kehinde, O. *Cell* **1974**, *1*, 113-116
(33) Armani, A.; Mammi, C.; Marzolla, V.; Calanchini, M.; Antelmi, A.; Rosano, G. M. C.; Fabbri, A.; Caprio, M. *Journal of Cellular Biochemistry* **2010**, *110*, 564-572.
(34) Zebisch, K.; Voigt, V.; Wabitsch, M.; Brandsch, M. *Analytical Biochemistry* **2012**, *425*, 88-90.
(35) Student, A. K.; Hsu, R. Y.; Lane, M. D. *Journal of Biological Chemistry* **1980**, *255*, 4745-4750.
(36) ATCC.
(37) Sigma-Aldrich.
(38) Hotamisligil, G. S.; Shargill, N. S.; Spiegelman, B. M. *Science* **1993**, *259*, 87-91.
(39) Speakman, J.; Hambly, C.; Mitchell, S.; Krol, E. *Laboratory Animals* **2008**, *42*, 413-432.
(40) Rosenthal, J.; Angel, A.; Farkas, J. *The American journal of physiology* **1974**, *226*, 411-418.
(41) Wang, C. Y.; Liao, J. K. *Mtor: Methods and Protocols* **2012**, *821*, 421-433.
(42) Watson, C. J.; Venton, B. J.; Kennedy, R. T. *Analytical Chemistry* **2006**, *78*, 1391-1399.
(43) Davies, M. I. *Analytica Chimica Acta* **1999**, *379*, 227-249.
(44) Ciriacks, C. M.; Bowser, M. T. *Neuroscience Letters* **2006**, *393*, 200-205.
(45) Hogerton, A. L.; Bowser, M. T. *Analytical Chemistry* **2013**, *85*, 9070-9077.
(46) Harstad, R. K.; Bowser, M. T. *Analytical Chemistry* **2016**, *88*, 8115-8122.
(47) Weisenberger, M. M.; Bowser, M. T. *Analytical Chemistry* **2017**, *89*, 1009-1014.
(48) Klinker, C. C.; Bowser, M. T. *Analytical Chemistry* **2007**, *79*, 8747-8754.
(49) Elmquist, W. F.; Sawchuk, R. J. *Pharmaceutical Research* **1997**, *14*, 267-288.
(50) Johnson, R. D.; Justice, J. B. *Brain Research Bulletin* **1983**, *10*, 567-571.
(51) Teltingdiaz, M.; Scott, D. O.; Lunte, C. E. *Analytical Chemistry* **1992**, *64*, 806-810.
(52) Scott, D. O.; Lunte, C. E. *Pharmaceutical Research* **1993**, *10*, 335-342.
(53) Sarre, S.; Deleu, D.; Vanbelle, K.; Ebinger, G.; Michotte, Y. *Trac-Trends in Analytical Chemistry* **1993**, *12*, 67-73.
(54) Palsmeier, R. K.; Lunte, C. E. *Life Sciences* **1994**, *55*, 815-825.
(55) Devineni, D.; KleinSzanto, A.; Gallo, J. M. *Cancer Chemotherapy and Pharmacology* **1996**, *38*, 499-507.
(56) Zuo, H.; Ye, M.; Davies, M. *Current Separations* **1995**, *14*, 54-57.
(57) Davies, M. I.; Lunte, C. E. *Drug Metabolism and Disposition* **1995**, *23*, 1072-1079.
(58) Davies, M. I.; Lunte, C. E. *Life Sciences* **1996**, *59*, 1001-1013.
(59) Kurata, N.; Inagaki, M.; Iwase, M.; Nishimura, Y.; Kiuchi, Y.; Yamazaki, Y.; Kobayashi, S.; Oguchi, K.; Uchida, E.; Yasuhara, H. *Research Communications in Molecular Pathology and Pharmacology* **1995**, *89*, 45-56.
(60) Ault, J. M.; Lunte, C. E.; Meltzer, N. M.; Riley, C. M. *Pharmaceutical Research* **1992**, *9*, 1256-1261.
(61) Ault, J. M.; Riley, C. M.; Meltzer, N. M.; Lunte, C. E. *Pharmaceutical Research* **1994**, *11*, 1631-1639.
(62) Zuo, H.; Ye, M.; Davies, M. *Current Separations* **1996**, *15*, 63-66.

(63) Nandi, P.; Lunte, S. M. *Analytica Chimica Acta* **2009**, *651*, 1-14.
(64) Davies, M. I.; Lunte, C. E. *Chemical Society Reviews* **1997**, *26*, 215-222.
(65) Wang, Y. F.; Wong, S. L.; Sawchuk, R. J. *Pharmaceutical Research* **1993**, *10*, 1411-1419.
(66) Jacobson, I.; Sandberg, M.; Hamberger, A. *Journal of Neuroscience Methods* **1985**, *15*, 263-268.
(67) Bungay, P. M.; Morrison, P. F.; Dedrick, R. L. *Life Sciences* **1990**, *46*, 105-119.
(68) Hsiao, J. K.; Ball, B. A.; Morrison, P. F.; Mefford, I. N.; Bungay, P. M. *Journal of Neurochemistry* **1990**, *54*, 1449-1452.
(69) Chaurasia, C. S. *Biomedical Chromatography* **1999**, *13*, 317-332.
(70) Stenken, J. A. *Analytica Chimica Acta* **1999**, *379*, 337-358.
(71) Hogan, B. L.; Lunte, S. M.; Stobaugh, J. F.; Lunte, C. E. *Analytical Chemistry* **1994**, *66*, 596-602.
(72) Jensen, S. M.; Hansen, H. S.; Johansen, T.; Malmlof, K. *Journal of Pharmaceutical and Biomedical Analysis* **2007**, *43*, 1751-1756.
(73) Takeda, S.; Sato, N.; Ikimura, K.; Nishino, H.; Rakugi, H.; Morishita, R. *Neuroscience* **2011**, *186*, 110-119.
(74) Lada, M. W.; Schaller, G.; Carriger, M. H.; Vickroy, T. W.; Kennedy, R. T. *Analytica Chimica Acta* **1995**, *307*, 217-225.
(75) Cano-Cebrian, M. J.; Zornoza, T.; Polache, A.; Granero, L. *Current Drug Metabolism* **2005**, *6*, 83-90.
(76) Yang, H.; Peters, J. L.; Allen, C.; Chern, S. S.; Coalson, R. D.; Michael, A. C. *Analytical Chemistry* **2000**, *72*, 2042-2049.
(77) Stahle, L.; Arner, P.; Ungerstedt, U. *Life Sciences* **1991**, *49*, 1853-1858.
(78) Larsson, C. I. *Life Sciences* **1991**, *49*, PL73-PL78.
(79) Parsons, L. H.; Smith, A. D.; Justice, J. B. *Journal of Neuroscience Methods* **1991**, *40*, 139-147.
(80) Lonnroth, P.; Jansson, P. A.; Smith, U. *American Journal of Physiology* **1987**, *253*, E228-E231.
(81) Stahle, L. *Advanced Drug Delivery Reviews* **2000**, *45*, 149-167.
(82) Morrison, P. F.; Bungay, P. M.; Dykstra, K. H.; Hsiao, J. K.; Mefford, I. N. *Monitoring Molecules in Neuroscience* **1991**, 47-50.
(83) Church, W. H.; Justice, J. B. *Analytical Chemistry* **1987**, *59*, 712-716.
(84) Andren, P. E.; Caprioli, R. M. *Journal of Mass Spectrometry* **1995**, *30*, 817-824.
(85) Wages, S. A.; Church, W. H.; Justice, J. B. *Analytical Chemistry* **1986**, *58*, 1649-1656.
(86) Chen, A. Q.; Lunte, C. E. *Journal of Chromatography A* **1995**, *691*, 29-35.
(87) Oshea, T. J.; Weber, P. L.; Bammel, B. P.; Lunte, C. E.; Lunte, S. M.; Smyth, M. R. *Journal of Chromatography* **1992**, *608*, 189-195.
(88) Kennedy, R. T.; Watson, C. J.; Haskins, W. E.; Powell, D. H.; Strecker, R. E. *Current Opinion in Chemical Biology* **2002**, *6*, 659-665.
(89) Huynh, B. H.; Fogarty, B. A.; Martin, R. S.; Lunte, S. M. *Analytical Chemistry* **2004**, *76*, 6440-6447.
(90) Sandlin, Z. D.; Shou, M. S.; Shackman, J. G.; Kennedy, R. T. *Analytical Chemistry* **2005**, *77*, 7702-7708.
(91) Caprioli, R. M.; Lin, S. N. *Proceedings of the National Academy of Sciences of the United States of America* **1990**, *87*, 240-243.
(92) Lin, S. N.; Slopis, J. M.; Butler, I. J.; Caprioli, R. M. *Journal of Neuroscience Methods* **1995**, *62*, 199-205.

(93) Berners, M. O. M.; Boutelle, M. G.; Fillenz, M. *Analytical Chemistry* **1994**, *66*, 2017-2021.
(94) Miele, M.; Berners, M.; Boutelle, M. G.; Kusakabe, H.; Fillenz, M. *Brain Research* **1996**, *707*, 131-133.
(95) Lemmo, A. V.; Jorgenson, J. W. *Analytical Chemistry* **1993**, *65*, 1576-1581.
(96) Hooker, T. F.; Jorgenson, J. W. *Analytical Chemistry* **1997**, *69*, 4134-4142.
(97) Lada, M. W.; Vickroy, T. W.; Kennedy, R. T. *Analytical Chemistry* **1997**, *69*, 4560-4565.
(98) Bowser, M. T.; Kennedy, R. T. *Electrophoresis* **2001**, *22*, 3668-3676.
(99) Zhou, J. X.; Heckert, D. M.; Zuo, H.; Lunte, C. E.; Lunte, S. M. *Analytica Chimica Acta* **1999**, *379*, 307-317.
(100) Wang, M.; Slaney, T.; Mabrouk, O.; Kennedy, R. T. *Journal of Neuroscience Methods* **2010**, *190*, 39-48.
(101) Ciriacks, C. M.; Bowser, M. T. *Analytical Chemistry* **2004**, *76*, 6582-6587.
(102) Ruiz-Jimenez, J.; de Castro, M. D. L. *Trac-Trends in Analytical Chemistry* **2006**, *25*, 563-571.
(103) Hu, T.; Zuo, H.; Riley, C. M.; Stobaugh, J. F.; Lunte, S. M. *Journal of Chromatography A* **1995**, *716*, 381-388.
(104) Hadwiger, M. E.; Torchia, S. R.; Park, S.; Biggin, M. E.; Lunte, C. E. *Journal of Chromatography B-Biomedical Applications* **1996**, *681*, 241-249.
(105) Parrot, S.; Sauvinet, V.; Riban, V.; Depaulis, A.; Renaud, B.; Denoroy, L. *Journal of Neuroscience Methods* **2004**, *140*, 29-38.
(106) Lada, M. W.; Vickroy, T. W.; Kennedy, R. T. *Journal of Neurochemistry* **1998**, *70*, 617-625.
(107) Tucci, S.; Rada, P.; Sepulveda, M. J.; Hernandez, L. *Journal of Chromatography B-Analytical Technologies in the Biomedical and Life Sciences* **1997**, *694*, 343-349.
(108) Zhou, S. Y.; Zuo, H.; Stobaugh, J. F.; Lunte, C. E.; Lunte, S. M. *Analytical Chemistry* **1995**, *67*, 594-599.
(109) Lada, M. W.; Kennedy, R. T. *Analytical Chemistry* **1996**, *68*, 2790-2797.
(110) O'Brien, K. B.; Esguerra, M.; Klug, C. T.; Miller, R. F.; Bowser, M. T. *Electrophoresis* **2003**, *24*, 1227-1235.
(111) Bardelmeijer, H. A.; Lingeman, H.; de Ruiter, C.; Underberg, W. J. M. *Journal of Chromatography A* **1998**, *807*, 3-26.
(112) Molnar-Perl, I.; Vasanits, A. *Journal of Chromatography A* **1999**, *835*, 73-91.
(113) Aoyama, C.; Santa, T.; Tsunoda, M.; Fukushima, T.; Kitada, C.; Imai, K. *Biomedical Chromatography* **2004**, *18*, 630-636.
(114) Johnson, R. D.; Navratil, M.; Poe, B. G.; Xiong, G. H.; Olson, K. J.; Ahmadzadeh, H.; Andreyev, D.; Duffy, C. F.; Arriaga, E. A. *Analytical and Bioanalytical Chemistry* **2007**, *387*, 107-118.
(115) Zetterstrom, T.; Vernet, L.; Ungerstedt, U.; Tossman, U.; Jonzon, B.; Fredholm, B. B. *Neuroscience Letters* **1982**, *29*, 111-115.
(116) Kennedy, R. T.; Thompson, J. E.; Vickroy, T. W. *Journal of Neuroscience Methods* **2002**, *114*, 39-49.
(117) Stenken, J. A.; Church, M. K.; Gill, C. A.; Clough, G. F. *Aaps Journal* **2010**, *12*, 73-78.
(118) O'Brien, K. B.; Esguerra, M.; Miller, R. F.; Bowser, M. T. *Analytical Chemistry* **2004**, *76*, 5069-5074.
(119) Langkilde, A.; Andersen, O.; Henriksen, J. H.; Langberg, H.; Petersen, J.; Eugen-Olsen, J. *Clinical Physiology and Functional Imaging* **2015**, *35*, 110-119.
(120) Rostami, E.; Bellander, B.-M. *Journal of diabetes science and technology* **2011**, *5*, 596-604.

(121) Dimopoulou, I.; Nikitas, N.; Orfanos, S. E.; Theodorakopoulou, M.; Vassiliadi, D.; Ilias, I.; Ikonomidis, I.; Boutati, E.; Maratou, E.; Tsangaris, I.; Karkouli, G.; Tsafou, E.; Diamantakis, A.; Kopterides, P.; Maniatis, N.; Kotanidou, A.; Armaganidis, A.; Ungerstedt, U. *Shock* **2011**, *35*, 343-348.
(122) Harstad, R.; Bowser, M.: submitted, 2016.
(123) Zarrin, F.; Dovichi, N. J. *Analytical Chemistry* **1985**, *37*, 1492-1496.
(124) Shackman, J. G.; Watson, C. J.; Kennedy, R. T. *Journal of Chromatography A* **2004**, *1040*, 273-282.
(125) Blomstrand, E.; Hassmen, P.; Ekblom, B.; Newsholme, E. A. *European Journal of Applied Physiology and Occupational Physiology* **1991**, *63*, 83-88.
(126) Marchianti, A. C. N.; Arimura, E.; Ushikai, M.; Horiuchi, M. *Environmental Health and Preventive Medicine* **2014**, *19*, 339-347.
(127) Mardinoglu, A.; Shoaie, S.; Bergentall, M.; Ghaffari, P.; Zhang, C.; Larsson, E.; Backhed, F.; Nielsen, J. *Molecular Systems Biology* **2015**, *11*.
(128) Enomoto, T.; Ohashi, K.; Shibata, R.; Higuchi, A.; Maruyama, S.; Izumiya, Y.; Walsh, K.; Murohara, T.; Ouchi, N. *Journal of Biological Chemistry* **2011**, *286*, 34552-34558.
(129) Envigo. 2017.
(130) Scudamore, C. L. In *A Practical Guide to the Histology of the Mouse*; John Wiley & Sons, Ltd.: Hoboken, NJ, 2014, pp 8-9.
(131) Category, T. R.; Aegis Creative Communications, Inc., 2013.
(132) Knoblaugh, S.; Habecker, R.; Rath, S.; Elsevier: Amsterdam, 2011, pp 15-41.
(133) Chusyd, D. E.; Wang, D.; Huffman, D. M.; Nagy, T. R. *Frontiers in Nutrition* **2016**, *3*.
(134) Himmshagen, J. *Faseb Journal* **1990**, *4*, 2890-2898.
(135) Ulmer, J., B.; Rappuoli, R.; John Wiley & Sons, Inc., 2003.
(136) Otto, K.; von Thaden, A.-K. In *The Laboratory Mouse*, Hedrich, P. H. J., Ed.; Elsevier Ltd., 2012, pp 739-759.
(137) Gargiulo, S.; Greco, A.; Gramanzini, M.; Esposito, S.; Affuso, A.; Brunetti, A.; Vesce, G. *Ilar Journal* **2012**, *53*, E55-E69.
(138) Flecknell, P.; Academic Press: London, 1987.
(139) Murray, W.; Fleming, P. In *Anesthesiology*, 1972, pp 620-625.
(140) Zuurbier, C.; Emons, V.; C, I.; Am. J. Physiol. Heart Circ. Physiol., 2002, pp H2099-H2105.
(141) Kohn, D.; Wixson, S.; White, W.; Benson, G. *Anesthesia and Analgesia in Laboratory Animals*; Academic Press: New York, 1997.
(142) Mazze, R.; Wilson, A.; Rice, S.; Baden, J.; Teratology, 1985, pp 339-345.
(143) Hildebrandt, I.; Su, H.; Weber, W. *Anesthesia and other considerations for in vivo imaging of small animals*; ILAR J, 2008; Vol. 49.
(144) Flecknell, P. In *Guide to Techniques in Mouse Development*; Academic Press: San Diego, CA, 1993, pp 16-33.
(145) Suez, J.; Korem, T.; Zeevi, D.; Zilberman-Schapira, G.; Thaiss, C. A.; Maza, O.; Israeli, D.; Zmora, N.; Gilad, S.; Weinberger, A.; Kuperman, Y.; Harmelin, A.; Kolodkin-Gal, I.; Shapiro, H.; Halpern, Z.; Segal, E.; Elinav, E. *Nature* **2014**, *514*, 181-+.
(146) Kroger, M.; Meister, K.; Kava, R. *Comprehensive Reviews in Food Science and Food Safety* **2006**, *5*, 35-47.
(147) Sardesai, V. M.; Waldshan, T. H. *Journal of Nutritional Biochemistry* **1991**, *2*, 236-244.

(148) Magnuson, B. A.; Burdock, G. A.; Doull, J.; Kroes, R. M.; Marsh, G. M.; Pariza, M. W.; Spencer, P. S.; Waddell, W. J.; Walker, R.; Williams, G. M. *Critical Reviews in Toxicology* **2007**, *37*, 629-727.
(149) Magnuson, B.; Academy of Nutrition and Dietetics, 2011.
(150) Lucas, E.; Kuznesof, P.; Joint Expert Committee for Food Additives, 2004.
(151) Geuns, J. M. C. *Phytochemistry* **2003**, *64*, 913-921.
(152) Ubukata, K.; Nakayama, A.; Mihara, R. *Food and Chemical Toxicology* **2011**, *49*, S8-S29.
(153) Chatsudthipong, V.; Muanprasat, C. *Pharmacology & Therapeutics* **2009**, *121*, 41-54.
(154) Roberts, A.; Renwick, A. G.; Sims, J.; Snodin, D. J. *Food and Chemical Toxicology* **2000**, *38*, S31-S41.
(155) *Who Technical Report Series* **1981**, 1-&.
(156) *Evaluation of Certain Food Additives and Contaminants* **1993**, *837*, 1-53.
(157) Colburn, W. A.; Bekersky, I.; Blumenthal, H. P. *Journal of Clinical Pharmacology* **1981**, *21*, 147-151.
(158) Ayala, J. E.; Samuel, V. T.; Morton, G. J.; Obici, S.; Croniger, C. M.; Shulman, G. I.; Wasserman, D. H.; McGuinness, O. P.; Co, N. I. H. M. M. P. C. *Disease Models & Mechanisms* **2010**, *3*, 525-534.
(159) McGuinness, O. P.; Ayala, J. E.; Laughlin, M. R.; Wasserman, D. H. *American Journal of Physiology-Endocrinology and Metabolism* **2009**, *297*, E849-E855.
(160) *WHO Technical Report Series* **1991**, *806*, 1-61.
(161) IPCS INCHEM.
(162) Close, B.; Banister, K.; Baumans, V.; Bernoth, E.; Bromage, N.; Bunyan, J.; al., e.; DGXT of the European Commission, 1996, pp 293-316.
(163) Close, B.; Banister, K.; Baumans, V.; Bernoth, E.; Bromage, N.; Bunyan, J.; al., e.; DGXT of the European Commission, 1997, pp 1-32.
(164) National Laboratory Research Council, I. o. L. A. R., Committee on Pain and Distress in Laboratory Animals. *Recognition and Alleviation of Pain and Distress in Laboratory Animals*; Academic Press: Washington DC, 1992.
(165) Kowalchuk, J. M.; Curi, R.; Newsholme, E. A. *Biochemical Journal* **1988**, *249*, 705-708.
(166) Felig, P.; Marliss, E.; Cahill, G. F. J. *New England Journal of Medicine* **1969**, *281*, 811-816.
(167) Nakaya, Y.; Minami, A.; Harada, N.; Sakamoto, S.; Niwa, Y.; Ohnaka, M. *American Journal of Clinical Nutrition* **2000**, *71*, 54-58.
(168) Berg, T. M.; Tymoczko, J. L.; Stryer, L.; WH Freeman: New York, 2002.
(169) Simon, B. R.; Parlee, S. D.; Learman, B. S.; Mori, H.; Scheller, E. L.; Cawthorn, W. P.; Ning, X. M.; Gallagher, K.; Tyrberg, B.; Assadi-Porter, F. M.; Evans, C. R.; MacDougald, O. A. *Journal of Biological Chemistry* **2013**, *288*, 32475-32489.
(170) Harstad, R. *Dissertation: Chapter 5* **2016**.
(171) Pelleymounter, M. A.; Cullen, M. J.; Baker, M. B.; Hecht, R.; Winters, D.; Boone, T.; Collins, F. *Science* **1995**, *269*, 540-543.
(172) Friedman, J. M.; Halaas, J. L. *Nature* **1998**, *395*, 763-770.
(173) Stump, C. S.; Henriksen, E. J.; Wei, Y. Z.; Sowers, J. R. *Annals of Medicine* **2006**, *38*, 389-402.
(174) Sinacore, D. R.; Gulve, E. A. *Physical Therapy* **1993**, *73*, 878-891.
(175) Rennie, M. J.; Wackerhage, H.; Spangenburg, E. E.; Booth, F. W. *Annual Review of Physiology* **2004**, *66*, 799-828.

(176) Zurlo, F.; Larson, K.; Bogardus, C.; Ravussin, E. *Journal of Clinical Investigation* **1990**, *86*, 1423-1427.
(177) Yaffe, D.; Saxel, O. *Nature* **1977**, *270*, 725-727.
(178) Morgan, J. E.; Moore, S. E.; Walsh, F. S.; Partridge, T. A. *Journal of Cell Science* **1992**, *102*, 779-&.
(179) Jing, L. In *Bio-Protocol 2(10): e172*, 2012.
(180) Barak, R.; Chet, I. *Soil Biology & Biochemistry* **1986**, *18*, 315-319.
(181) Bjorntorp, P.; Sjostrom, L. *Metabolism* **1971**, *20*, 703-713.
(182) McMahon, D. K.; Anderson, P. A. W.; Nassar, R.; Bunting, J. B.; Saba, Z.; Oakeley, A. E.; Malouf, N. N. *American Journal of Physiology* **1994**, *266*, C1795-C1802.